

# Observational and numerical modeling constraints on the global ocean biological carbon pump

Scott C. Doney<sup>1</sup>, Kayla Alexis Mitchell<sup>1</sup>, Stephanie Anne Henson<sup>2</sup>, Emma L Cavan<sup>3</sup>, Timothy DeVries<sup>4</sup>, Nicolas Gruber<sup>5</sup>, Judith Hauck<sup>6</sup>, Colleen B. Mouw<sup>7</sup>, Jens Daniel Müller<sup>5</sup>, and Francois W. Primeau<sup>8</sup>

<sup>1</sup>University of Virginia

<sup>2</sup>National Oceanography Centre

<sup>3</sup>University of Tasmania

<sup>4</sup>University of California Santa Barbara

<sup>5</sup>ETH Zürich

<sup>6</sup>Alfred Wegener Institute Helmholtz Centre for Polar and Marine Research

<sup>7</sup>University of Rhode Island

<sup>8</sup>University of California, Irvine

April 05, 2024

## Abstract

This study characterized ocean biological carbon pump metrics in the second iteration of the REgional Carbon Cycle Assessment and Processes (RECCAP2) project, a coordinated, international effort to constrain contemporary ocean carbon air-sea fluxes and interior carbon storage trends using a combination of observation-based estimates, inverse models, and global ocean biogeochemical models. The analysis here focused on comparisons of global and biome-scale regional patterns in particulate organic carbon production and sinking flux from the RECCAP2 model ensemble against observational products derived from satellite remote sensing, sediment traps, and geochemical methods. There was generally encouraging model-data agreement in large-scale spatial patterns, though with substantial spread across the model ensemble and observational products. The global-integrated, model ensemble-mean export production, taken as the sinking particulate organic carbon flux at 100 m ( $6.41 \pm 1.52$  Pg C yr $^{-1}$ ), and export ratio defined as sinking flux divided by net primary production ( $0.154 \pm 0.026$ ) both fell at the lower end of observational estimates. Comparison with observational constraints also suggested that the model ensemble may have underestimated regional biological CO<sub>2</sub> drawdown and air-sea CO<sub>2</sub> flux in high productivity regions. Reasonable model-data agreement was found for global-integrated, ensemble-mean sinking particulate organic carbon flux into the deep ocean at 1000 m ( $0.95 \pm 0.64$  Pg C yr $^{-1}$ ) and the transfer efficiency defined as flux at 1000m divided by flux at 100m ( $0.121 \pm 0.035$ ), with both variables exhibiting considerable regional variability. Future modeling studies are needed to improve system-level simulation of interaction between model ocean physics and biogeochemical response.

1  
2 **Observational and numerical modeling constraints on the global ocean biological**  
3 **carbon pump**

4  
5 **Scott C. Doney<sup>1</sup>, Kayla A. Mitchell<sup>1,2</sup>, Stephanie A. Henson<sup>3</sup>, Emma Cavan<sup>4</sup>, Tim DeVries<sup>5</sup>,**  
6 **Nicolas Gruber<sup>6</sup>, Judith Hauck<sup>7</sup>, Colleen B. Mouw<sup>8</sup>, Jens D. Müller<sup>6</sup>, and Francois W.**  
7 **Primeau<sup>2</sup>**

8  
9 **Submitted, March 4<sup>th</sup>, 2024**

10  
11 <sup>1</sup> Department of Environmental Sciences, University of Virginia, Charlottesville, VA, USA,

12 <sup>2</sup> Department of Earth System Science, University of California, Irvine, Irvine, CA, USA,

13 <sup>3</sup> National Oceanography Centre, Southampton, UK,

14 <sup>4</sup> Department of Life Sciences, Silwood Park Campus, Imperial College London, Berkshire, UK,

15 <sup>5</sup> Earth Research Institute and Department of Geography, University of California, Santa

16 Barbara, Santa Barbara, CA, USA,

17 <sup>6</sup> Environmental Physics, Institute of Biogeochemistry and Pollutant Dynamics, ETH Zurich,  
18 Zürich, Switzerland

19 <sup>7</sup> Alfred-Wegener-Institut, Helmholtz-Zentrum für Polar- und Meeresforschung, Bremerhaven,  
20 Germany

21 <sup>8</sup> Graduate School of Oceanography, University of Rhode Island, Narragansett, RI, USA.

22

23 Corresponding author: Scott Doney ([sdoney@virginia.edu](mailto:sdoney@virginia.edu)) ORCID: 0000-0002-3683-2437

24

25 **Key Points:**

26

- 27 • Global-scale, ocean biogeochemical simulations are compared with observation-based  
estimates of the marine biological carbon pump.
- 28 • A multi-model ensemble exhibits relatively good agreement with observation-based  
metrics for carbon export flux and transfer efficiency.
- 30 • Based on identified model-observation and inter-model differences, we provide guidance  
31 for future model evaluations and development.

32

33 **Abstract**

34 This study characterized ocean biological carbon pump metrics in the second iteration of  
35 the REgional Carbon Cycle Assessment and Processes (RECCAP2) project, a coordinated,  
36 international effort to constrain contemporary ocean carbon air-sea fluxes and interior carbon  
37 storage trends using a combination of observation-based estimates, inverse models, and global  
38 ocean biogeochemical models. The analysis here focused on comparisons of global and biome-  
39 scale regional patterns in particulate organic carbon production and sinking flux from the  
40 RECCAP2 model ensemble against observational products derived from satellite remote sensing,  
41 sediment traps, and geochemical methods. There was generally encouraging model-data  
42 agreement in large-scale spatial patterns, though with substantial spread across the model ensemble  
43 and observational products. The global-integrated, model ensemble-mean export production, taken  
44 as the sinking particulate organic carbon flux at 100 m ( $6.41 \pm 1.52 \text{ Pg C yr}^{-1}$ ), and export ratio  
45 defined as sinking flux divided by net primary production ( $0.154 \pm 0.026$ ) both fell at the lower end  
46 of observational estimates. Comparison with observational constraints also suggested that the  
47 model ensemble may have underestimated regional biological CO<sub>2</sub> drawdown and air-sea CO<sub>2</sub> flux  
48 in high productivity regions. Reasonable model-data agreement was found for global-integrated,  
49 ensemble-mean sinking particulate organic carbon flux into the deep ocean at 1000 m ( $0.95 \pm 0.64$   
50 Pg C yr<sup>-1</sup>) and the transfer efficiency defined as flux at 1000m divided by flux at 100m ( $0.121 \pm$   
51 0.035), with both variables exhibiting considerable regional variability. Future modeling studies  
52 are needed to improve system-level simulation of interaction between model ocean physics and  
53 biogeochemical response.

54

55 **Plain Language Summary**

56 Phytoplankton in the surface ocean create each year an amount of organic carbon  
57 approximately equivalent to all the annual photosynthesis by plants on land. A small fraction of  
58 this newly formed organic carbon is exported below the surface layer, and an even smaller amount  
59 makes it all the way to the deep ocean. The transport of organic carbon to the sub-surface ocean,  
60 called the biological carbon pump, influences the global-scale distributions of ocean nutrients,  
61 oxygen, and inorganic carbon as well as the amount of carbon dioxide in the atmosphere. The  
62 global rates and geographic patterns of photosynthesis and carbon flux out of the surface ocean  
63 have previously been constructed from ship measurements and satellite remote sensing. Here, we  
64 compare these observation-based estimates to a suite of three-dimensional, numerical ocean  
65 models and find broadly similar results. The model simulations also capture aspects of the  
66 biological carbon pump deeper in the water column, where there are fewer direct constraints from  
67 field observations. Our comparison of observations and simulations identifies some deficiencies  
68 in the models that should be corrected in order to better simulate climate change impacts on the  
69 biological carbon pump.

70

71 **1 Introduction**

72 Marine biogeochemical processes play a central role in the global Earth System,  
73 modulating the distribution of inorganic carbon, oxygen, and nutrients within the ocean and the  
74 partitioning of carbon between ocean and atmosphere reservoirs (Broecker and Peng, 1982;  
75 Sarmiento and Gruber, 2002; Devries, 2022; Iversen, 2023; Siegel et al., 2023). Because of the

76 strong oceanic influence on atmospheric CO<sub>2</sub> concentration and thus planetary climate, there is  
77 considerable scientific focus on quantifying both the baseline and trends in ocean carbon storage  
78 and fluxes arising from the uptake of anthropogenic CO<sub>2</sub> and climate change impacts on marine  
79 biogeochemical and physical dynamics (Henson et al., 2016; DeVries et al., 2019; Hauck et al.,  
80 2020; Canadell et al., 2021; Crisp et al., 2022; Wilson et al., 2022; Gruber et al., 2023). The  
81 REgional Carbon Cycle Assessment and Processes (RECCAP) project is a coordinated,  
82 international effort to constrain contemporary ocean carbon air-sea fluxes and interior storage  
83 trends using a combination of observation-based estimates, inverse models, and global ocean  
84 biogeochemical models (GOBMs) (Wanninkhof et al., 2013; Khatiwala et al., 2013). The second  
85 phase, RECCAP2, extends the original synthesis using additional years of ocean observations and  
86 updated methodology and numerical results (DeVries et al., 2023; Hauck et al., 2023) as well as  
87 expanding the scope of the analysis, in this case into biological carbon pump magnitude and  
88 efficiency.

89 In a simple 1-D form, the marine biological carbon pump can be viewed as the net  
90 production of particulate organic carbon (POC) and inorganic carbon (PIC) in the surface ocean,  
91 downward vertical transport of particulate carbon into the thermocline and deep sea, and  
92 subsequent respiration and remineralization of particulate carbon back into dissolved inorganic  
93 carbon (DIC) (Volk and Hoffert, 1985). The downward organic carbon transport, or export flux,  
94 drives subsurface marine biogeochemistry, fuels deep-ocean ecosystems, and influences ocean  
95 carbon storage and atmospheric CO<sub>2</sub>. The biological pump accentuates the vertical gradient in DIC  
96 already established from CO<sub>2</sub> system thermal solubility and temperature gradients, and deep-ocean  
97 carbon storage reflects a net balance between the biological carbon pump source and physical  
98 ocean circulation processes that return elevated deep-ocean DIC waters back to the surface ocean  
99 via upwelling and vertical mixing (Sarmiento and Gruber, 2006). The relationship between ocean  
100 carbon storage and the strength of the biological pump is not necessarily straightforward because  
101 of physical-biological interactions; for example, stronger overturning circulation can enhance both  
102 biological export through increased nutrient supply and the physical return of high-DIC deep-  
103 ocean waters to the surface (Doney et al., 2006). The vertical structure of the biological carbon  
104 pump is also important. Sinking POC fluxes decline rapidly in the thermocline (0 to ~1000 m  
105 depth), with only a fraction of surface export flux reaching the deep ocean below 1000 m (Martin  
106 et al., 1987; Lutz et al., 2007; Lima et al., 2014; Dinauer et al., 2022). Deeper remineralization  
107 depths, that is the transport of a greater fraction of POC into the lower thermocline or deep ocean  
108 prior to respiration, enhances ocean carbon storage because of generally reduced physical return  
109 rates to the surface ocean for deeper waters, and therefore longer retention times for the  
110 remineralized DIC, although with substantial regional variations associated with circulation  
111 pathways and rates (Kwon et al., 2009; Siegel et al., 2021).

112 Net primary production (NPP) by surface ocean phytoplankton generates POC and  
113 dissolved organic carbon (DOC), and most marine NPP is converted rapidly back to DIC through  
114 zooplankton grazing of living biomass and detritus or through the microbial loop involving  
115 consumption of POC and DOC pools. Export fluxes require an excess of community production  
116 of organic carbon over respiration that in turn must be supported by an external supply of new  
117 nutrients over sufficient time and space scales (Ducklow and Doney, 2013). The fraction of NPP  
118 that is exported (export ratio = export flux/NPP), is modulated by the magnitude and seasonality  
119 of NPP, environmental conditions, and phytoplankton and zooplankton community composition  
120 (Laufkötter et al., 2016). Export flux from the euphotic zone occurs through multiple pathways  
121 including gravitational sinking of POC (e.g., living and dead cells; fecal pellets; marine snow),

122 physical subduction and mixing of POC and DOC below the surface layer, and active biological  
123 transport by vertically migrating organisms (Siegel et al., 2016). Contemporary models capture,  
124 with varying levels of sophistication and skill, biological processes involved in NPP and export  
125 flux from the upper ocean (Fennel et al., 2022), though models tend to focus on gravitational  
126 particle sinking and many do not incorporate all of the relevant export pathways (Boyd et al., 2019;  
127 Henson et al., 2022) or dynamics governing vertical carbon fluxes from the surface to the deep sea  
128 (Burd, 2024). Here we focus on simulated export via gravitational particle sinking, which is  
129 incorporated in virtually all global ocean biogeochemical models in some form. Observation-based  
130 estimates of the global export flux have a large range ( $\sim 5\text{--}12 \text{ Pg C yr}^{-1}$ ; Siegel et al., 2016), which  
131 is almost identical to the range in export estimates for the modern-day era simulated by coupled  
132 climate models ( $4.5\text{--}12 \text{ Pg C yr}^{-1}$ ; Henson et al., 2022), i.e. the observations-based estimates of  
133 export flux provide a poor constraint for biogeochemical models. Because of differences in model  
134 climate responses and parameterizations of the ocean biological carbon pump, substantial  
135 uncertainties also plague projections of future changes in export flux in response to climate change.  
136 For example, Henson et al. (2022) found a large inter-model spread in projected changes in export  
137 flux by 2100 of between  $+0.16$  and  $-1.98 \text{ Pg C yr}^{-1}$  ( $+1.8$  to  $-41\%$ ) under the high-emission SSP5-  
138 8.5 scenario.

139 Much of the export flux of organic carbon from the euphotic zone, taken here as the  
140 downward flux through 100m ( $F_{100}$ ), is consumed by respiration in the mesopelagic zone (100 –  
141 1000 m). The diverse mechanisms for vertical transport and remineralization of organic matter in  
142 the mesopelagic are only partially captured in models (Fennel et al., 2022). A steep decline with  
143 depth in the gravitational sinking flux of particles is well documented from mid-depth sediment  
144 traps (e.g., Lutz et al., 2007; Lima et al., 2014; Dinauer et al., 2022), but the exact processes  
145 involved are less well quantified and may include physical and biological particle fragmentation  
146 (Briggs et al., 2020) as well as particle consumption and repackaging by zooplankton (Stukel et  
147 al., 2019). Particle fluxes and the depth-scale of remineralization are affected by particle  
148 composition, size, density, and sinking speeds. Particles can vary widely from small, slowly  
149 sinking dead cells and detrital material, to large marine snow aggregates with enhanced sinking  
150 speeds from captured ballast material, to large rapidly sinking fecal pellets (Lam et al., 2011;  
151 Omand et al., 2020). Vertical migrators transport organic carbon downward from the euphotic  
152 zone into the mesopelagic, respiring  $\text{CO}_2$  and releasing fecal pellets at depth (Archibald et al.,  
153 2019). Sinking particle fluxes and mesopelagic biological processes typically are not modeled in  
154 great mechanistic detail in contemporary global ocean biogeochemical models, and often relatively  
155 simplistic empirical relationships such as variants of the Martin power-law flux curve (Martin et  
156 al., 1987) are used in place of explicit representation of the processes controlling mesopelagic flux  
157 attenuation.

158 The proportion of sinking exported POC that survives remineralization in the mesopelagic  
159 zone to reach depths  $> 1000$  meters is referred to as the transfer efficiency, given here as the ratio  
160 of sinking fluxes at 100 and 1000 meters ( $E_{1000/100}$ ). POC reaching 1000m depth is remineralized  
161 below the main thermocline and is likely sequestered on timescales of  $>100$  years, thus  
162 contributing to the long-term ocean carbon sink (Siegel et al., 2021). There is currently little  
163 consensus on the global magnitude or spatial patterns of transfer efficiency, with some approaches  
164 suggesting that  $E_{1000/100}$  is high at high latitudes and low at low latitudes (Marsay et al., 2015;  
165 Weber et al., 2016; DeVries and Weber, 2017), whilst others imply the opposite pattern (Lam et  
166 al., 2011; Henson et al., 2012; Guidi et al., 2015; Mouw et al., 2016b; Dinauer et al. 2022). A  
167 variety of approaches have been used to generate these estimates, including paired in situ

168 observations of  $^{234}\text{Th}$ -derived export flux and deep sediment trap flux (Henson et al. 2012), vertical  
 169 profiles of flux from drifting sediment traps (Marsay et al., 2015) or inverting the observed nutrient  
 170 and/or oxygen distributions using an inverse model (Weber et al., 2016; Devries and Weber, 2017;  
 171 Cram et al., 2018). The differing approaches, and differing time and space scales that they integrate  
 172 over, are likely a significant source of the uncertainty in global  $E_{1000/100}$  patterns. In CMIP6  
 173 models, there are substantial differences in both the preindustrial mean  $E_{1000/100}$  (varying from 3%  
 174 to 25% across models) and its response to 21<sup>st</sup> century climate change, with projections showing  
 175 both increases and decreases in  $E_{1000/100}$  over time (Wilson et al., 2022).

176 Early model skill assessments relied heavily on model-data comparisons to transient  
 177 tracers, ocean physics, and sub-surface nutrient and oxygen fields that reflect the imprint of  
 178 biological pump fluxes and ocean circulation (e.g., Matsumoto et al., 2004; Doney et al. 2004;  
 179 Najjar et al. 2007). However, observational constraints on the ocean biological carbon pump have  
 180 advanced considerably since the early global 3-D ocean biogeochemical modelling efforts (e.g.,  
 181 Bacastow and Maier-Reimer, 1990; Maier-Reimer, 1993). Global-scale data compilations of  
 182 primary production, surface export and mesopelagic sinking carbon fluxes are now available based  
 183 on a wealth of satellite remote sensing, sediment traps, and geochemical methods (e.g., Henson et  
 184 al. 2012; Mouw et al., 2016a). Past model-data skill assessments using multi-model ensembles  
 185 have highlighted differences in simulated ocean biological carbon pump patterns, magnitudes, and  
 186 mechanisms and identified model biases relative to admittedly imperfect observational estimates  
 187 (Laufkötter et al., 2015; Laufkötter et al., 2016). This study expands on these past assessment  
 188 efforts of the ocean biological carbon pump to include the current generation of global ocean  
 189 biogeochemical models compiled for RECCAP2 (DeVries et al., 2023).

190 The objective of this study is to characterize the global-scale biological carbon pump from  
 191 RECCAP2 models and compare the simulation results with observation-based metrics. The focus  
 192 is on the spatial patterns and global-integrated rates from the multi-model ensemble mean taking  
 193 into consideration inter-model spread. Key metrics include export of sinking POC from the surface  
 194 euphotic zone and the efficiency of POC transfer through the mesopelagic ocean, both of which  
 195 are central to ocean carbon storage. Based on identified model-observation and inter-model  
 196 differences, we also provide guidance for future global ocean biogeochemical model evaluations  
 197 and development that could include targeted, more detailed analyses of dynamics and biases within  
 198 individual RECCAP models.

199

## 200 **2 Methods and Data**

### 201 **2.1 RECCAP2 model simulations and observational data products**

202 This study leveraged a collection of ocean simulation and observational data sets, outlined  
 203 in Table 1, assembled for RECCAP2 following standardized protocols and data reporting for  
 204 numerical and observation-based pCO<sub>2</sub> products (RECCAP2 Ocean Science Team, 2022; DeVries  
 205 et al., 2023; Müller, 2023). The RECCAP2 ocean data sets included monthly surface and annual  
 206 ocean interior output for the contemporary period from more than a dozen global ocean  
 207 biogeochemical model hindcast simulations, including both forward and data-assimilated models,  
 208 along with observation-based surface ocean pCO<sub>2</sub> interpolation products. Many of the models  
 209 included in the RECCAP2 suite have been used in the Global Carbon Project to assess the ocean  
 210 carbon sink (Hauck et al., 2020; Friedlingstein et al., 2022). Here, we present model results for

1985 to 2018 from RECCAP2 simulation A, which was forced with historical atmospheric reanalysis data and increasing atmospheric CO<sub>2</sub>, and hence represents both steady-state and variable climate processes and both natural, pre-industrial carbon fluxes and anthropogenic carbon fluxes caused by rising atmospheric CO<sub>2</sub> (DeVries et al., 2023).

215

**Table 1.** Description of RECCAP2 global ocean biogeochemical hindcast models, global data-assimilated models, and observation-based products used in this study. For more details see Tables S1 and S2 in DeVries et al. (2023). The World Ocean Atlas (WOA) data set was also used in the model-data evaluation.

220

221 <b>Global hindcast models</b>	222 <b>Data range</b>	223 <b>References</b>
222 CCSM-WHOI	1958-2017	Doney et al. (2009)
223 CESM-ETHZ	1980-2018	Lindsay et al. (2014); Yang and Gruber (2016)
224 CNRM-ESM2 -1	1980-2018	Séférian et al. (2019; 2020); Berthet et al. (2019)
225 EC-Earth3	1980-2018	Döscher et al. (2021)
226 FESOM-RECoM-LR	1980-2018	Hauck et al. (2020)
227 MPIOM-HAMOCC	1980-2018	Ilyina et al. (2013); Mauritzen et al. (2019)
228 MOM6-Princeton	1980-2018	Liao et al. (2020); Stock et al. (2020)
229 MRI-ESM2-1	1980-2018	Urakawa et al. (2020); Tsujino et al. (2017)
230 NorESM-OC1.2	1980-2018	Schwinger et al. (2016)
231 NEMO-PlankTOM12.1	1980-2018	Le Quéré et al. (2016); Wright et al. (2021)
232 ORCA1-LIM3-PISCES	1980-2018	Aumont et al. (2015)

233

#### 234 **Data-assimilated models**

235 ECCO-Darwin	1995-2018	Carroll et al. (2020; 2022)
236 SIMPLE-TRIM	Climatology	DeVries and Weber (2017)

237

#### 238 **pCO<sub>2</sub> interpolation products**

239 CMEMS-LSCE-FFNN	1985-2018	Chau et al. (2022)
240 JenaMLS	1985-2018	Rödenbeck et al. (2013); Rödenbeck et al. (2022)
241 MPI-SOMFFN	1982-2018	Landschützer et al. (2016)
242 NIES-ML3	1980-2020	Zeng et al. (2022)
243 OceanSODA-ETHZ	1985-2018	Gregor and Gruber (2021)
244 LDEO_HPD	1985-2018	Gloegge et al. (2022)
245 UOEX_Wat20	1985-2019	Watson et al. (2020)

246

#### 247 **World Ocean Atlas**

248 Oxygen and AOU	Climatology	Garcia et al. (2019)
--------------------	-------------	----------------------

249

#### 250 **Biological carbon pump metrics**

251 net primary production, export production,		
252 and sinking POC flux	Climatology	Mouw et al. (2016a; 2016b)

253

254

255 Spatial 2D model output and pCO<sub>2</sub> interpolation products were provided to RECCAP2  
256 with 1° x 1° resolution at monthly time steps, and 3D model output was resolved at annual time

257 steps. All estimates derived in this study were computed on the  $1^\circ \times 1^\circ$  grid. Global multi-model  
 258 ensembles, spatial integrals and averages were computed as needed from the gridded results. For  
 259 the aggregation to sub-basin ocean regions, ocean biomes based on Fay and McKinley (2014) were  
 260 used in most instances to facilitate consistent regional intercomparison across RECCAP2 studies  
 261 (e.g., Hauck et al., 2023). Longhurst provinces (Supplement Figure S1; Reygondeau et al., 2013)  
 262 were additionally used in some of the biological pump model-observational comparisons to be  
 263 consistent with one of the key observational data synthesis products (Mouw et al., 2016a). The  
 264 notation and units for the biological, chemical and physical variables used in this study are  
 265 described in Table 2. More details on the RECCAP2 ocean data sets can be found in DeVries et  
 266 al. (2023).

267 We also used an observational compilation of surface ocean export production and sinking  
 268 POC flux combined with satellite ocean color data products for primary production synthesized in  
 269 Mouw et al. (2016a) and as aggregated to Longhurst regional provinces in Mouw et al. (2016b).  
 270 The full dataset includes over 15000 individual sediment trap and  $^{234}\text{Th}$  POC flux measurements  
 271 at 673 locations, combined with satellite-derived estimates of NPP. Chlorophyll measurements  
 272 collected from the SeaWiFS sensor on the OrbView-2 ocean color satellite, spanning from August  
 273 1997 to December 2010, were used to derive NPP using the vertically generalized production  
 274 model (VGPM) (Behrenfeld and Falkowski, 1997) on an equal-area grid with 9-km resolution.  
 275 The climatology in Mouw et al. (2016a) used an interpolation approach to combine the satellite  
 276 timeseries and short-deployment (<30 days trap cup intervals) sediment trap POC flux  
 277 measurements at overlapping locations. Over 43% of the POC flux measurements were collected  
 278 after 1997, overlapping with the satellite record. For each POC flux location, median monthly  
 279 values are computed and binned into biogeochemical Longhurst provinces for the climatology.  
 280 The POC flux climatology also has a depth dimension, with depth bins centered at 20 m for a near-  
 281 surface layer, in 50 m intervals in the upper thermocline, and in 200 m intervals from 500 m to  
 282 5000 m.

283  
 284 **Table 2.** Glossary and description of modeled, observed, and derived variables including  
 285 notation and units.  
 286

Variable Name	Units	Output frequency	Description
<b>2D or surface ocean properties</b>			
$p\text{CO}_2$	$\mu\text{atm}$	monthly	Surface ocean $p\text{CO}_2$
$NPP$	$\text{mol C m}^{-2} \text{yr}^{-1}$	monthly	Vertically-integrated net primary production of organic carbon
$F_{100}$	$\text{mol C m}^{-2} \text{yr}^{-1}$	monthly	POC sinking flux at 100 m
$F_{1000}$	$\text{mol C m}^{-2} \text{yr}^{-1}$	monthly	POC sinking flux at 1000 m
<b>3D or Interior Ocean Properties</b>			
T	$^\circ\text{C}$	annual	Seawater potential temperature
S	-	annual	Salinity (PSS-78)
$F_{3D}$	$\text{mol C m}^{-2} \text{yr}^{-1}$	annual	3D field of POC sinking flux

O <sub>2</sub>	mol O <sub>2</sub> m <sup>-3</sup>	annual	Dissolved oxygen concentration
<b>Derived Variables</b>			
$E_{100/NPP} = F_{100}/NPP$	-	monthly	Surface Export Ratio
$E_{1000/100} = F_{1000}/F_{100}$	-	monthly	Mesopelagic Transfer Efficiency
$E_{1000/NPP} = F_{1000}/NPP$	-	monthly	Surface to Deep-sea Export Efficiency
AOU	μmol kg <sup>-1</sup>	monthly	Apparent oxygen utilization

287

288

289 **2.2 Ocean biological pump and biogeochemical metrics**

290 Our analysis utilized biogeochemical model estimates of vertically integrated NPP and  
 291 export fluxes of sinking POC flux across a shallow surface at the approximate base of the euphotic  
 292 zone (100 m,  $F_{100}$ ) and at the base of the main thermocline (1000 m,  $F_{1000}$ ). Note that the 1000 m  
 293 fluxes were not provided for all models (see Figure 2c), and therefore the ensemble means for  $F_{100}$   
 294 and  $F_{1000}$  were constructed from different subsets of RECCAP2 simulations. The export ratio,  
 295  $E_{100/NPP}$ , was computed as the ratio of POC sinking flux at 100 m divided by net integrated primary  
 296 production:

$$297 \quad E_{100/NPP} = \frac{F_{100}}{NPP} \quad (1)$$

298 The transfer efficiency across the 1000 m depth horizon,  $E_{1000/100}$ , was similarly computed as the  
 299 ratio of sinking POC fluxes at 100 m and 1000 m:

$$301 \quad E_{1000/100} = \frac{F_{1000}}{F_{100}} \quad (2)$$

303 A depth of 1000 m is taken as an approximate boundary between the main thermocline with  
 304 ventilation timescales of years to decades and the deep ocean with time-scales of a century and  
 305 longer (Siegel et al., 2021).

306 The relationship between the biological pump and the inorganic CO<sub>2</sub> system was examined  
 307 by partitioning the seasonal variability in surface seawater pCO<sub>2</sub> into thermal and non-thermal  
 308 components following Takahashi et al. (2002). We refer readers interested in a thorough analysis  
 309 of RECCAP2 CO<sub>2</sub> system seasonality to Rodgers et al. (2023). The temperature effect on pCO<sub>2</sub>  
 310 was calculated for isochemical seawater using the approximation  $\frac{\partial(\ln(pCO_2))}{\partial T} = 0.0423 ({}^\circ C^{-1})$  from  
 311 the experimental value from Takahashi et al. (1993). The seasonal cycle in monthly surface  
 312 temperature anomalies relative to the annual mean surface temperature generated a corresponding  
 313 seasonal variation in the thermal (temperature-dependent) pCO<sub>2</sub> component about the pCO<sub>2</sub> annual  
 314 mean:

$$315 \quad pCO_2^{thermal} = (pCO_2)_{mean} \times \exp[0.0423(T_{monthly} - T_{mean})] \quad (3)$$

316

317 Ocean hindcast simulations typically capture quite well the seasonal cycle of sea surface  
318 temperature because the ocean models are forced by atmospheric reanalysis products and heat flux  
319 boundary conditions that effectively contain information on the observed temperature record  
320 (Doney et al., 2007); the same model-data agreement transfers to the thermal pCO<sub>2</sub> seasonal  
321 component. The non-thermal pCO<sub>2</sub> component was computed by subtracting the thermal  
322 component from the monthly pCO<sub>2</sub> values, and the seasonal amplitude  $\Delta pCO_2, \text{non-thermal}$  was  
323 calculated as the seasonal peak-to-trough difference. The non-thermal pCO<sub>2</sub> component reflects  
324 seasonal variations in DIC and alkalinity from biological organic and inorganic carbon production  
325 and remineralization, air-sea CO<sub>2</sub> gas exchange, and physical transport and mixing. Note that the  
326 seasonal phasing of the non-thermal pCO<sub>2</sub> component can be distinct from the phasing of the total  
327 pCO<sub>2</sub> cycle. This is especially the case in the low latitudes, where the thermal component  
328 dominates the seasonal cycle (Takahashi et al., 1993; Landschützer et al., 2018; Rodgers et al.,  
329 2023).

330 We also computed apparent oxygen utilization (AOU) using modeled dissolved oxygen,  
331 salinity, and potential temperature fields. Modeled average AOU at 100 m (AOU<sub>100</sub>) and 1000 m  
332 depth (AOU<sub>1000</sub>) were found using nearest depth bins in model products (bins centered within 50  
333 m of depths). The simulated AOU fields are compared against the World Ocean Atlas (WOA) data  
334 product (Garcia et al., 2019).

335

### 336 3 Results

#### 337 3.1 Simulated ocean biological carbon pump metrics

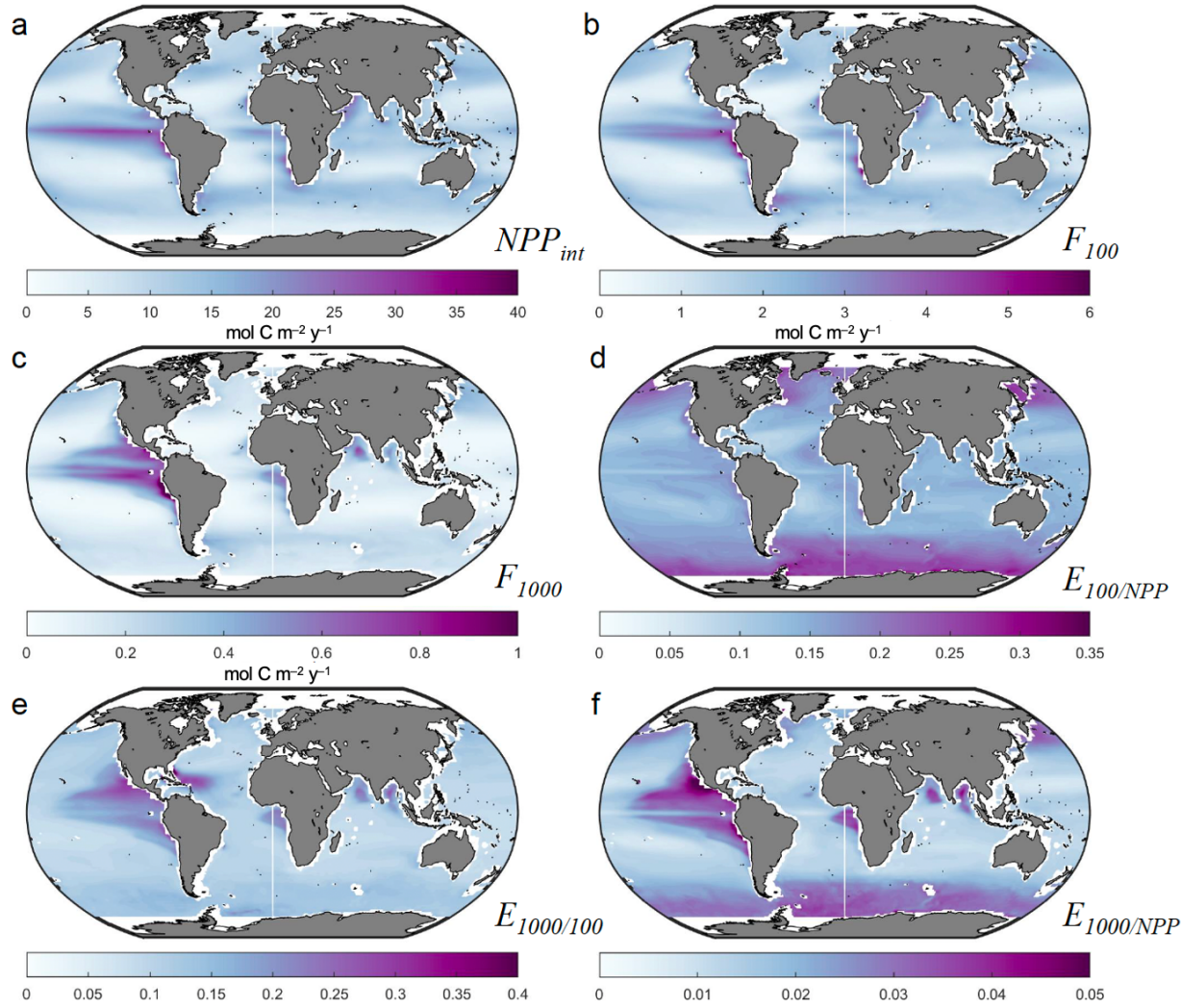
338 Global spatial fields of present-day biological carbon pump variables are displayed in  
339 Figure 1 for the RECCAP2 model ensemble mean with the corresponding ensemble standard  
340 deviation in Figure S1. Biome-scale ensemble-mean averages and within-ensemble standard  
341 deviation values for the biological pump metrics are reported in Table 3 using the standard  
342 RECCAP2 biomes by ocean basin (Figure S2; Fay and McKinley, 2014).

343 The magnitude and spatial patterns of simulated annual mean NPP and export flux from  
344 sinking POC ( $F_{100}$ ) (Figure 1a and 1b) are broadly similar to observational estimates (Section 3.2).  
345 Simulated upper-ocean biological pump variables showed large geographic variations with annual-  
346 mean NPP ranging on biome scales (Table 3) from 8 to 21 mol C m<sup>-2</sup> yr<sup>-1</sup> and  $F_{100}$  ranging from  
347 1.1 to 2.9 mol C m<sup>-2</sup> yr<sup>-1</sup>. The simulated spatial patterns reflect euphotic zone temperature, nutrient  
348 supply, and grazing and loss rates that govern phytoplankton standing stock in the models  
349 (Falkowski et al., 1998; Laufkötter et al., 2015; Laufkötter et al., 2016). The imprint of nutrient  
350 supply was particularly evident in the elevated NPP and export fluxes found in equatorial and  
351 coastal upwelling regions, western boundary currents, and mid-latitude bands of deep seasonal  
352 mixing. Within-ensemble standard deviations ( $\sigma$ ) of NPP and  $F_{100}$  were elevated in the equatorial  
353 band, and high  $\sigma_{NPP}$  values were found also in the Southern Ocean indicating substantial model  
354 disagreement within the ensemble (Figure S1a and S1b). Biome-scale  $\sigma_{NPP}$  values ranged from 2.1  
355 to 6.6 mol C m<sup>-2</sup> yr<sup>-1</sup> (from as low as 0.22 to nearly 0.72 times the ensemble mean in parts of the  
356 Southern Ocean); biome-scale  $\sigma_{F100}$  values varied from 0.4 to >1.0 mol C m<sup>-2</sup> yr<sup>-1</sup> with the largest  
357 absolute and fractional within-ensemble variation of >0.7 times the ensemble mean occurring in  
358 the western equatorial Pacific.

359 The local POC sinking flux at the base of the mesopelagic ( $F_{1000}$ ) ranged at biome scale  
360 from 0.09 to 0.54 mol C m<sup>-2</sup> yr<sup>-1</sup> with broadly similar patterns to  $F_{100}$ , though with some notable  
361 exceptions such as the high  $F_{1000}$  values in tropical low-oxygen zones in the eastern tropical Pacific  
362 and Arabian Sea (Figure 1c). Note the roughly half to full order of magnitude decline in scale in  
363 Figure 1 from NPP to  $F_{100}$  and then  $F_{100}$  to  $F_{1000}$ . This indicates first that the bulk of simulated  
364 NPP is recycled within the euphotic zone above 100 m, rather than exported as sinking POC flux,  
365 and second that most of the sinking POC flux at 100 m is remineralized in the mesopelagic, rather  
366 than reaching the deep ocean below 1000 m. As for NPP and  $F_{100}$ , some correspondence was found  
367 for the spatial patterns of ensemble-mean  $F_{1000}$  and  $\sigma_{F1000}$ . Highest biome-scale  $\sigma_{F1000}$  values of  
368 0.26 to 0.29 mol C m<sup>-2</sup> yr<sup>-1</sup> occurred in the North Pacific and eastern equatorial Pacific, equal to  
369 0.85 and 0.53 times the ensemble-mean  $F_{1000}$  for those biomes; biome-scale  $\sigma_{F1000}$  values of ~0.5  
370 or more of the ensemble-mean were common, with even higher fractional values locally such as in  
371 the eastern subtropical North Pacific (Figure S1c; Table 3).

372 The fraction of NPP exported across 100 m, or export ratio ( $E_{100/NPP}$ , Figure 1d; Table 3)  
373 varies at the biome scale in the ensemble mean from 0.12 to 0.21 with elevated values in high  
374 latitudes. The spatial patterns for within-ensemble  $E_{100/NPP}$  standard deviation (Figure S1d) mirror  
375 that of the mean  $E_{100/NPP}$  with biome-mean standard deviations of 0.035 to 0.050 in most biomes  
376 and up to 0.091 in the sub-polar Southern Ocean biome where there is more within-ensemble  
377 model spread.

378  
379  
380

381  
382

383 **Figure 1.** Multi-model ensemble averages of biological pump parameters from 1985 to 2018  
 384 across all RECCAP2 model simulations (simulation A). Maps of annual mean (a) integrated net  
 385 primary productivity  $NPP$ , (b) particulate organic carbon export fluxes at 100 m  $F_{100}$ , and (c) 1000  
 386 m depth  $F_{1000}$ , all in  $\text{mol C m}^{-2} \text{ yr}^{-1}$ . Ensemble mean (d) surface export efficiency ratio  $E_{100/NPP} =$   
 387  $F_{100}/NPP$  (Eq. 1), (e) mesopelagic transfer efficiency at 1000 m  $E_{1000/100} = F_{1000}/F_{100}$  (Eq. 2), and  
 388 (f) export efficiency to the deep ocean  $E_{1000/NPP} = F_{1000}/NPP$ , all ratios unitless.

389

390 The ensemble-mean transfer efficiency through the mesopelagic,  $E_{1000/100}$  (Figure 1e; Table  
 391 3), exhibited background levels at the biome-scale of 0.09-0.14 for most biomes and ranging as  
 392 high as 0.18 in the eastern equatorial Pacific biome; sub-biome regional values up to 0.3 occurred  
 393 in the eastern tropical Pacific, western and eastern tropical Atlantic, and Arabian Sea and Bay of  
 394 Bengal. Some ocean biogeochemical models reduce sub-surface POC remineralization in low-  
 395 oxygen zones, using a parameterization based on local oxygen concentrations, driving higher  
 396  $E_{1000/100}$  values in low-oxygen regions such as the eastern tropical Pacific, Arabian Sea and Bay of  
 397 Bengal. Furthermore, POC flux mineral ballasting from Saharan dust deposition, prescribed as an

398 external forcing, is likely an important contributor in at least some models (CCSM-WHOI and  
 399 CESM-ETHZ) to high  $E_{1000/100}$  in the western tropical Atlantic (Lima et al., 2014). The ensemble  
 400  $E_{1000/100}$  standard deviation (Figure S1e) generally followed  $E_{1000/100}$  with particularly large  
 401  $\sigma E_{1000/100}$  values up to 0.3 in the western tropical Atlantic reflecting differences across models in  
 402 the parameterization of POC sinking in the presence of desert dust. The metric  $E_{1000/NPP}$  (Figure  
 403 1f), combining surface export and mesopelagic transfer efficiencies, had generally similar spatial  
 404 patterns to  $E_{1000/100}$  but with lower values, reflecting the small fraction of NPP that sinks below  
 405 1000 m and is sequestered in the deep ocean. More than a factor of two variation was found for  
 406 metric  $E_{1000/NPP}$  across biomes (0.012 to 0.027) with large within-ensemble variation for some  
 407 biomes where the standard deviation approached or exceeded the ensemble mean.

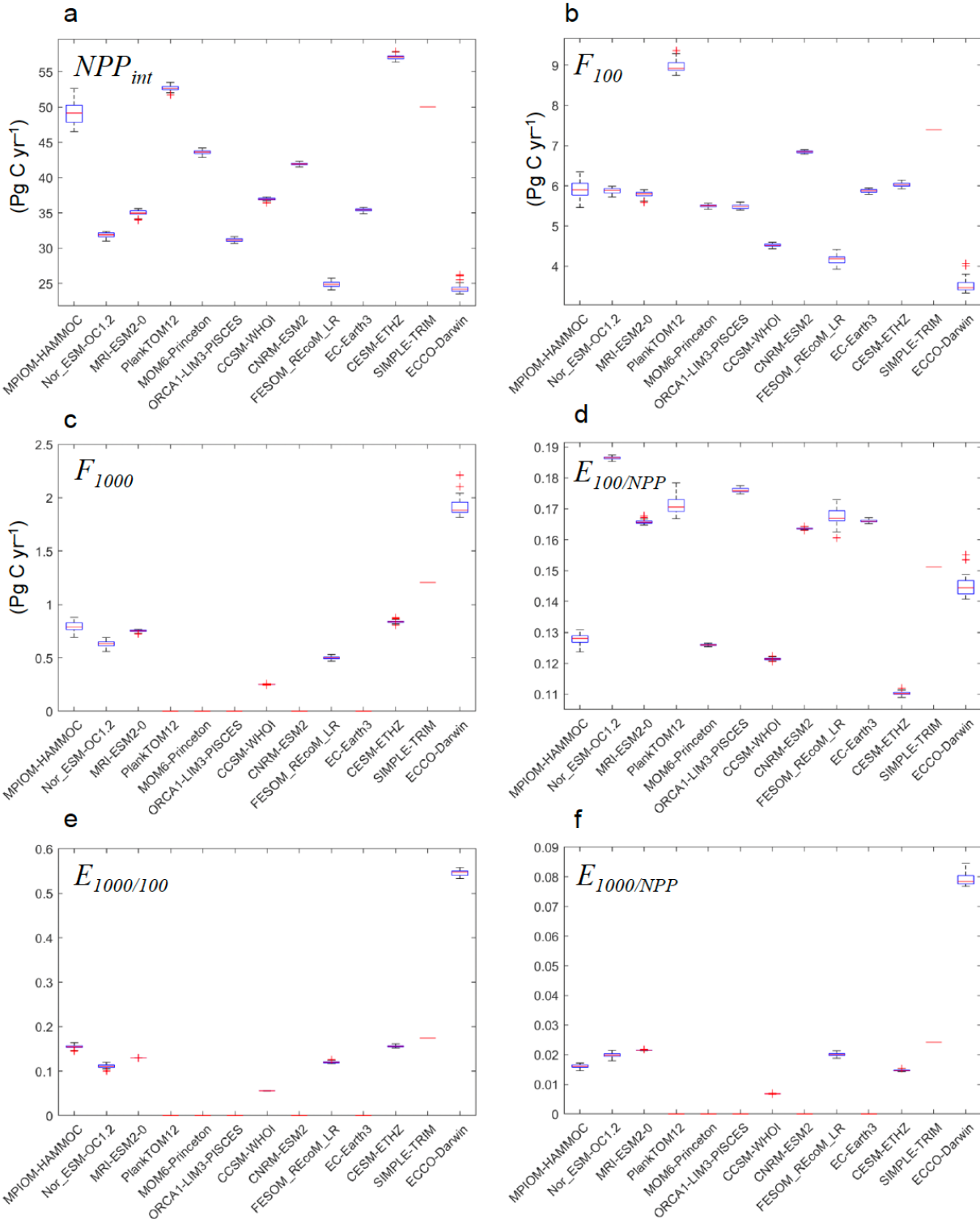
408  
 409 **Table 3.** Model ensemble averages and standard deviations of biological pump parameters by  
 410 RECCAP2 regional biomes (Figure S2) (see also Figure 1) grouped as Sub-Polar Seasonally  
 411 Stratified (SPSS), Sub-Tropical Seasonally Stratified (STSS), Sub-Tropical Permanently Stratified  
 412 (STPS), Equatorial (EQU), and Mediterranean (MED). Table includes annual means and standard  
 413 deviations for vertically integrated net primary productivity  $NPP$ , particulate organic carbon export  
 414 fluxes at 100 m  $F_{100}$ , and 1000 m depth  $F_{1000}$ , all in mol C m<sup>-2</sup> yr<sup>-1</sup>, and average surface export  
 415 efficiency ratio  $E_{100/NPP} = F_{100}/NPP$ , mesopelagic transfer efficiency at 1000 m  $E_{1000/100} =$   
 416  $F_{1000}/F_{100}$ , and export efficiency to the deep ocean  $E_{1000/NPP} = F_{1000}/NPP$ , all ratios unitless.  
 417 Ensemble were not computed for the small, high-latitude polar ice biomes due to noisy and/or  
 418 missing data across the full ensemble.  
 419

	$NPP$	$F_{100}$	$F_{1000}$	$E_{100/NPP}$	$E_{1000/100}$	$E_{1000/NPP}$
<b>SPSS</b>						
N. PACIFIC	11.89±4.81	2.21±0.65	0.307±0.263	0.206±0.076	0.124±0.071	0.018±0.012
N. ATLANTIC	9.30±3.00	1.77±0.65	0.177±0.156	0.211±0.075	0.116±0.060	0.014±0.009
SOUTHERN	9.24±6.64	1.59±0.60	0.197±0.119	0.213±0.091	0.132±0.071	0.023±0.025
<b>STSS</b>						
N. PACIFIC	13.53±3.68	2.04±0.70	0.206±0.117	0.161±0.040	0.114±0.049	0.014±0.006
N. ATLANTIC	12.98±3.28	1.93±0.54	0.165±0.069	0.162±0.049	0.099±0.036	0.014±0.006
SOUTHERN	13.91±5.02	2.12±0.39	0.222±0.087	0.173±0.053	0.109±0.040	0.016±0.009
<b>STPS</b>						
N. PACIFIC	8.92±3.24	1.18±0.61	0.177±0.102	0.131±0.047	0.132±0.049	0.017±0.010
N. ATLANTIC	7.70±2.37	0.97±0.44	0.092±0.057	0.121±0.051	0.140±0.097	0.013±0.008
S. ATLANTIC	9.78±2.16	1.33±0.41	0.138±0.090	0.130±0.043	0.104±0.040	0.012±0.008
INDIAN	16.67±4.75	2.25±0.85	0.284±0.162	0.143±0.035	0.130±0.063	0.016±0.008
<b>EQU</b>						
W. PACIFIC	11.03±5.31	1.44±1.06	0.10±0.078	0.134±0.059	0.089±0.050	0.013±0.011
E. PACIFIC	21.16±5.16	2.91±0.74	0.542±0.288	0.151±0.043	0.178±0.086	0.027±0.015
ATLANTIC	14.33±4.71	1.94±0.65	0.272±0.137	0.145±0.039	0.140±0.043	0.019±0.010
<b>MED</b>	9.21±3.71	1.34±0.79	0.074±0.062	0.141±0.060	0.119±0.107	0.011±0.008

420

421 To illustrate differences among the models making up the RECCAP2 multi-model  
422 ensemble, global integrals of the annual average biological pump metrics are displayed in Figure  
423 2. A box-whisker plot is shown for each model ensemble member quantifying the interannual  
424 variability for each model for the RECCAP2 reporting period (1985-2018). Note that some  
425 RECCAP2 models did not report  $F_{1000}$ , resulting in missing estimates for  $E_{1000/100}$  and  $E_{1000/NPP}$ .  
426 Some models stood out as either anomalously low (e.g. FESOM-REcom-LR for NPP) or high  
427 (e.g. NEMO-PlankTOM12.1 for  $F_{100}$ ) relative to the other RECCAP2 ensemble members, though  
428 inter-model agreement alone was not necessarily a robust indicator of model skill (see Section  
429 3.2). For global  $E_{100/NPP}$ , the models were roughly split into low (0.10-0.12) and high (0.16-0.19)  
430 groups (Figure 2d). Global  $F_{1000}$ ,  $E_{1000/100}$ , and  $E_{1000/NPP}$  varied widely for the smaller number of  
431 available models (Figure 2c, 2e, and 2f).

432

433  
434

435 **Figure 2.** Boxplots showing median values (1985-2018), interannual interquartile ranges, and  
 436 outliers of biological pump metrics across model products in RECCAP2 ensemble (simulation A).  
 437 Globally integrated, annual (a) net primary productivity  $NPP$ , (b) particulate organic carbon export  
 438 fluxes at 100 m  $F_{100}$ , and (c) 1000 m depth  $F_{1000}$ , all in  $\text{Pg C yr}^{-1}$ . Global and annual average (d)

439 surface export efficiency ratio  $E_{100/NPP} = F_{100}/NPP$  (Eq. 1), (e) mesopelagic transfer efficiency at  
 440 1000 m  $E_{1000/100} = F_{1000}/F_{100}$  (Eq. 2), and (f) export efficiency to the deep ocean  $E_{1000/NPP} =$   
 441  $F_{1000}/NPP$ , all ratios unitless. CCSM-WHOI output does not include the year 2018 and SIMPLE-  
 442 TRIM does not simulate interannual variability. Efficiency ratios are not given in panels d, e, and  
 443 f for models lacking the corresponding  $NPP$ ,  $F_{100}$ , or  $F_{1000}$ .  
 444

### 445 3.2 Model-observational comparisons

446 The global ocean biological carbon pump metrics from the RECCAP2 multi-model  
 447 ensemble were compared against corresponding literature values in Table 4 and Figure 3. The  
 448 RECCAP2 multi-model ensemble global-integrated NPP value,  $42.7 \pm 10.9 \text{ Pg C yr}^{-1}$ , was at the  
 449 lower end of literature estimates (43.5-68 Pg C yr $^{-1}$ ), and the inter-quartiles have limited overlap.  
 450 Similarly, global-integrated  $F_{100}$  from the multi-model ensemble of  $6.41 \pm 1.52 \text{ Pg C yr}^{-1}$  was  
 451 lower than the mean of the literature estimates of sinking POC flux ( $\sim 8 \text{ Pg C yr}^{-1}$ , range 4-13 Pg  
 452 C yr $^{-1}$ ), though the inter-quartiles overlapped substantially because of the large range in  
 453 observation-based estimates. The global-integrated model ensemble  $F_{1000}$  value of  $0.95 \pm 0.64 \text{ Pg}$   
 454 C yr $^{-1}$  fell between one low estimate of  $0.66 \text{ Pg C yr}^{-1}$  (Henson et al., 2012) and two other literature  
 455 estimates of  $1.1 \text{ Pg C yr}^{-1}$ . The global multi-model ensemble-mean export and transfer efficiencies,  
 456  $E_{100/NPP}$  ( $0.15 \pm 0.03$ ) and  $E_{1000/100}$  ( $0.12 \pm 0.04$ ), were within the range of literature values after  
 457 removing the high  $E_{100}$  values (0.3 and 0.38) from Laws et al. (2000) and acknowledging one low  
 458 outlier model for global  $E_{1000/100}$  ( $\sim 0.05$ ; CCSM-WHOI; Figure 2e).

459 The wide range of literature estimates reflects differences in measurement methodologies,  
 460 biases, and uncertainties in the datasets used for biological carbon pump metric estimation, as well  
 461 as uncertainties introduced by data sampling biases, aggregation, time/space interpolation and  
 462 modeling approaches. At global scales, in situ observational sampling for some variables remains  
 463 sparse and regionally patchy, and satellites, empirical relationships, and numerical models have  
 464 been used to gap-fill for global-scale product generation. For example, even with field data sets  
 465 available for ocean NPP based on  $^{14}\text{C}$  uptake incubation studies, satellite remote sensing has been  
 466 required to create uniform global NPP products, which have been calibrated/validated against  $^{14}\text{C}$   
 467 NPP field data. A variety of in situ methods have been used to estimate surface ocean export flux  
 468 estimates ( $\sim F_{100}$ ) – drifting sediment traps,  $^{234}\text{Th}$  deficit, etc. To derive global-scale fields of  
 469 export, extrapolation from the limited in situ data is required which generates uncertainties in the  
 470 derived estimates due to the underlying data sparsity (Henson et al., 2024). Typically, satellite data  
 471 is used to build an empirical relationship between flux and readily derived variables, such as sea  
 472 surface temperature or chlorophyll concentration. Other approaches include merging satellite data  
 473 with food-web models (e.g., Siegel et al., 2014). Observation-based global  $F_{1000}$  estimates have  
 474 been generated from sediment trap data (Mouw et al., 2016a), and estimates of both global  $F_{100}$   
 475 and  $F_{1000}$  have been derived from inverse and data-assimilation ocean models (e.g., Devries and  
 476 Weber, 2017; Nowicki et al., 2022).  
 477

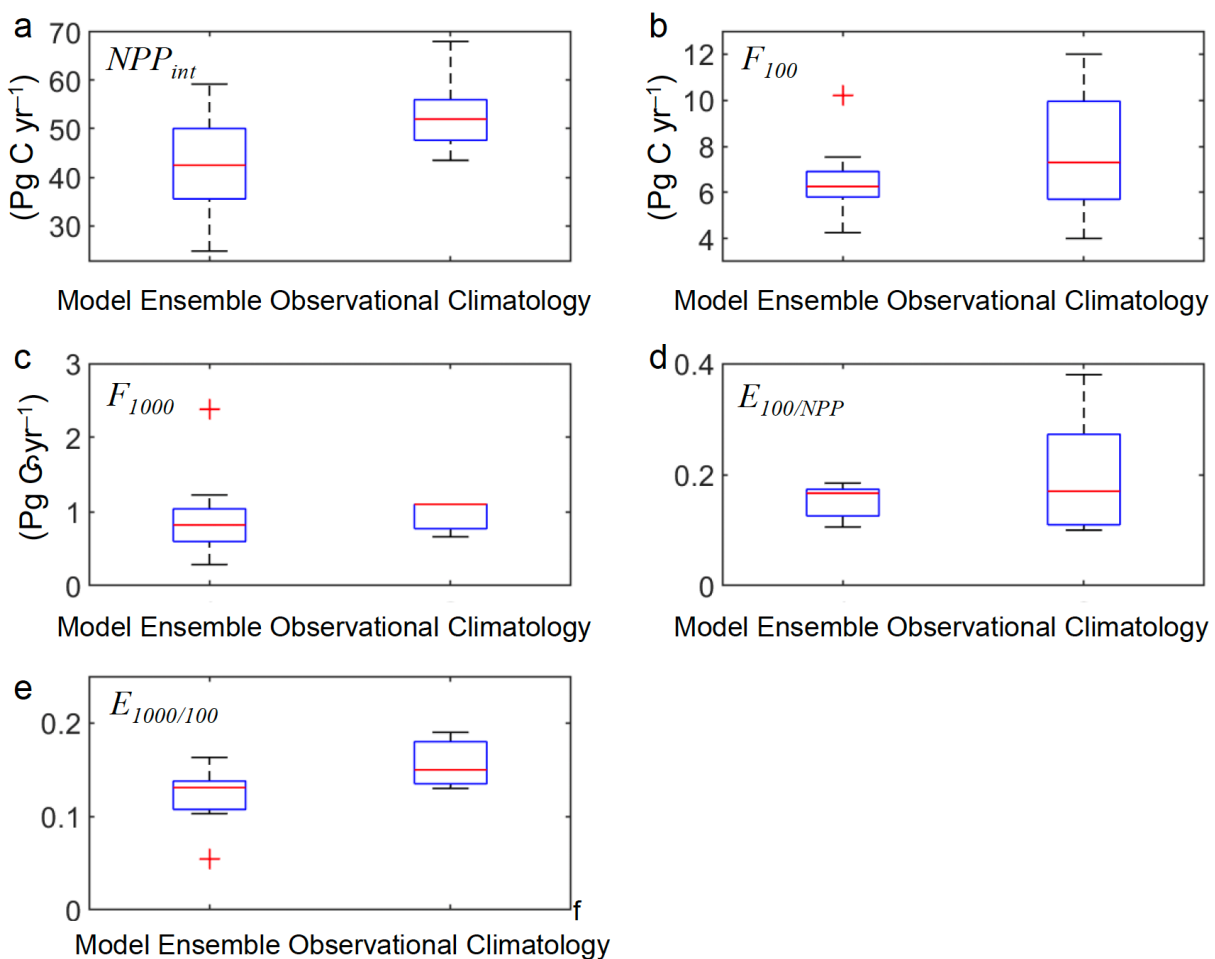
478 **Table 4.** Comparison of literature-based, global observation-based ocean biological carbon pump  
 479 metrics with the RECCAP2 model ensemble means and within-ensemble standard deviations.  
 480 Note that SIMPLE-TRIM data assimilation results from Devries and Weber (2017) are also  
 481 included in the RECCAP-2 model ensemble.

482

Net Primary Production $NPP$ (Pg C $yr^{-1}$ )	References
43.5	VGPM Behrenfeld & Falkowski (1997)
52	CAFÉ Silsbe et al. 2016
68	Carr (2002) & Carr et al. 2006
49	Marra et al. (2003)
52	CbPM2 Behrenfeld et al. 2005
<b>42.7 ± 10.9</b>	<b>RECCAP2 model ensemble mean and STD</b>
POC Export $\sim F_{100}$ (Pg C $yr^{-1}$ )	
4	Henson et al. (2012)
9.6	Dunne et al. (2007)
11.1-12.9	Laws et al. (2000)
5.7	Siegel et al. (2014)
9.6	Schlitzer (2000); inversion
9-13	Laws et al. (2011)
8.8 (7.3 at 100 m)	DeVries & Weber (2017); data assimilating
7.3 (6.4 at 100 m)	Nowicki et al. (2022)
<b>6.41 ± 1.52</b>	<b>RECCAP2 model ensemble-mean and STD</b>
POC Flux 1000 m $F_{1000}$ (Pg C $yr^{-1}$ )	
0.66	Henson et al. (2012)
1.1	DeVries & Weber (2017)
1.1	Nowicki et al. (2022)
<b>0.95 ± 0.64</b>	<b>RECCAP2 model ensemble mean and STD</b>
Export Ratio $\sim E_{100/NPP}$	
0.1	Henson et al. (2012)
0.19	Dunne et al. (2007)
0.3	Laws et al. (2000); food web
0.38	Laws et al. (2000); empirical
0.103	Siegel et al. (2014)
0.17	DeVries & Weber (2017)

0.13 (for POC only)	Nowicki et al. (2022)
0.18 (for POC + DOC + vertical migration)	
<b>0.154 ± 0.026</b>	<b>RECCAP2 model ensemble mean and STD</b>
<b>Transfer Flux Efficiency <math>E_{1000/100}</math></b>	
0.19	Henson et al. (2012)
0.13	DeVries & Weber (2017)
0.15	Nowicki et al. (2022)
<b>0.121 ± 0.035</b>	<b>RECCAP2 model ensemble mean</b>

483



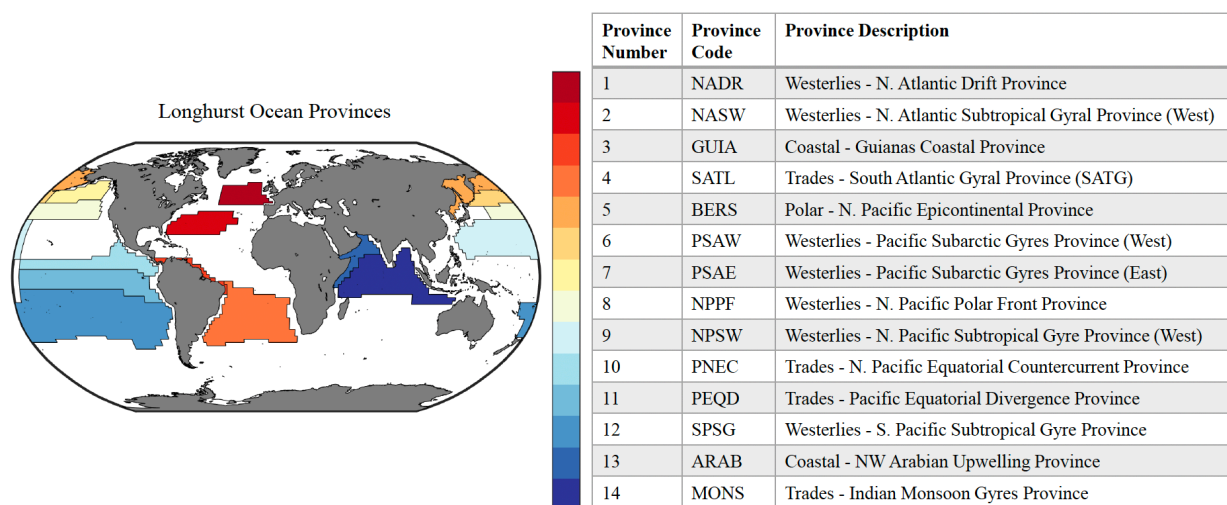
484

485

486 **Figure 3.** Box-whisker plots showing median values and interquartile ranges of biological pump  
 487 parameters from 1985-2018 averaged across model products in RECCAP2 ensemble (simulation  
 488 A). Global integrated, annual (a) net primary productivity  $NPP$ , (b) particulate organic carbon  
 489 export fluxes at 100 m  $F_{100}$ , and (c) 1000 m depth  $F_{1000}$ , all in Pg C yr<sup>-1</sup> (note that the median line  
 490 for  $F_{1000}$  is also the upper interquartile because two of the three observational estimates match).

491 Global and annual average surface export efficiency ratio (d)  $E_{100/NPP} = F_{100}/NPP$  (Eq. 1), and (e)  
492 mesopelagic transfer efficiency at 1000 m  $E_{1000/100} = F_{1000}/F_{100}$  (Eq. 2), all ratios unitless.

493

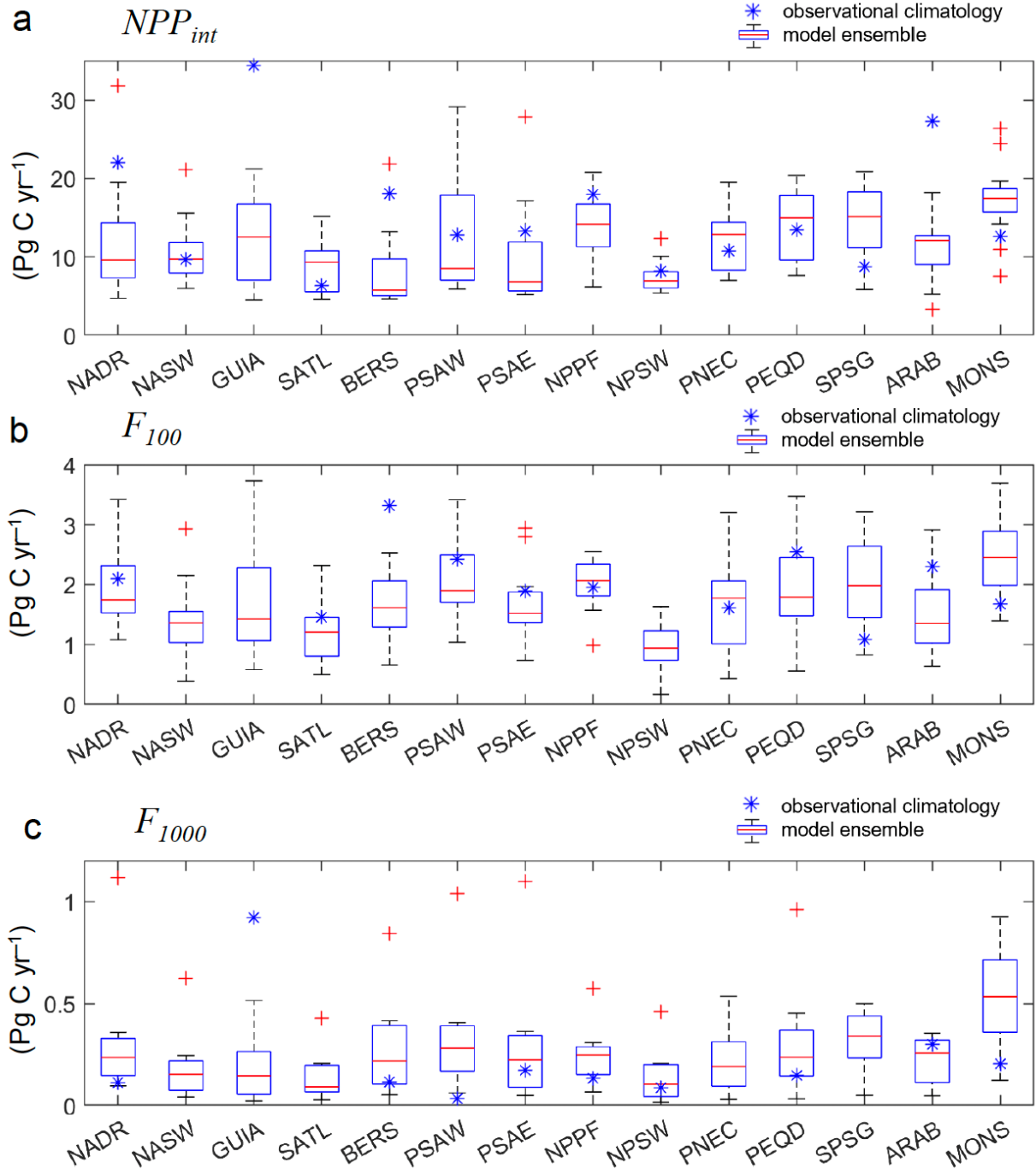


494

495

496 **Figure 4.** Map of Longhurst provinces (Reygondeau et al., 2013) used in analysis of biological  
 497 pump field observations and model results (Mouw et al., 2016a).

498

499  
500

501 **Figure 5.** Box-whisker plot of RECCAP2 multi-model ensemble medians, interquartile ranges,  
 502 and outliers for annual-mean (a) vertical integrated primary production ( $NPP_{int}$ ), (b) sinking POC  
 503 fluxes at 100m ( $F_{100}$ ), and (c) sinking POC flux at 1000m ( $F_{1000}$ ), all in  $\text{Pg C yr}^{-1}$ , pooled into  
 504 biogeochemical Longhurst ocean provinces (Figure 4) and compared to the observational  
 505 climatology for the same provinces constructed by Mouw et al. (2016b). Robust uncertainty  
 506 estimates are not available for the observational climatology which averages available data that is

507 often spatially sparse and/or concentrated in brief time intervals. Note that only provinces with  
 508 sufficient observational data are plotted (see Figure 4).

509

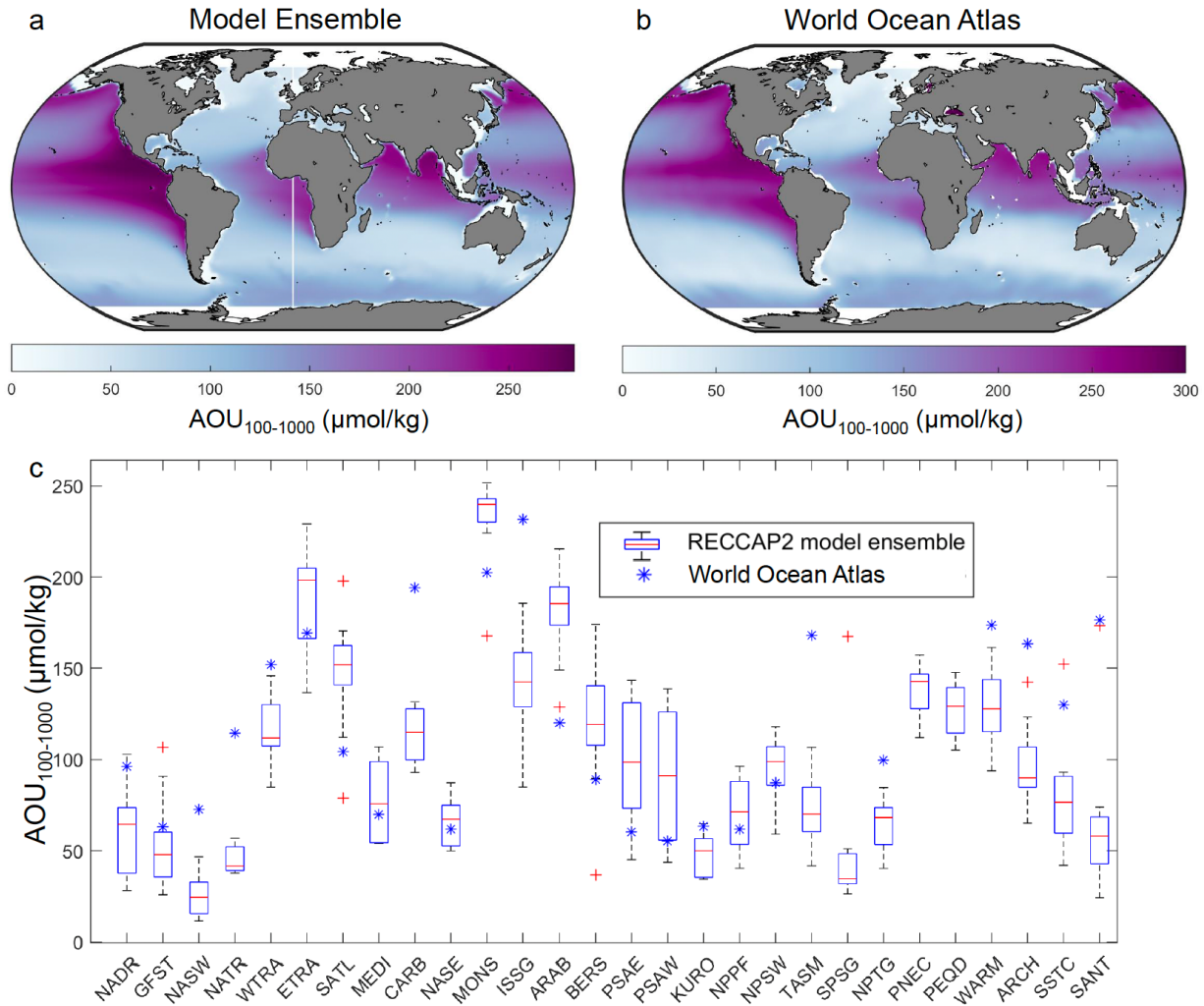
510 The biological carbon pump model comparison to observation-based estimates was  
 511 extended in Figure 5 to a regional level using the observational data of Mouw et al. (2016a) as  
 512 aggregated by Mouw et al. (2016b) into monthly climatological values for Longhurst  
 513 biogeographic provinces (Figure 4). The Mouw et al. (2016a) date set aggregates the limited  
 514 available field data that is often spatially sparse and locally high frequency with considerable  
 515 mesoscale variability, some of which may be aliased into monthly and province scale averages.  
 516 Therefore, robust uncertainty estimates are not available for the Mouw et al. (2016b) observational  
 517 climatology. The variations across the RECCAP2 models are displayed as box-whisker plots. The  
 518 members of the model ensemble exhibited a wide range of NPP,  $F_{100}$  and  $F_{1000}$  values for many  
 519 provinces, but still the observational climatology falls within the multi-model ensemble inter-  
 520 quartiles for only about half of the provinces. The substantial model-observational offsets indicate  
 521 recurring regional differences consistent across multiple models in the RECCAP2 ensemble; these  
 522 disagreements could be targets for future ocean biogeochemical model development and analyses  
 523 of observational sampling biases. The model ensemble members also exhibited extreme model-  
 524 data differences in some provinces where the observational climatology value falls outside the  
 525 simulated range including model outliers. The RECCAP2 models consistently underestimated the  
 526 strength of biological carbon pump metrics, relative to the observational climatology, in polar and  
 527 sub-polar provinces in the North Pacific (N. Pacific epicontinental sea, BERS, low NPP and  $F_{100}$ )  
 528 and North Atlantic (N. Atlantic Drift, NADR, low NPP); and in equatorial provinces in the Indian  
 529 (Northwest Arabian Sea upwelling, ARAB, low NPP), Pacific (Trades-Pacific Equatorial  
 530 Divergence, PEQD, low  $F_{100}$ ) and Atlantic (Guianas coast, GUIA, low  $F_{1000}$ ; note, the observed  
 531 high Guianas coast value reflects a small, productive region that may not be well represented in  
 532 global-scale models). In other provinces, the model ensemble overestimated the biological pump  
 533 in the South Pacific gyre (SPSG, high NPP and  $F_{100}$ ), Indian monsoon gyre (MONS, high NPP  
 534 and  $F_{100}$ ), and Western Pacific subarctic gyres (PSAW, high  $F_{1000}$ ).

535

### 536 **3.3 Biological pump imprint on ocean CO<sub>2</sub> system and biogeochemistry**

537 The ocean biological carbon pump imprints on surface and sub-surface biogeochemistry  
 538 (see Introduction), and these effects are simulated in the RECCAP2 models. A strong positive  
 539 mesopelagic AOU signal is generated by cumulative biological O<sub>2</sub> consumption along the  
 540 ventilation paths of subsurface waters (Najjar et al., 2007). AOU fields thus integrate non-local,  
 541 large-scale biogeochemical dynamics and physical resupply of O<sub>2</sub> from the surface. A key  
 542 contributor to AOU is the remineralization of sinking POC flux in the mesopelagic, quantified by  
 543 the large decline between  $F_{100}$  and  $F_{1000}$  and low transfer efficiency through the mesopelagic  
 544  $E_{1000/100}$  (Figures 1–3; Tables 3 and 4). For the RECCAP2 model ensemble, there was generally  
 545 good model-data agreement in the geographic pattern in AOU averaged over the mesopelagic  
 546 (100–1000 m) (Figure 6). The model ensemble captured the regional AOU variation of <50 to  
 547 >250  $\mu\text{mol kg}^{-1}$ , though substantial disagreement arose on the scale of Longhurst provinces where  
 548 the model-ensemble interquartile spans the observational data for only a handful of provinces  
 549 (Figure 6c). The RECCAP2 models did not exhibit a strong inter-model relationship between  
 550 global mean AOU and  $F_{100}$  (not shown). The weak relationship between AOU and  $F_{100}$  across  
 551 models likely highlights the influence on AOU of substantial variations in the strength of model

552 thermocline ventilation rates that could also influence simulated anthropogenic CO<sub>2</sub> uptake (e.g.,  
 553 Dutay et al., 2002; Matsumoto et al., 2004). Model deep-ocean AOU was not evaluated because  
 554 model spin-up time scales were too short for the simulations to reach steady-state (Séférian et al.,  
 555 2019), an issue that also would affect simulated deep-ocean preindustrial DIC (Mikaloff Fletcher  
 556 et al., 2007). Some imprint of the observational fields used for model initial conditions could also  
 557 be retained in the simulated mesopelagic AOU depending on the model spin-up procedure.  
 558

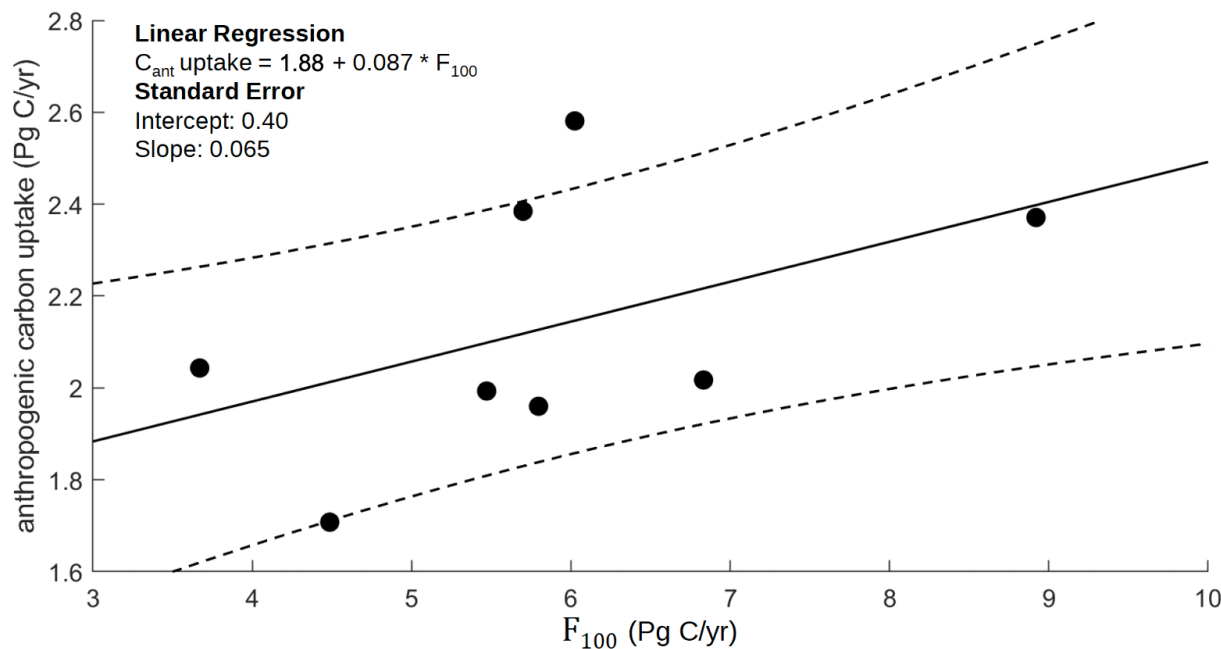


559  
 560  
 561 **Figure 6.** Analysis of apparent oxygen utilization (AOU,  $\mu\text{mol kg}^{-1}$ ) vertically averaged over the  
 562 mesopelagic zone (100-1000 m): (a) spatial map of RECCAP2 multi-model ensemble average,  
 563 and (b) spatial map from WOA observational data set, and (c) box-whisker plot of RECCAP2  
 564 multi-model ensemble medians, interquartile ranges, and outliers pooled into biogeochemical  
 565 Longhurst ocean provinces (Figure 4).  
 566

567 The simulated regional patterns and global integrated surface POC export  $F_{100}$  (Figures 1  
 568 –3; Tables 3 and 4) must be balanced on appropriate time and space scales by new production and  
 569 external nutrient supply, largely from physical upwelling and mixing for most ocean regions

570 (Ducklow and Doney, 2013). As an indicator of physical controls on export associated with  
 571 nutrient supply, the individual RECCAP2 model, global-integrated  $F_{100}$  values exhibited a positive  
 572 correlation with global-ocean anthropogenic CO<sub>2</sub> uptake (Figure 7) (DeVries et al., 2023). This is  
 573 consistent with findings from previous model intercomparison exercises where models with  
 574 stronger thermocline ventilation had both larger export flux and anthropogenic CO<sub>2</sub> uptake (Najjar  
 575 et al., 2007). The  $F_{100}$ –anthropogenic CO<sub>2</sub> uptake correlation, therefore, is indirect through a  
 576 common underlying physical mechanism whereby stronger ventilation enhances both the  
 577 downward transport of anthropogenic CO<sub>2</sub> correlation and the upward transport of nutrients and  
 578 thus  $F_{100}$ . The physical-chemical solubility mechanisms controlling ocean anthropogenic CO<sub>2</sub>  
 579 uptake are well documented, and there is no evidence of any significant role for biogeochemical  
 580 processes, though climate-change biogeochemical feedbacks on ocean carbon storage may become  
 581 more important in the future (Canadell et al., 2021).

582



583

584

585 **Figure 7.** Scatter plot of global-integrated ocean anthropogenic CO<sub>2</sub> uptake (mean of 1985–2018)  
 586 (Pg C yr<sup>-1</sup>) versus particulate organic carbon (POC) export flux ( $F_{100}$ , Pg C yr<sup>-1</sup>) for individual  
 587 RECCAP2 models. Anthropogenic CO<sub>2</sub> uptake for the same RECCAP2 models was taken from  
 588 DeVries et al. (2023). A linear regression and confidence intervals for the regression are overlain.  
 589 The  $F_{100}$ –anthropogenic CO<sub>2</sub> uptake correlation was indirect through a common underlying  
 590 physical mechanism whereby stronger ventilation enhances both the downward transport of  
 591 anthropogenic CO<sub>2</sub> correlation and the upward transport of nutrients and thus  $F_{100}$ .

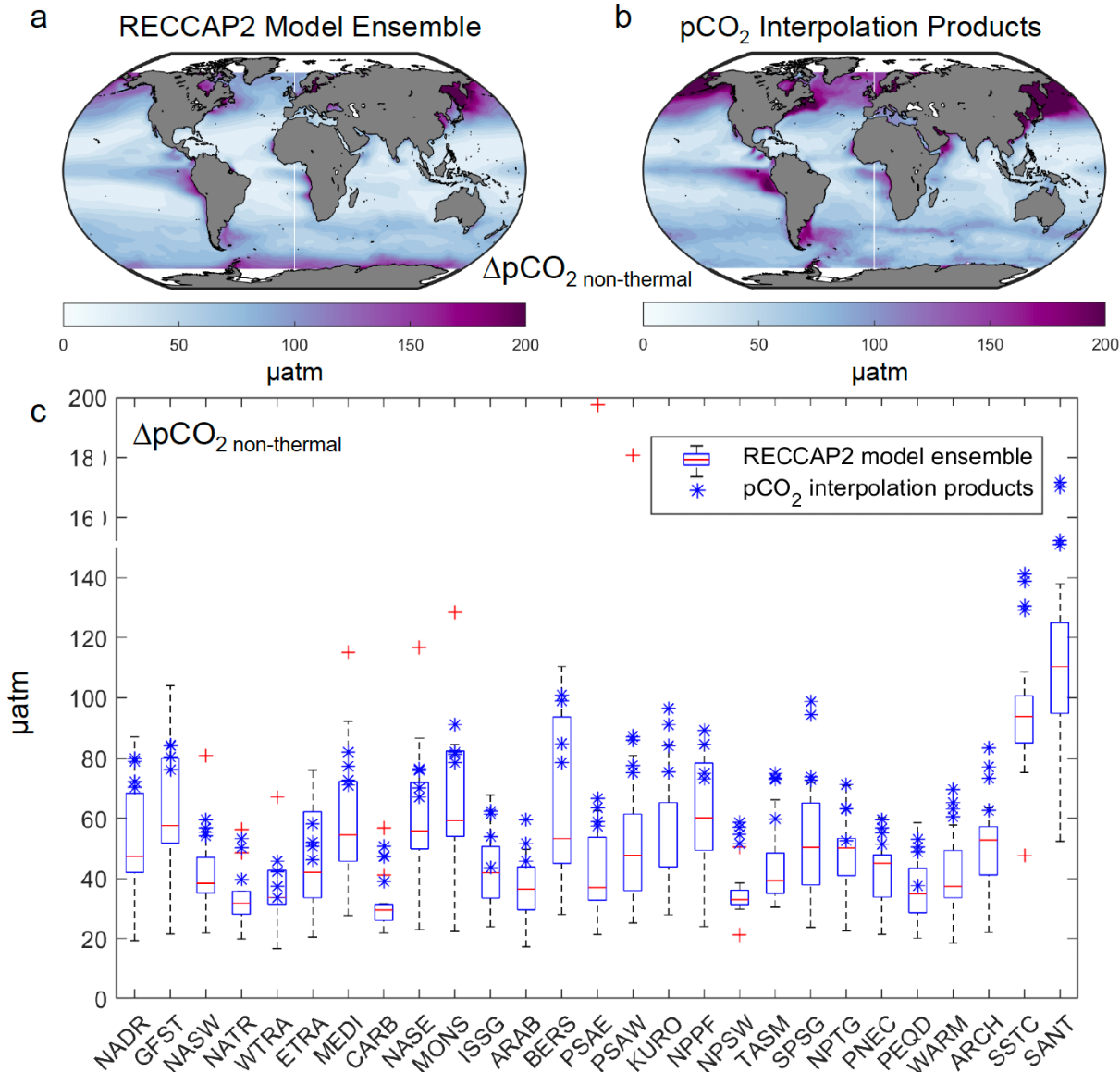
592

593

594 Seasonal variations in upper-ocean biogeochemistry were used as a metric of the physical  
 595 controls associated with seasonal mixing and nutrient supply, which are reflected in simulated  
 596 POC export. By correcting for seasonal thermal variations in pCO<sub>2</sub> (Equation 3), we used model  
 597 monthly pCO<sub>2</sub> fields to quantify the combined effects of seasonal biogeochemical, gas-exchange  
 598 and physical processes through the seasonal amplitude of non-thermal pCO<sub>2</sub>,  $\Delta p\text{CO}_{2,\text{non-thermal}}$   
 (Takahashi et al., 2002). The geographic pattern of  $\Delta p\text{CO}_{2,\text{non-thermal}}$  from the RECCAP2 model

599 ensemble was similar to the pattern from the mean of the  $\text{pCO}_2$  observational products (Figure 8a  
600 and 8b). Both the model ensemble and observational products exhibited regional variations of  
601  $\Delta\text{pCO}_{2,\text{non-thermal}}$  that ranged from 30 to  $>150 \mu\text{atm}$  with elevated values in mid- to high latitudes  
602 as well as equatorial and eastern boundary current upwelling regions. However, the magnitude of  
603  $\Delta\text{pCO}_{2,\text{non-thermal}}$  in the model ensemble was considerably lower in the mid- to high latitude northern  
604 hemisphere, eastern tropical Pacific, and Brazil-Malvinas convergence region, suggesting a  
605 generally weaker modeled seasonal cycling of DIC. The same low bias in the RECCAP2 models  
606 was evident on the scale of Longhurst provinces where the observational products fell at the top  
607 end or well above the model-ensemble interquartile (Figure 8c). In many ocean regions, strong  
608 seasonality in mixed layer depth modulates vertical nutrient supply and annual-mean biological  
609 productivity. The weaker model ensemble  $\Delta\text{pCO}_{2,\text{non-thermal}}$  values (Figure 8), therefore, may be  
610 linked to regional patterns of lower NPP and  $F_{100}$  relative to observations (Figure 5) in the North  
611 Pacific (BERS province), North Atlantic (NADR province), eastern equatorial Pacific (PEQD),  
612 and Brazil-Malvinas convergence (western part of SATL province).

613

614  
615

616 **Figure 8.** Analysis characterizing the combined effects of seasonal biogeochemical, gas-exchange  
617 and physical processes using the seasonal amplitude of non-thermal  $\Delta pCO_{2,non-thermal}$  (a) spatial  
618 map of RECCAP2 multi-model ensemble average, (b) spatial map from pCO<sub>2</sub> observational data  
619 products, and (c) box-whisker plot of RECCAP2 multi-model ensemble medians, interquartile  
620 ranges, and outliers pooled into biogeochemical Longhurst ocean provinces (Figure 4). The  
621 province means from each observational product are plotted in panel (c) as individual points rather  
622 than as box-whiskers because of the limited number of observational products.  
623

#### 624 4 Discussion and Conclusions

625 Our analysis of the ocean biological carbon pump fields from the RECCAP2 multi-model  
626 ensemble revealed generally encouraging agreement with many aspects of observed patterns.

627 Global-integrated NPP and surface export flux ( $F_{100}$ ) from the RECCAP2 models tended to fall at  
 628 the lower end of observational estimates (Figure 3 and Table 4), and geographic patterns in NPP  
 629 were generally consistent with observational data products (Figures 1 and 5). Similar to previous  
 630 model intercomparison studies (Laufkötter et al., 2015; Laufkötter et al., 2016), we found  
 631 substantial within-ensemble variation in global biological carbon pump metrics, including the  
 632 presence of model outliers (Figure 3), indicating that these aspect of biogeochemical models have  
 633 not necessarily converged with time.

634 Regional patterns in the RECCAP2 model-mean ensemble included elevated NPP, surface  
 635 export flux ( $F_{100}$ ) and export efficiency ( $E_{100}$ ) in high-latitudes and coastal and equatorial  
 636 upwelling regions, with lower values in more oligotrophic regions. These results are in line with  
 637 previous studies that found that a substantial proportion of NPP in nutrient-rich regions is driven  
 638 by large phytoplankton such as diatoms and, combined with an active zooplankton population, this  
 639 can generate a significant export flux in the form of both dense aggregates and fecal pellets. High-  
 640 latitude elevated biomass, colder temperatures (Dunne et al., 2005), and strong seasonality also  
 641 have been implicated in observations of higher POC export fluxes in spring and/or summer months  
 642 contributing to the annual mean (Buesseler et al., 2001; Lampitt et al., 2001; Bol et al., 2018;  
 643 Henson et al., 2023). In low nutrient regimes, such as the lower latitude oligotrophic gyres,  
 644 previous studies report export flux to be low (Henson et al., 2012) but relatively constant  
 645 throughout the year with small seasonal increases in fluxes (Karl et al., 2012). Future studies of  
 646 the RECCAP2 ensemble could investigate in more detail the seasonality in NPP,  $F_{100}$ , and  $E_{100}$ ,  
 647 exploring, for example, the seasonal variability in export ratio that can be substantial due in part  
 648 to the time lag between NPP and export flux (Henson et al., 2015; Giering et al., 2017; Laws and  
 649 Maiti, 2019; Henson et al., 2015).

650 The sinking POC flux into the deep ocean ( $F_{1000}$ ) and mesopelagic transfer efficiency  
 651 across the mesopelagic zone ( $E_{1000/100}$ ) in the RECCAP2 multi-model ensemble (Figures 1 and 5)  
 652 exhibited different spatial patterns than found for surface export, similar to findings of previous  
 653 studies (e.g., Henson et al., 2012). Simulated  $F_{1000}$  and  $E_{1000/100}$  were greater in the tropical eastern  
 654 Pacific, eastern Atlantic, and Arabian Sea, and  $E_{1000/100}$  was also elevated in the western tropical  
 655 North Atlantic and, to a lesser extent, Southern Ocean. Previous model studies have also found  
 656 substantial regional variations due to particle size and composition effects (Lima et al., 2014) that  
 657 modify empirical power curves used for modeling POC sinking and remineralization (Martin et  
 658 al., 1987). Model parameterizations tend to increase the effective remineralization length scales  
 659 and thus transfer to depth in regions with high mineral fluxes (e.g., dust,  $\text{CaCO}_3$ , silica) (Armstrong  
 660 et al., 2002) or in tropical oxygen minimum zones (Laufkötter et al., 2017; Dinauer et al., 2022).  
 661 The RECCAP2 regional variations in mesopelagic transfer efficiency, modulated with basin-scale  
 662 variations in physical circulation-driven sequestration time-scale (Siegel et al., 2021), influence  
 663 the effect of the biological pump on ocean carbon storage (Kwon et al., 2009).

664 While we focused primarily on long-term mean NPP and export fluxes, the RECCAP2  
 665 models also exhibited year-to-year variability (Table S1), though typically much lower than  
 666 within-ensemble model differences (Figure 2), and small long-term temporal trends (Table S2).  
 667 No consistent positive or negative trend was observed across the models in simulated NPP and  
 668 sinking POC fluxes at 100m and 1000m, with NPP trends of order  $\pm 0.01 \text{ Pg C yr}^{-1}/\text{year}$  over the  
 669 33 years of the time series (1985-2018). Although these trends could contain a signal from climate  
 670 change, the relatively short duration of the RECCAP2 analysis period resulted in large signal to  
 671 noise due to interannual variability. Previous modeling studies indicate that chlorophyll and NPP

672 time series of 30-40 years length are needed to distinguish climate change trends from natural  
 673 variability (Henson et al., 2010). Hence, the RECCAP2 analysis period may indeed not be long  
 674 enough to separate trends from interannual variability. While a recent study suggests that climate-  
 675 change trends can emerge more rapidly in ocean color remote-sensing reflectance (Cael et al.,  
 676 2023), any actual climate change signal in models may be masked by temporal biases associated  
 677 with incomplete model spin-up and resulting temporal drift (Séférian et al., 2016).

678 Our analysis of the biological carbon pump was relevant in several ways to the primary  
 679 focus of the RECCAP2 ocean project on air-sea CO<sub>2</sub> fluxes and ocean uptake of anthropogenic  
 680 CO<sub>2</sub> (DeVries et al., 2023). Biological net CO<sub>2</sub> uptake and carbon export modulate the background,  
 681 pre-industrial and contemporary spatial and seasonal patterns of surface ocean pCO<sub>2</sub> and sea-air  
 682 CO<sub>2</sub> flux that must be accounted for to determine anthropogenic CO<sub>2</sub> perturbations. The low model  
 683  $F_{100}$  values globally (Figure 3) and for mid- to high-latitude Northern Hemisphere and eastern  
 684 equatorial Pacific provinces (Figure 5), relative to observations, suggested that the RECCAP2  
 685 model ensemble may have underestimated biological CO<sub>2</sub> drawdown in high productivity regions.  
 686 Potential issues were also identified in simulated seasonal biogeochemical, gas-exchange and  
 687 physical dynamics as captured in the seasonal amplitude of non-thermal pCO<sub>2</sub> variations, with  
 688 weaker  $\Delta pCO_{2,non-thermal}$  values found at mid- to high-latitudes and in the eastern equatorial Pacific  
 689 in the model ensemble relative to observations (Figure 8). Future work with more detailed model  
 690 diagnostics could explore the connections between regional biases in simulated annual-mean and  
 691 seasonal export production and biases in air-sea CO<sub>2</sub> flux as observed in other RECCAP2 studies  
 692 (DeVries et al., 2023; Hauck et al., 2023).

693 Ocean circulation modulates biological export flux on basin to global scales (Najjar et al.,  
 694 2007), and the range in RECCAP2 global-integrated  $F_{100}$  values indicated that substantial  
 695 differences exist in simulated ocean physics within the RECCAP2 marine biogeochemical models  
 696 (Doney et al., 2004). The same ocean circulation variations also likely influenced the  
 697 anthropogenic CO<sub>2</sub> uptake estimates from DeVries et al. (2023) as indicated by the positive  
 698 correlation between anthropogenic CO<sub>2</sub> uptake and  $F_{100}$  across individual RECCAP2 models  
 699 (Figure 7). This is supported by further analysis of the RECCAP2 models demonstrating that the  
 700 rate of ocean overturning circulation is strongly correlated with anthropogenic CO<sub>2</sub> uptake in the  
 701 models (Terhaar et al., 2023). Variations in model export could also be compared against metrics  
 702 of physical stratification (Fu et al., 2022). The substantial inter-model spread in both physical and  
 703 biogeochemical metrics likely reflects common factors resulting from differences in simulated  
 704 thermocline ventilation and exchange between the surface and mid-depth ocean.

705 A set of additional model development recommendations emerge from our analyses. One  
 706 path forward would leverage independent model skill evaluation for inert chemical tracers (e.g.,  
 707 CFC-11, CFC-12, SF<sub>6</sub>) using standard ocean model intercomparison protocols (e.g., CMIP6 Ocean  
 708 Model Intercomparison Project; Orr et al., 2017). The transient tracer simulations would help  
 709 decipher the physical-biological factors controlling simulated AOU (Figure 6). Remineralization  
 710 of sinking biological organic matter structures sub-surface ocean dissolved inorganic carbon, O<sub>2</sub>,  
 711 and nutrient fields, a signal that must be addressed in observational estimates of anthropogenic  
 712 CO<sub>2</sub>. While the predominant pathway for ocean anthropogenic CO<sub>2</sub> uptake involves physical-  
 713 chemical dynamics, rather than biological dynamics, the same physical circulation and mixing  
 714 processes influence biogeochemical rates such as nutrient supply. Therefore, evaluation and  
 715 improvement of the ocean biological pump may provide additional insight.

716 The substantial variation in biological pump metrics shown here highlighted the need to  
717 reconcile inter-model and model-observational differences. Challenges arise for model  
718 improvement because there is limited agreement on the appropriate parameterizations for many  
719 key processes of biological carbon export (Henson et al., 2022), subsurface particle sinking, and  
720 remineralization. Many global models include detailed representation of euphotic zone processes  
721 but rather more simplistic representation of mesopelagic processes. Thus, the simulated global-  
722 scale biological carbon pump responses to interannual variability, let alone decadal climate  
723 change, remain poorly constrained (Henson et al., 2016). Following the mechanistic approach  
724 reported in previous model intercomparison studies for primary production (Laufkötter et al.,  
725 2015) and export production (Laufkötter et al., 2016), future studies could emphasize how overall  
726 model behavior reflects differences in model parameterizations, functional equations, and  
727 parameter values in both the euphotic and mesopelagic zones.

728 Opportunities exist to leverage process-level information from lab and field studies to  
729 improve model treatment of POC production, sinking POC flux and extension of export pathways  
730 beyond POC gravitational sinking, for example physical subduction and active migration by  
731 organisms (Boyd et al., 2019; Siegel et al., 2016; Henson et al., 2022; Siegel et al., 2023).  
732 Phytoplankton community structure, captured to some degree in many models, influences  
733 magnitude and composition of export flux from the euphotic zone, the heterotrophic consumers of  
734 sinking POC and zooplankton community structure (Boyd and Newton, 1995; Cavan et al., 2019).  
735 Model treatments could be improved for grazers, such as zooplankton, that act to decrease particle  
736 flux by consuming phytoplankton and sinking POC, while also increasing flux by packaging POC  
737 into fecal pellets with a wide range of sinking speeds (Turner, 2015; Steinberg and Landry, 2017).  
738 Grazer diel vertical migration may also need to be incorporated as a carbon shunt below the depth  
739 horizons of most intense heterotrophic activity (i.e., upper mesopelagic zone), consuming POC in  
740 the surface ocean and respiring it at grazer resident daytime depth (Bianchi et al., 2013). More  
741 mechanistic treatment of particle dynamics may also be feasible. Particle disaggregation,  
742 physically through shear or biologically through fragmentation by grazers, likely contributes  
743 substantially to the decline in POC flux with depth while also providing a POC source for  
744 mesopelagic microbes (Laurenceau-Cornec et al., 2020; Briggs et al., 2020). Microbes also can  
745 reduce POC flux directly, as they constantly attach and detach from sinking POC (Kiørboe et al.,  
746 2002; Kiørboe et al., 2003), hydrolyzing and respiring the POC. While variable particle sinking  
747 speed is included in some model parameterizations, large meta-analyses of empirical data have  
748 struggled to find a strong link between sinking rate and size of particles, because of the vast  
749 variability in particle type, methods used to measure sinking rate, and environment the particles  
750 were collected from (Cael et al., 2021).

751 Many of these process-level insights are already driving progress on mechanistic  
752 parameterizations for sinking particle flux (e.g., Dinauer et al., 2022), vertical migration (e.g.,  
753 Archibald et al., 2019), and other key factors in the marine biological pump. Together with global-  
754 scale ocean biogeochemical data compilations and syntheses (e.g., Mouw et al., 2016a; Mouw et  
755 al., 2016b, Clements et al., 2023) there are now promising new opportunities to evaluate, constrain,  
756 and improve ocean biological carbon pump simulations. Based on the model-data analysis  
757 presented here, the RECCAP2 multi-model ensemble exhibited relatively good agreement with  
758 observed biological carbon pump metrics, where there is sufficient data. The analysis also  
759 identified model-data biases and substantial differences among some of the models included in  
760 RECCAP2. These biases should be used to guide directions for future model development.

761  
762  
763

#### 764 **Funding**

765 S.C. Doney and K.A. Mitchell acknowledge support from the U.S. National Science Foundation  
766 via the Center for Chemical Currencies of a Microbial Planet (NSF 2019589). S.A. Henson  
767 received support from a European Research Council Consolidator grant (GOCART, agreement  
768 number 724416). S. Henson and J. Hauck received support from the European Union's Horizon  
769 2020 research and innovation programme under grant agreement no. 820989 (COMFORT), and  
770 the European Union's Horizon Europe research and innovation programme under grant agreement  
771 no. 101083922 (OceanICU). Funding to J. Hauck was provided by the Initiative and Networking  
772 Fund of the Helmholtz Association (Helmholtz Young Investigator Group Marine Carbon and  
773 Ecosystem Feedbacks in the Earth System, MarESys, Grant VH-NG-1301). J.D. Müller and N.  
774 Gruber acknowledge support from the European Union's Horizon 2020 research and innovation  
775 programme under grant agreement no. 821003 (project 4C) and no. 820989 (project COMFORT).  
776 T. DeVries acknowledges support from NSF grant OCE-1958955. E.L. Cavan was funded by an  
777 Imperial College Research Fellowship.

778

#### 779 **Acknowledgements**

780 Conceptualization (Ideas; formulation or evolution of overarching research goals and aims):  
781 S.C.D, S.A.H.

782 Data curation (Management activities to annotate (produce metadata), scrub data and maintain  
783 research data (including software code, where it is necessary for interpreting the data itself) for  
784 initial use and later re-use): K.A.M, J.D.M.

785 Formal analysis (Application of statistical, mathematical, computational, or other formal  
786 techniques to analyze or synthesize study data): S.C.D., K.A.M., S.A.H.

787 Funding acquisition (Acquisition of the financial support for the project leading to this  
788 publication): S.C.D, S.A.H.

789 Investigation (Conducting a research and investigation process, specifically performing the  
790 experiments, or data/evidence collection): All co-authors

791 Methodology (Development or design of methodology; creation of models): S.C.D., K.A.M.,  
792 S.A.H.

793 Project administration (Management and coordination responsibility for the research activity  
794 planning and execution): S.C.D., S.A.H., J.D.M.

795 Software (Programming, software development; designing computer programs; implementation  
796 of the computer code and supporting algorithms; testing of existing code components): K.A.M.,  
797 J.D.M.

798 Supervision (Oversight and leadership responsibility for the research activity planning and  
799 execution, including mentorship external to the core team): S.C.D, S.A.H., J.D.M.

800 Visualization (Preparation, creation and/or presentation of the published work, specifically  
801 visualization/data presentation): S.C.D., K.A.M.

802 Writing – original draft (Preparation, creation and/or presentation of the published work,  
803 specifically writing the initial draft (including substantive translation)): S.C.D., K.A.M., S.A.H.,  
804 E.C.

805 Writing – review and editing (Preparation, creation and/or presentation of the published work by  
806 those from the original research group, specifically critical review, commentary or revision –  
807 including pre- or post-publication stages): All co-authors

808

## 809 **Open Research**

810 The RECCAP2 ocean data collection can be found in Müller (2023).

811 Müller, Jens Daniel. (2023). RECCAP2-ocean data collection [Data set]. Zenodo.

812 1631 <https://doi.org/10.5281/zenodo.7990823>

813

## 814 **References**

815

816 Archibald, K., Siegel, D. A., & Doney, S. C. (2019) Modeling the impact of zooplankton diel  
817 vertical migration on the carbon export flux of the biological pump. *Global Biogeochemical  
818 Cycles*, 33, 181–199. <https://doi.org/10.1029/2018GB005983>

819

820 Armstrong, R. A., Lee, C., Hedges, J. I., Honjo, S., & Wakeham, S. G. (2001). A new, mechanistic  
821 model for organic carbon fluxes in the ocean based on the quantitative association of POC with  
822 ballast minerals, *Deep Sea Research Part II*, 49, 219–236. [https://doi.org/10.1016/S0967-0645\(01\)00101-1](https://doi.org/10.1016/S0967-<br/>823 0645(01)00101-1)

824

825 Aumont, O., Ethé, C., Tagliabue, A., Bopp, L., & Gehlen, M. (2015). PISCES-v2: An ocean  
826 biogeochemical model for carbon and ecosystem studies. *Geoscientific Model Development*, 8,  
827 2465–2513. <https://doi.org/10.5194/gmd-8-2465-2015>

828

829 Bacastow, R., & Maier-Reimer, E. (1990). Ocean-circulation model of the carbon cycle. *Climate  
830 Dynamics*, 4, 95–125. <https://doi.org/10.1007/BF00208905>

831

832 Behrenfeld, M. J., & Falkowski, P. G. (1997). Photosynthetic rates derived from satellite-based  
833 chlorophyll concentration. *Limnology and Oceanography*, 42, 1–20.  
834 <https://doi.org/10.4319/lo.1997.42.1.0001>

835

836 Behrenfeld, M. J., Boss, E., Siegel, D. A., & Shea, D. M. (2005). Carbon-based ocean  
837 productivity and phytoplankton physiology from space, *Global Biogeochemical Cycles*, 19,  
838 GB1006. <https://doi.org/10.1029/2004GB002299>.

839

840 Berthet, S., Séférian, R., Bricaud, C., Chevallier, M., Volodire, A., & Ethé, C. (2019). Evaluation  
841 of an online grid-coarsening algorithm in a global eddy-admitting ocean-biogeochemical model.  
842 *Journal of Advances in Modeling Earth Systems*, 11(6), 1759–1783.  
843 <https://doi.org/10.1029/2019ms001644>

844

845 Bianchi, D., Stock, C., Galbraith, E. D., & Sarmiento, J. L. (2013). Diel vertical migration:  
846 Ecological controls and impacts on the biological pump in a one-dimensional ocean model.  
847 *Global Biogeochemical Cycles*, 27, 478–491. <https://doi.org/10.1002/gbc.20031>

848

849 Bol, R., Henson, S. A., Rumyantseva, A., & Briggs, N. (2018). High-frequency variability of  
850 small-particle carbon export flux in the Northeast Atlantic. *Global Biogeochemical Cycles*, 32,  
851 1803–1814. <https://doi.org/10.1029/2018GB005963>

852

853 Boyd, P., & Newton, P. (1995). Evidence of the potential influence of planktonic community  
854 structure on the interannual variability of particulate organic carbon flux, *Deep Sea Research*  
855 Part I, 42, 619–639. [https://doi.org/10.1016/0967-0637\(95\)00017-Z](https://doi.org/10.1016/0967-0637(95)00017-Z)

856

857 Boyd, P.W., Claustre, H., Levy, M., Siegel, D. A., & Weber, T. (2019). Multi-faceted particle  
858 pumps drive carbon sequestration in the ocean. *Nature*, 568, 327–335.  
859 <https://doi.org/10.1038/s41586-019-1098-2>

860

861 Briggs, N., Dall'Olmo, G., & Claustre, H. (2020). Major role of particle fragmentation in  
862 regulating biological sequestration of CO<sub>2</sub> by the oceans, *Science*, 367, 791–793.  
863 <https://doi.org/10.1126/science.aay1790>

864

865 Broecker, W. S. and T. H. Peng (1982). *Tracers in the Sea*, Eldigio Press, Palisades, NY, 690 pp.  
866 [https://www.ideo.columbia.edu/~broecker/Home\\_files/TracersInTheSea\\_searchable.pdf](https://www.ideo.columbia.edu/~broecker/Home_files/TracersInTheSea_searchable.pdf)

867

868 Buesseler, K. O., Ball, K. O. L., Andrews, J., Cochran, J. K., Hirschberg, D. J., Bacon, M. P., et  
869 al. (2001). Upper ocean export of particulate organic carbon and biogenic silica in the Southern  
870 Ocean along 170°W, *Deep Sea Research Part II*, 48, 4275–4297. [https://doi.org/10.1016/S0967-0645\(01\)00089-3](https://doi.org/10.1016/S0967-0645(01)00089-3)

872

873 Burd, A. B. (2024). Modeling the vertical flux of organic carbon in the global ocean, *Annual  
874 Review of Marine Science*, 16, 135–161, <https://doi.org/10.1146/annurev-marine-022123-102516>

875

876 Cael, B. B., Cavan, E. L., & Britten, G. L. (2021). Reconciling the size-dependence of marine  
877 particle sinking speed. *Geophysical Research Letters*, 48, e2020GL091771.  
878 <https://doi.org/10.1029/2020GL091771>

879

880 Cael, B. B., Bisson, K., Boss, E., Dutkiewicz, S., & Henson. S. (2023). Global climate-change  
881 trends detected in indicators of ocean ecology. *Nature*, 619, 551–554.  
882 <https://doi.org/10.1038/s41586-023-06321-z>

883

884 Canadell, J. G., Monteiro, P. M. S., Costa, M. H., Cotrim da Cunha, L., Cox, P. M., Eliseev, A.  
885 V., et al. (2021). Global Carbon and other Biogeochemical Cycles and Feedbacks. In *Climate  
886 Change 2021: The Physical Science Basis. Contribution of Working Group I to the Sixth  
887 Assessment Report of the Intergovernmental Panel on Climate Change* [Masson-Delmotte, V., P.  
888 Zhai, A. Pirani, S.L. Connors, C. Péan, S. Berger, N. Caud, Y. Chen, L. Goldfarb, M.I. Gomis,  
889 M. Huang, K. Leitzell, E. Lonnoy, J.B.R. Matthews, T.K. Maycock, T. Waterfield, O. Yelekçi,  
890 R. Yu, and B. Zhou (eds.)]. Cambridge University Press, Cambridge, United Kingdom and New  
891 York, NY, USA, pp. 673–816. <https://doi.org/10.1017/9781009157896.007>

892

893 Carroll, D., Menemenlis, D., Adkins, J. F., Bowman, K. W., Brix, H., Dutkiewicz, S., et al.  
894 (2020). The ECCO-Darwin data-assimilative global ocean biogeochemistry model: Estimates of

895 seasonal to multidecadal surface ocean pCO<sub>2</sub> and air-sea CO<sub>2</sub> flux. *Journal of Advances in*  
896 *Modeling Earth Systems*, 12(10), e2019MS001888.

897

898 Carroll, D., Menemenlis, D., Dutkiewicz, S., Lauderdale, J. M., Adkins, J. F., Bowman, K. W., et  
899 al. (2022). Attribution of space-time variability in global-ocean dissolved inorganic carbon.  
900 *Global Biogeochemical Cycles*, 36(3), e2021GB007162.

901

902 Carr, M. E. (2002). Estimation of potential productivity in Eastern Boundary Currents using  
903 remote sensing, *Deep Sea Research Part II*, 49(1–3), 59–80.

904

905 Carr, M., Friedrichs, M., Schmeltz, M., Noguchiaita, M., Antoine, D., Arrigo, K., & et al. (2006).  
906 A comparison of global estimates of marine primary production from ocean color. *Deep-Sea*  
907 *Research Part II*, 53, 741–770. <https://doi.org/10.1016/j.dsr2.2006.01.028>

908

909 Cavan, E. L., Laurenceau-Cornec, E. C., Bressac, M., Boyd, P. W. (2019). Exploring the ecology  
910 of the mesopelagic biological pump. *Progress in Oceanography*, 176, 102125.  
911 <https://doi.org/10.1016/j.pocean.2019.102125>

912

913 Chau, T. T. T., Gehlen, M., & Chevallier, F. (2022). A seamless ensemble-based reconstruction of  
914 surface ocean pCO<sub>2</sub> and air-sea CO<sub>2</sub> fluxes over the global coastal and open oceans.  
915 *Biogeosciences*, 19(4), 1087–1109. <https://doi.org/10.5194/bg-19-1087-2022>

916

917 Clements, D. J., Yang, S., Weber, T., McDonnell, A. M. P., Kiko, R., Stemmann, L., Bianchi, D.  
918 (2023). New estimate of organic carbon export from optical measurements reveals the role of

919 particle size distribution and export horizon. *Global Biogeochemical Cycles*, 37,  
920 e2022GB007633. <https://doi.org/10.1029/2022GB007633>

921

922 Cram, J. A., Weber, T., Leung, S. W., McDonnell, A. M. P., Liang, J.-H., & Deutsch, C. (2018).  
923 The role of particle size, ballast, temperature, and oxygen in the sinking flux to the deep sea.  
924 *Global Biogeochemical Cycles*, 32, 858–876. <https://doi.org/10.1029/2017GB005710>

925

926 Crisp, D., Dolman, H., Tanhua, T., McKinley, G. A., Hauck, J., Bastos, A., et al. (2022). How  
927 well do we understand the land-ocean-atmosphere carbon cycle? *Reviews of Geophysics*, 60,  
928 e2021RG000736. <https://doi.org/10.1029/2021RG000736>

929

930 DeVries, T. (2022). The ocean carbon cycle, *Annual Review of Environment and Resources*, 47,  
931 317–341. <https://doi.org/10.1146/annurev-environ-120920-111307>

932

933 DeVries, T., & Weber, T. (2017). The export and fate of organic matter in the ocean: New  
934 constraints from combining satellite and oceanographic tracer observations. *Global  
935 Biogeochemical Cycles*, 31, 535–555. <https://doi.org/10.1002/2016GB005551>

936

937 DeVries, T., Le Quéré, C., Andrews, O., Berthet, S., Hauck, J., Ilyina, T., et al. (2019). Decadal  
938 trends in the ocean carbon sink. *Proceedings of the National Academy of Sciences*, 116(24),  
939 11646–11651. <https://doi.org/10.1073/pnas.1900371116>

940

941 DeVries, T., Yamamoto, K., Wanninkhof, R., Gruber, N., Hauck, J., Müller, J. D., et al. (2023).  
942 Magnitude, trends, and variability of the global ocean carbon sink from 1985–2018, *Global  
943 Biogeochemical Cycles*, 37 e2023GB007780. <https://doi.org/10.1029/2023GB007780>

944

945 Dinauer, A., Laufkötter, C., Doney, S. C., & Joos, F. (2022). What controls the large-scale  
946 efficiency of carbon transfer through the ocean's mesopelagic zone? Insights from a new,  
947 mechanistic model (MSPACMAM). *Global Biogeochemical Cycles*, 36, e2021GB007131.  
948 <https://doi.org/10.1029/2021GB007131>

949

950 Doney, S. C., Lindsay, K., Caldeira, K., Campin, J.-M., Drange, H., Dutay, J. C., et al. (2004).  
951 Evaluating global ocean carbon models: The importance of realistic physics. *Global  
952 Biogeochemical Cycles*, 18(3), GB3017. <https://doi.org/10.1029/2003GB002150>

953

954 Doney, S. C., Lindsay, K., Fung, I., J. John, J. (2006). Natural variability in a stable 1000 year  
955 coupled climate-carbon cycle simulation. *Journal of Climate*, 19(13), 3033–3054.  
956 <https://doi.org/10.1175/JCLI3783.1>

957

958 Doney, S. C., Yeager, S., Danabasoglu, G., Large, W. G., McWilliams, J. C. (2007). Mechanisms  
959 governing interannual variability of upper ocean temperature in a global hindcast simulation.  
960 *Journal of Physical Oceanography*, 37, 1918–1938. <https://doi.org/10.1175/JPO3089.1>

961

962 Doney, S. C., Lima, I., Feely, R. A., Glover, D. M., Lindsay, K., Mahowald, N., Moore, J. K.,  
963 Wanninkhof, R. (2009): Mechanisms governing interannual variability in upper-ocean inorganic  
964 carbon system and air-sea CO<sub>2</sub> fluxes: Physical climate and atmospheric dust. *Deep Sea*

965 *Research Part II: Topical Studies in Oceanography*, 56(8–10) 640–655.  
966 <https://doi.org/10.1016/j.dsr2.2008.12.006>

967

968 Döscher, R., Acosta, M., Alessandri, A., Anthoni, P., Arsouze, T., Bergman, T., et al. (2022). The  
969 EC-Earth3 Earth system model for the Coupled Model Intercomparison Project 6. *Geoscientific  
970 Model Development*, 15(7), 2973–3020. <https://doi.org/10.5194/gmd-15-2973-2022>

971

972 Ducklow, H. W., & Doney, S. C. (2013). What is the metabolic state of the oligotrophic ocean? A  
973 debate. *Annual Review of Marine Science*, 5, 525–533. <https://doi.org/10.1146/annurev-marine-121211-172331>

974

975

976 Dunne, J. P., Armstrong, R. A., Gnanadesikan, A., & Sarmiento, J. L. (2005). Empirical and  
977 mechanistic models for the particle export ratio, *Global Biogeochemical Cycles*, 19, GB4026.  
978 <https://doi.org/10.1029/2004GB002390>.

979

980 Dunne, J. P., Sarmiento, J. L., & Gnanadesikan, A. (2007). A synthesis of global particle export  
981 from the surface ocean and cycling through the ocean interior and on the seafloor. *Global  
982 Biogeochemical Cycles*, 21, GB4006. <https://doi.org/10.1029/2006GB002907>

983

984 Dutay, J.-C., Bullister, J. L., Doney, S. C., Orr, J. C., Najjar, R., Caldeira, K., et al. (2002).  
985 Evaluation of ocean model ventilation with CFC-11: comparison of 13 global ocean models.  
986 *Ocean Modelling*, 4, 89–120. [https://doi.org/10.1016/S1463-5003\(01\)00013-0](https://doi.org/10.1016/S1463-5003(01)00013-0)

987

988 Falkowski, P. G., Barber, R. T., & Smetacek, V. (1998). Biogeochemical controls and feedbacks  
989 on ocean primary production. *Science*, 281(5374), 200–206.  
990 <https://doi.org/10.1126/science.281.5374.200>

991

992 Fay, A. R., & McKinley, G. A. (2014). Global open-ocean biomes: mean and temporal  
993 variability. *Earth System Science Data*, 6, 273–284. <https://doi.org/10.5194/essd-6-273-2014>.

994

995 Fennel, K., Mattern, J. P., Doney, S. C., Bopp, L., Moore, A. M., Wang, B., & Yu, L. (2022).  
996 Ocean biogeochemical modelling. *Nature Reviews Methods Primers*, 2, 76.  
997 <https://doi.org/10.1038/s43586-022-00154-2>

998

999 Friedlingstein, P., O’Sullivan, M., Jones, M. W., Andrew, R. M., Gregor, L., Hauck, J., et al.  
1000 (2022). Global carbon budget 2022. *Earth System Science Data*, 14, 4811–4900.  
1001 <https://doi.org/10.5194/essd-14-4811-2022>

1002

1003 Fu, W., Moore, J. K., Primeau, F., Collier, N., Ogunro, O. O., Hoffman, F. M., & Randerson, J. T.  
1004 (2022). Evaluation of ocean biogeochemistry and carbon cycling in CMIP earth system models  
1005 with the International Ocean Model Benchmarking (IOMB) software system. *Journal of  
1006 Geophysical Research: Oceans*, 127, e2022JC018965. <https://doi.org/10.1029/2022JC018965>

1007

1008 Garcia, H. E., Weathers, K., Paver, C. R., Smolyar, I., Boyer, T. P., Locarnini, R. A., et al. (2019).  
1009 World Ocean Atlas 2018, Volume 3: Dissolved Oxygen, Apparent Oxygen Utilization, and

1010 Oxygen Saturation. A. Mishonov Technical Ed., *NOAA Atlas NESDIS 83*, 38pp.  
1011 [https://www.ncei.noaa.gov/sites/default/files/2020-04/woa18\\_vol3.pdf](https://www.ncei.noaa.gov/sites/default/files/2020-04/woa18_vol3.pdf)

1012

1013 Giering, S., Sanders, R., Lampitt, R., Anderson, T. R., Tamburini, C., Boutrif, M., et al. (2014).  
1014 Reconciliation of the carbon budget in the ocean's twilight zone. *Nature*, 507, 480–483.  
1015 <https://doi.org/10.1038/nature13123>

1016

1017 Giering, S. L. C., Sanders, R., Martin, A. P., Henson, S. A., Riley, J. S., Marsay, C. M., & Johns,  
1018 D. G. (2017). Particle flux in the oceans: Challenging the steady state assumption, *Global*  
1019 *Biogeochemical Cycles*, 31, 159–171. <https://doi.org/10.1002/2016GB005424>

1020

1021 Gloege, L., Yan, M., Zheng, T., & McKinley, G. A. (2022). Improved quantification of ocean  
1022 carbon uptake by using machine learning to merge global models and pCO<sub>2</sub> data. *Journal of*  
1023 *Advances in Modeling Earth Systems*, 14(2), e2021MS002620.  
1024 <https://doi.org/10.1029/2021ms002620>

1025

1026 Glover, D. M., Jenkins, W. J., & Doney, S. C. (2011). *Modeling Methods for Marine Science*.  
1027 Cambridge, United Kingdom: Cambridge University Press.  
1028 <https://doi.org/10.1017/CBO9780511975721>

1029

1030 Gregor, L., & Gruber, N. (2021). OceanSODA-ETHZ: A global gridded data set of the surface  
1031 ocean carbonate system for seasonal to decadal studies of ocean acidification. *Earth System*  
1032 *Science Data*, 13(2), 777–808. <https://doi.org/10.5194/essd-13-777-2021>

1033

1034 Gruber, N., Bakker, D.C.E., DeVries, T., Gregor, L., Hauck, J., Landschützer, P., McKinley, G.  
1035 A., & Müller, J. D. (2023). Trends and variability in the ocean carbon sink. *Nature Reviews Earth*  
1036 *and Environment*, 4, 119–134. <https://doi.org/10.1038/s43017-022-00381-x>

1037

1038 Guidi, L., Legendre, L., Reygondeau, G., Uitz, J., Stemmann, L., & Henson, S. A. (2015). A new  
1039 look at ocean carbon remineralization for estimating deep water sequestration. *Global*  
1040 *Biogeochemical Cycles*, 29, 1044–1059. <https://doi.org/10.1002/2014GB005063>

1041

1042 Hauck, J., Zeising, M., Le Quéré, C., Gruber, N., Bakker, D. C. E., Bopp, L., et al. (2020).  
1043 Consistency and challenges in the ocean carbon sink estimate for the global carbon budget.  
1044 *Frontiers in Marine Science*, 7, 571720. <https://doi.org/10.3389/fmars.2020.571720>

1045

1046 Hauck, J., Gregor, L., Nissen, C., Patara, L., Hague, M., Mongwe, P., et al. (2023). The Southern  
1047 Ocean carbon cycle 1985–2018: Mean, seasonal cycle, trends, and storage. *Global*  
1048 *Biogeochemical Cycles*, 37, e2023GB007848. <https://doi.org/10.1029/2023GB007848>

1049

1050 Henson, S. A., Sarmiento, J. L., Dunne, J. P., Bopp, L., Lima, I., Doney, S. C., et al. (2010).  
1051 Detection of anthropogenic climate change in satellite records of ocean chlorophyll and  
1052 productivity. *Biogeosciences*, 7, 621–640. <https://doi.org/10.5194/bg-7-621-2010>

1053

1054 Henson, S. A., Sanders, R., & Madsen, E. (2012). Global patterns in efficiency of particulate  
1055 organic carbon export and transfer to the deep ocean. *Global Biogeochemical Cycles*, 26,  
1056 GB1028. <https://doi.org/10.1029/2011GB004099>

1057

1058 Henson, S. A., Yool, A., & Sanders, R. (2015). Variability in efficiency of particulate organic  
1059 carbon export: A model study, *Global Biogeochemical Cycles*, 29, 33–45.  
1060 doi:10.1002/2014GB004965

1061

1062 Henson, S. A., Beaulieu, C., & Lampitt, R. (2016). Observing climate change trends in ocean  
1063 biogeochemistry: When and where. *Global Change Biology*, 22(4), 1561–1571.  
1064 <https://doi.org/10.1111/gcb.13152>

1065

1066 Henson, S. A., Laufkötter, C., Leung, S. Giering, S. L. C., Palevsky, H. I., & Cavan, E. L. (2022).  
1067 Uncertain response of ocean biological carbon export in a changing world. *Nature Geoscience*,  
1068 15, 248–254. <https://doi.org/10.1038/s41561-022-00927-0>

1069

1070 Henson, S. A., Briggs, N., Carvalho, F., Manno, C., Mignot, A., Thomalla, S. (2023). A seasonal  
1071 transition in biological carbon pump efficiency in the northern Scotia Sea, Southern Ocean. *Deep  
1072 Sea Research Part II*, 208, 105274. <https://doi.org/10.1016/j.dsr2.2023.105274>

1073

1074 Henson, S. A., Kelsey Bisson, K., Hammond, M. L., Martin, A., Mouw, C., Yool, A. (2024).  
1075 Effect of sampling bias on global estimates of ocean carbon export. *Environmental Research  
1076 Letters*, 19, 024009. <http://dx.doi.org/10.1088/1748-9326/ad1e7f>

1077

1078 Ilyina, T., Six, K. D., Segschneider, J., Maier-Reimer, E., Li, H., & Núñez-Riboni, I. (2013).  
1079 Global ocean biogeochemistry model HAMOCC: Model architecture and performance as  
1080 component of the MPI-Earth system model in different CMIP5 experimental realizations.  
1081 *Journal of Advances in Modeling Earth Systems*, 5(2), 287–315.  
1082 <https://doi.org/10.1029/2012ms000178>

1083

1084 Iversen, M. H. (2023). Carbon export in the ocean: a biologist's perspective. *Annual Review of  
1085 Marine Science*, 15, 357–381. <https://doi.org/10.1146/annurev-marine-032122-035153>

1086

1087 Karl, D. M., Church, M. J., Dore, J. E., Letelier, R., & Mahaffey, C. (2012). Predictable and  
1088 efficient carbon sequestration in the North Pacific Ocean supported by symbiotic nitrogen  
1089 fixation, *Proceedings of the National Academy of Sciences USA*, 109, 1842–1849.  
1090 <https://doi.org/10.1073/pnas.1120312109>

1091

1092 Khatiwala, S., Tanhua, T., Mikaloff Fletcher, S., Gerber, M., Doney, S. C., Graven, H. D., et al.  
1093 (2013). Global ocean storage of anthropogenic carbon, *Biogeosciences*, 10, 2169–2191.  
1094 <https://doi.org/10.5194/bg-10-2169-2013>

1095

1096 Kiørboe, T., Grossart, H.-P., Ploug, H., & Tang, K. (2002). Mechanisms and rates of bacterial  
1097 colonization of sinking aggregates, *Applied and Environmental Microbiology*, 68, 3996–4006.  
1098 <https://doi.org/10.1128/AEM.68.8.3996-4006.2002>

1099

1100 Kiørboe, T., Tang, K., Grossart, H.-P., & Ploug, H. (2003). Dynamics of microbial communities  
1101 on marine snow aggregates: colonization, growth, detachment, and grazing mortality of attached  
1102 bacteria, *Applied and Environmental Microbiology*, 69, 3036–3047.  
1103 <https://doi.org/10.1128/AEM.69.6.3036-3047.2003>

1104

1105 Kwon, E., Primeau, F., & Sarmiento, J. (2009). The impact of remineralization depth on the air–  
1106 sea carbon balance, *Nature Geoscience*, 2, 630–635. <https://doi.org/10.1038/ngeo612>

1107

1108 Lam, P. J., Doney, S. C., & Bishop, J. K. B. (2011). The dynamic ocean biological pump:  
1109 Insights from a global compilation of particulate organic carbon, CaCO<sub>3</sub>, and opal concentration  
1110 profiles from the mesopelagic. *Global Biogeochemical Cycles*, 25, GB3009.  
1111 <https://doi.org/10.1029/2010GB003868>.

1112

1113 Lampitt, R. S., Bett, B. J., Kiriakoulakis, K., Popova, E. E., Ragueneau, O., Vangriesheim, A., &  
1114 Wolff, G. A. (2001). Material supply to the abyssal seafloor in the Northeast Atlantic, *Progress in  
1115 Oceanography*, 50, 27–63. [https://doi.org/10.1016/S0079-6611\(01\)00047-7](https://doi.org/10.1016/S0079-6611(01)00047-7)

1116

1117 Landschützer, P., Gruber, N., & Bakker, D. C. (2016). Decadal variations and trends of the global  
1118 ocean carbon sink. *Global Biogeochemical Cycles*, 30(10), 1396–1417.  
1119 <https://doi.org/10.1002/2015gb005359>

1120

1121 Landschützer, P., Gruber, N., Bakker, D. C. E., Stemmler, I., Six, K. D. (2018). Strengthening  
1122 seasonal marine CO<sub>2</sub> variations due to increasing atmospheric CO<sub>2</sub>. *Nature Climate Change*, 8,  
1123 146–150. <https://doi.org/10.1038/s41558-017-0057-x>

1124

1125 Laufkötter, C., Vogt, M., Gruber, N., Aita-Noguchi, M., Aumont, O., Bopp, L., et al. (2015).  
1126 Drivers and uncertainties of future global marine primary production in marine ecosystem  
1127 models. *Biogeosciences*, 12(23), 6955–6984. <https://doi.org/10.5194/bg-12-6955-2015>

1128

1129 Laufkötter, C., Vogt, M., Gruber, N., Aumont, O., Bopp, L., Doney, S. C., et al. (2016). Projected  
1130 decreases in future marine export production: The role of the carbon flux through the upper  
1131 ocean ecosystem. *Biogeosciences*, 13, 4023–4047. <https://doi.org/10.5194/bg-13-4023-2016>

1132

1133 Laufkötter, C., John, J. G., Stock, C. A., & Dunne, J. P. (2017). Temperature and oxygen  
1134 dependence of the remineralization of organic matter. *Global Biogeochemical Cycles*, 31, 1038–  
1135 1050. <https://doi.org/10.1002/2017GB005643>

1136

1137 Laurenceau-Cornec, E. C., Le Moigne, F. A. C., Gallinari, M., Moriceau, B., Toullec, J., Iversen,  
1138 M. I., Engel, A., & De La Rocha, C. L. (2020). New guidelines for the application of Stokes'  
1139 models to the sinking velocity of marine aggregates, *Limnology and Oceanography*, 65, 1264–  
1140 1285. <https://doi.org/10.1002/lno.11388>

1141

1142 Laws, E. A., Falkowski, P. G., Smith Jr, W. O., Ducklow, H., & McCarthy, J. J. (2000).  
1143 Temperature effects on export production in the open ocean. *Global Biogeochemical Cycles*, 14,  
1144 1231–1246. <https://doi.org/10.1029/1999GB001229>

1145

1146 Laws, E. A., & Maiti, K. (2019). The relationship between primary production and export  
1147 production in the ocean: Effects of time lags and temporal variability, *Deep Sea Research Part I*,  
1148 148, 100–107. <https://doi.org/10.1016/j.dsr.2019.05.006>

1149

1150 Laws, E. A., D'sa, E., & Naik, P. (2011). Simple equations to estimate ratios of new or export  
1151 production to total production from satellite-derived estimates of sea surface temperature and  
1152 primary production. *Limnology and Oceanography: Methods*, 9(12), 593–601.  
1153 <https://doi.org/10.4319/lom.2011.9.593>

1154

1155 Le Quéré, C., Buitenhuis, E. T., Moriarty, R., Alvain, S., Aumont, O., Bopp, L., et al. (2016).  
1156 Role of zooplankton dynamics for Southern Ocean phytoplankton biomass and global  
1157 biogeochemical cycles. *Biogeosciences*, 13(14), 4111–4133. <https://doi.org/10.5194/bg-13-4111-2016>

1159

1160 Liao, E., Resplandy, L., Liu, J., & Bowman, K. W. (2020). Amplification of the ocean carbon  
1161 sink during El Niños: Role of poleward Ekman transport and influence on atmospheric CO<sub>2</sub>.  
1162 *Global Biogeochemical Cycles*, 34(9), e2020GB006574. <https://doi.org/10.1029/2020gb006574>

1163

1164 Lima, I. D., Lam, P. J., & Doney, S. C. (2014). Dynamics of particulate organic carbon flux in a  
1165 global ocean model, *Biogeosciences*, 11, 1177–1198. <https://doi.org/10.5194/bg-11-1177-2014>

1166

1167 Lindsay, K., Bonan, G. B., Doney, S. C., Hoffman, F. M., Lawrence, D. M., Long, M. C., et al.  
1168 (2014). Preindustrial-control and twentieth-century carbon cycle experiments with the Earth  
1169 System Model CESM1(BGC). *Journal of Climate*, 27(24), 8981–9005. <https://doi.org/10.1175/jcli-d-12-00565.1>

1171

1172 Lutz, M. J., Caldeira, K., Dunbar, R. B., & Behrenfeld, M. J. (2007). Seasonal rhythms of net  
1173 primary production and particulate organic carbon flux to depth describe the efficiency of  
1174 biological pump in the global ocean. *Journal of Geophysical Research Oceans*, 112, C10011.  
1175 <https://doi.org/10.1029/2006JC003706>

1176

1177 Maier-Reimer, E. (1993). Geochemical cycles in an ocean general circulation model.  
1178 Preindustrial tracer distributions, *Global Biogeochemical Cycles*, 7, 645–677.  
1179 <https://doi.org/10.1029/93GB01355>

1180

1181 Marinov, I., Gnanadesikan, A., Sarmiento, J. L., Toggweiler, J. R., Follows, M., & Mignone, B.  
1182 K. (2008). Impact of oceanic circulation on biological carbon storage in the ocean and  
1183 atmospheric pCO<sub>2</sub>, *Global Biogeochemical Cycles*, 22, GB3007.  
1184 <https://doi.org/10.1029/2007GB002958>

1185

1186 Marra, J., Ho, C., & Trees, C. C. (2003). An alternative algorithm for the calculation of primary  
1187 production from remote sensing data, Rep. LDEO 2003–1, Lamont-Doherty Earth Observatory,  
1188 Palisades, New York. <https://www.ledo.columbia.edu/~marra/MarraAlgorithm.pdf> (Accessed  
1189 August, 2022).

1190

1191 Marsay, C. M., Sanders, R. J., Henson, S. A., Pabortsava, K., Achterberg, E. P., & Lampitt, R. S.  
1192 (2015). Attenuation of sinking particulate organic carbon flux through the mesopelagic ocean,  
1193 *Proceedings of the National Academy of Sciences USA*, 112(4) 1089–1094.  
1194 <https://doi.org/10.1073/pnas.1415311112>

1195

1196 Martin, J. H., Knauer, G. A., Karl, D. M., & Broenkow, W. W. (1987). VERTEX: carbon cycling  
1197 in the northeast Pacific, *Deep-Sea Research*, 34, 267–285. [https://doi.org/10.1016/0198-0149\(87\)90086-0](https://doi.org/10.1016/0198-0149(87)90086-0)

1198

1199

1200 Matsumoto, K., Sarmiento, J. L., Key, R. M., Bullister, J. L., Caldeira, K., Campin, J.-M., et al.  
1201 (2004). Evaluation of ocean carbon cycle models with data-based metrics, *Geophysical Research  
Letters*, 31, L07303. <https://doi.org/10.1029/2003GL018970>

1202

1203

1204 Mauritsen, T., Bader, J., Becker, T., Behrens, J., Bittner, M., Brokopf, R., et al. (2019).  
1205 Developments in the MPI-M Earth system model version 1.2 (MPI-ESM1. 2) and its response to  
1206 increasing CO<sub>2</sub>. *Journal of Advances in Modeling Earth Systems*, 11(4), 998–1038.  
1207 <https://doi.org/10.1029/2018ms001400>

1208

1209 Mayor, D. J., Sanders, R., Giering, S. L. C., & Anderson, T. R. (2014). Microbial gardening in  
1210 the ocean's twilight zone: Detritivorous metazoans benefit from fragmenting, rather than  
1211 ingesting, sinking detritus, *BioEssays*, 36, 1132–1137. <https://doi.org/10.1002/bies.201400100>

1212

1213 Mikaloff Fletcher, S. E., Gruber, N., Jacobson, A. R., Gloor, M., Doney, S. C., Dutkiewicz, S., et  
1214 al. (2007). Inverse estimates of the oceanic sources and sinks of natural CO<sub>2</sub> and their implied  
1215 oceanic transport. *Global Biogeochemical Cycles*, 21, GB1010.  
1216 <https://doi.org/10.1029/2006GB002751>

1217

1218 Mouw, C. B., Barnett, A., McKinley, G. A., Gloege, L., & Pilcher, D. (2016a). Global ocean  
1219 particulate organic carbon flux merged with satellite parameters, *Earth System Science Data*, 8,  
1220 531–541. <https://doi.org/10.5194/essd-8-531-2016>

1221

1222 Mouw, C. B., Barnett, A., McKinley, G. A., Gloege, L., & Pilcher, D. (2016b). Phytoplankton  
1223 size impact on export flux in the global ocean, *Global Biogeochemical Cycles*, 30, 1542–1562.  
1224 <https://doi.org/10.1002/2015GB005355>

1225

1226 Müller, Jens Daniel. (2023). RECCAP2-ocean data collection [Data set]. Zenodo. 1631.  
1227 <https://doi.org/10.5281/zenodo.7990823>

1228

1229 Najjar, R. G., X. Jin, F. Louanchi, O. Aumont, K. Caldeira, S.C. Doney, et al. (2007). Impact of  
1230 circulation on export production, dissolved organic matter and dissolved oxygen in the ocean:  
1231 Results from Phase II of the Ocean Carbon-cycle Model Intercomparison Project (OCMIP-2),  
1232 *Global Biogeochemical Cycles*, 21, GB3007. <https://doi.org/10.1029/2006GB002857>.

1233

1234 Nowicki, M., DeVries, T., & Siegel, D. A. (2022). Quantifying the carbon export and  
1235 sequestration pathways of the ocean's biological carbon pump. *Global Biogeochemical Cycles*,  
1236 36, e2021GB007083. <https://doi.org/10.1029/2021GB007083>

1237

1238 Omand, M. M., Govindarajan, R., He, J., & Mahadevan, A. (2020). Sinking flux of particulate  
1239 organic matter in the oceans: Sensitivity to particle characteristics. *Scientific Reports*, 10, 5582.  
1240 <https://doi.org/10.1038/s41598-020-60424-5>

1241

1242 Orr, J. C., R.G. Najjar, O. Aumont, L. Bopp, J.L. Bullister, G. Danabasoglu, et al. (2017).  
1243 Biogeochemical protocols and diagnostics for the CMIP6 Ocean Model Intercomparison Project  
1244 (OMIP). *Geoscientific Model Development*, 10, 2169–2199. <https://doi.org/10.5194/gmd-10-2169-2017>

1245

1246

1247 RECCAP2 Ocean Science Team (2022). RECCAP2 Ocean Protocols, accessed August 3<sup>rd</sup>, 2022.  
1248 <https://reccap2-ocean.github.io/protocols/>

1249

1250 Reygondeau, G., Longhurst, A., Martinez, E., Beaugrand, G., Antoine, D., & Maury, O. (2013),  
1251 Dynamic biogeochemical provinces in the global ocean, *Global Biogeochemical Cycles*, 27,  
1252 1046–1058. <https://doi.org/10.1002/gbc.20089>

1253

1254 Rödenbeck, C., DeVries, T., Hauck, J., Le Quéré, C., & Keeling, R. F. (2022). Data-based  
1255 estimates of interannual sea–air CO<sub>2</sub> flux variations 1957–2020 and their relation to  
1256 environmental drivers. *Biogeosciences*, 19(10), 2627–2652. <https://doi.org/10.5194/bg-19-2627-2022>

1257

1258

1259 Rödenbeck, C., Keeling, R. F., Bakker, D. C., Metzl, N., Olsen, A., Sabine, C., & Heimann, M.  
1260 (2013). Global surface-ocean pCO<sub>2</sub> and sea–air CO<sub>2</sub> flux variability from an observation-driven  
1261 ocean mixed-layer scheme. *Ocean Science*, 9(2), 193–216. <https://doi.org/10.5194/os-9-193-2013>

1262

1263

1264 Rodgers, K. B., Schwinger, J., Fassbender, A. J., Landschützer, P., Yamaguchi, R., Frenzel, H., et  
1265 al. (2023). Seasonal variability of the surface ocean carbon cycle: A synthesis. *Global  
1266 Biogeochemical Cycles*, 37, e2023GB007798. <https://doi.org/10.1029/2023GB007798>

1267

1268 Sarmiento, J. L., & Gruber, N. (2002). Anthropogenic carbon sinks. *Physics Today*, 55(8), 30–36.  
1269 <https://doi.org/10.1063/1.1510279>

1270

1271 Sarmiento, J. L., & Gruber, N. (2006). *Ocean Biogeochemical Dynamics*. Princeton University  
1272 Press. <https://doi.org/10.1017/S0016756807003755>

1273

1274 Schlitzer, R. (2000). Applying the adjoint method for biogeochemical modeling: Export of  
1275 particulate organic matter in the World Ocean, *Inverse methods in biogeochemical cycles*, ed. P.  
1276 Kasibhata, AGU Monograph 114, pp. 107–124.

1277

1278 Schwinger, J., Goris, N., Tjiputra, J. F., Kriest, I., Bentsen, M., Bethke, I., et al. (2016).  
1279 Evaluation of NorESM-OC (versions 1 and 1.2), the ocean carbon-cycle stand-alone  
1280 configuration of the Norwegian Earth System Model (NorESM1). *Geoscientific Model  
1281 Development*, 9(8), 2589–2622. <https://doi.org/10.5194/gmd-9-2589-2016>

1282

1283 Séférian, R., Gehlen, M., Bopp, L., Resplandy, L., Orr, J. C., Marti, O., et al. (2016). Inconsistent  
1284 strategies to spin up models in CMIP5: implications for ocean biogeochemical model  
1285 performance assessment, *Geoscientific Model Development*, 9, 1827–1851.  
1286 <https://doi.org/10.5194/gmd-9-1827-2016>

1287

1288 Séférian, R., Berthet, S., Yool, A., Palmiéri, J., Bopp, L., Tagliabue, A., et al. (2020). Tracking  
1289 improvement in simulated marine biogeochemistry between CMIP5 and CMIP6. *Current*  
1290 *Climate Change Reports*, 6(3), 95–119. <https://doi.org/10.1007/s40641-020-00160-0>

1291

1292 Séférian, R., Nabat, P., Michou, M., Saint-Martin, D., Volodire, A., Colin, J., et al. (2019).  
1293 Evaluation of CNRM Earth-System model, CNRM-ESM2-1: Role of Earth system processes in  
1294 present-day and future climate. *Journal of Advances in Modeling Earth Systems*, 11(12),  
1295 4182–4227. <https://doi.org/10.1029/2019ms001791>

1296

1297 Siegel, D. A., Buesseler, K. O., Doney, S. C., Sailley, S. F., Behrenfeld, M. J., & Boyd, P. W.  
1298 (2014). Global assessment of ocean carbon export by combining satellite observations and food-  
1299 web models. *Global Biogeochemical Cycles*, 28(3), 181–196.  
1300 <https://doi.org/10.1002/2013gb004743>

1301

1302 Siegel, D. A., Buesseler, K. O., Behrenfeld, M. J., Benitez-Nelson, C. R., Boss, E., Brzezinski,  
1303 M. A., et al. (2016). Prediction of the export and fate of global ocean net primary production: the  
1304 EXPORTS science plan, *Frontiers in Marine Science*, 3, 22.  
1305 <http://doi.org/10.3389/fmars.2016.00022>

1306

1307 Siegel, D. A., DeVries, T., Doney, S. C., & T. Bell, T. (2021). Assessing the sequestration time  
1308 scales of some ocean-based carbon dioxide reduction strategies, *Environmental Research Letters*,  
1309 16, 104003. <https://doi.org/10.1088/1748-9326/ac0be0>

1310

1311 Siegel, D. A., DeVries, T., Cetinić, I., & K Bisson, K. M. (2023). Quantifying the ocean's  
1312 biological pump and Its carbon cycle impacts on global scales, *Annual Review of Marine*  
1313 *Science*, 15, 329–356. <https://doi.org/10.1146/annurev-marine-040722-115226>

1314

1315 Silsbe, G. M., Behrenfeld, M. J., Halsey, K. H., Milligan, A. J., & Westberry, T. K. (2016). The  
1316 CAFE model: A net production model for global ocean phytoplankton, *Global Biogeochemical*  
1317 *Cycles*, 30, 1756–1777. doi:10.1002/2016GB005521

1318

1319 Steinberg, D. K., & M.R. Landry, M. R. (2017). Zooplankton and the ocean carbon cycle, *Annual*  
1320 *Review of Marine Science*, 9, 413–444. <https://doi.org/10.1146/annurev-marine-010814-015924>

1321

1322 Stock, C. A., Dunne, J. P., Fan, S., Ginoux, P., John, J., Krasting, J. P., et al. (2020). Ocean  
1323 biogeochemistry in GFDL's Earth system model 4.1 and its response to increasing atmospheric  
1324 CO<sub>2</sub>. *Journal of Advances in Modeling Earth Systems*, 12(10), e2019MS002043. <https://doi.org/10.1029/2019ms002043>

1325

1326

1327 Stukel, M. R., Ohman, M. D., Kelly, T. B., & Biard, T. (2019). The roles of suspension-feeding  
1328 and flux-feeding zooplankton as gatekeepers of particle flux into the mesopelagic ocean in the  
1329 Northeast Pacific. *Frontiers in Marine Science*, 6, 397. <https://doi.org/10.3389/fmars.2019.00397>

1330

1331 Takahashi, T., Olafsson, J., Goddard, J. G., Chipman, D. W., & Sutherland, S. C. (1993).  
1332 Seasonal variation of CO<sub>2</sub> and nutrients in the high-latitude surface oceans: A comparative study,  
1333 *Global Biogeochemical Cycles*, 7(4), 843–878. <https://doi.org/10.1029/93GB02263>

1334

1335 Takahashi, T., Sutherland, S. C., Sweeney, C., Poisson, A., Metzl, N., Tilbrook, B., et al. (2002).  
1336 Global sea-air CO<sub>2</sub> flux based on climatological surface ocean pCO<sub>2</sub>, and seasonal biological  
1337 and temperature effects. *Deep Sea Research Part II: Topical Studies in Oceanography*, 49(9–10),  
1338 1601–1622. [https://doi.org/10.1016/S0967-0645\(02\)00003-6](https://doi.org/10.1016/S0967-0645(02)00003-6)

1339

1340 Terhaar, T., Goris, N., Müller, J. D., DeVries, T., Gruber, N., Hauck, J., et al. (2023). Assessment  
1341 of global ocean biogeochemistry models for ocean carbon sink estimates in RECCAP2 and  
1342 recommendations for future studies. *ESS Open Archive*.  
1343 <https://doi.org/10.22541/essoar.168394734.41886821/v1>

1344

1345 Turner, J. T. (2015). Zooplankton fecal pellets, marine snow, phytodetritus and the ocean's  
1346 biological pump, *Progress in Oceanography*, 130, 205–248.  
1347 <https://doi.org/10.1016/j.pocean.2014.08.005>

1348

1349 Tsujino, H., Nakano, H., Sakamoto, K., Urakawa, S., Hirabara, M., Ishizaki, H., & Yamanaka, G.  
1350 (2017). Reference manual for the meteorological research institute community ocean model  
1351 version 4 (MRI. COMv4) (Vol. 80, p. 306). Technical Reports of the Meteorological Research  
1352 Institute.

1353

1354 Urakawa, L. S., Tsujino, H., Nakano, H., Sakamoto, K., Yamanaka, G., & Toyoda, T. (2020). The  
1355 sensitivity of a depth-coordinate model to diapycnal mixing induced by practical  
1356 implementations of the isopycnal tracer diffusion scheme. *Ocean Modelling*, 154, 101693.  
1357 <https://doi.org/10.1016/j.ocemod.2020.101693>

1358

1359 Volk, T., & Hoffert, M. I. (1985). Ocean carbon pumps: Analysis of relative strengths and  
1360 efficiencies in ocean-driven atmospheric CO<sub>2</sub> changes. In E. Sundquist & W. Broecker (Eds.),  
1361 *The carbon cycle and atmospheric CO<sub>2</sub>: Natural variations archean to present* (Vol. 32, pp. 99–  
1362 110). American Geophysical Union (AGU). <https://doi.org/10.1029/GM032P0099>

1363

1364 Wanninkhof, R., Park, G.-H., Takahashi, T., Sweeney, C., Feely, R., Nojiri, Y., et al. (2013).  
1365 Global ocean carbon uptake: magnitude, variability and trends, *Biogeosciences*, 10, 1983–2000.  
1366 <https://doi.org/10.5194/bg-10-1983-2013>

1367

1368 Watson, A. J., Schuster, U., Shutler, J. D., Holding, T., Ashton, I. G., Landschützer, P., et al.  
1369 (2020). Revised estimates of ocean-atmosphere CO<sub>2</sub> flux are consistent with ocean carbon  
1370 inventory. *Nature Communications*, 11(1), 1–6. <https://doi.org/10.1038/s41467-020-18203-3>

1371

1372 Weber, T., Cram, J. A., Leung, S. W., DeVries, T., & Deutsch, C. (2016). Deep ocean nutrients  
1373 imply large latitudinal variation in particle transfer efficiency, *Proceedings of the National  
1374 Academy of Sciences*, 113, 8606–8611. <https://doi.org/10.1073/pnas.1604414113>

1375

1376 Wilson, J. D., Andrews, O., Katavouta, A., de Melo Viríssimo, F., Death, R. M., Adloff, M., et al.  
1377 (2022). The biological carbon pump in CMIP6 models: 21st century trends and uncertainties.  
1378 *Proceedings of the National Academy of Sciences USA*, 119(29), e2204369119.  
1379 <https://doi.org/10.1073/pnas.2204369119>

1380

1381 Wright, R. M., Le Quéré, C., Buitenhuis, E., Pitois, S., & Gibbons, M. J. (2021). Role of jellyfish  
1382 in the plankton ecosystem revealed using a global ocean biogeochemical model. *Biogeosciences*,  
1383 18(4), 1291–1320. <https://doi.org/10.5194/bg-18-1291-2021>

1384

1385 Yang, S., & Gruber, N. (2016). The anthropogenic perturbation of the marine nitrogen cycle by  
1386 atmospheric deposition: Nitrogen cycle feedbacks and the  $^{15}\text{N}$  Haber-Bosch effect. *Global  
1387 Biogeochemical Cycles*, 30(10), 1418–1440. <https://doi.org/10.1002/2016gb005421>

1388

1389 Zeng, J., Iida, Y., Matsunaga, T., & Shirai, T. (2022). Surface ocean  $\text{CO}_2$  concentration and air-  
1390 sea flux estimate by machine learning with modelled variable trends. *Frontiers in Marine  
1391 Science*, 9, 989233. <https://doi.org/10.3389/fmars.2022.989233>

1392

1393

**Supporting Information:**

1394     **Observational and numerical modeling constraints on the global ocean biological carbon pump**

1395

1396     **Scott C. Doney<sup>1</sup>, Kayla A. Mitchell<sup>1,2</sup>, Stephanie A. Henson<sup>3</sup>, Emma Cavan<sup>4</sup>, Tim DeVries<sup>5</sup>,**  
1397     **Nicolas Gruber<sup>6</sup>, Judith Hauck<sup>7</sup>, Colleen B. Mouw<sup>8</sup>, Jens D. Müller<sup>6</sup>, and Francois W.**  
1398     **Primeau<sup>2</sup>**

1399

1400     **February 4<sup>th</sup>, 2024**

1401

1402     <sup>1</sup> Department of Environmental Sciences, University of Virginia, Charlottesville, VA, USA,

1403     <sup>2</sup> Department of Earth System Science, University of California, Irvine, Irvine, CA, USA,

1404     <sup>3</sup> National Oceanography Centre, Southampton, UK,

1405     <sup>4</sup> Department of Life Sciences, Silwood Park Campus, Imperial College London, Berkshire, UK,

1406     <sup>5</sup> Earth Research Institute and Department of Geography, University of California, Santa  
1407     Barbara, Santa Barbara, CA, USA,

1408     <sup>6</sup> Environmental Physics, Institute of Biogeochemistry and Pollutant Dynamics, ETH Zurich,  
1409     Zürich, Switzerland

1410     <sup>7</sup> Alfred-Wegener-Institut, Helmholtz-Zentrum für Polar- und Meeresforschung, Bremerhaven,  
1411     Germany

1412     <sup>8</sup> Graduate School of Oceanography, University of Rhode Island, Narragansett, RI, USA.

1413

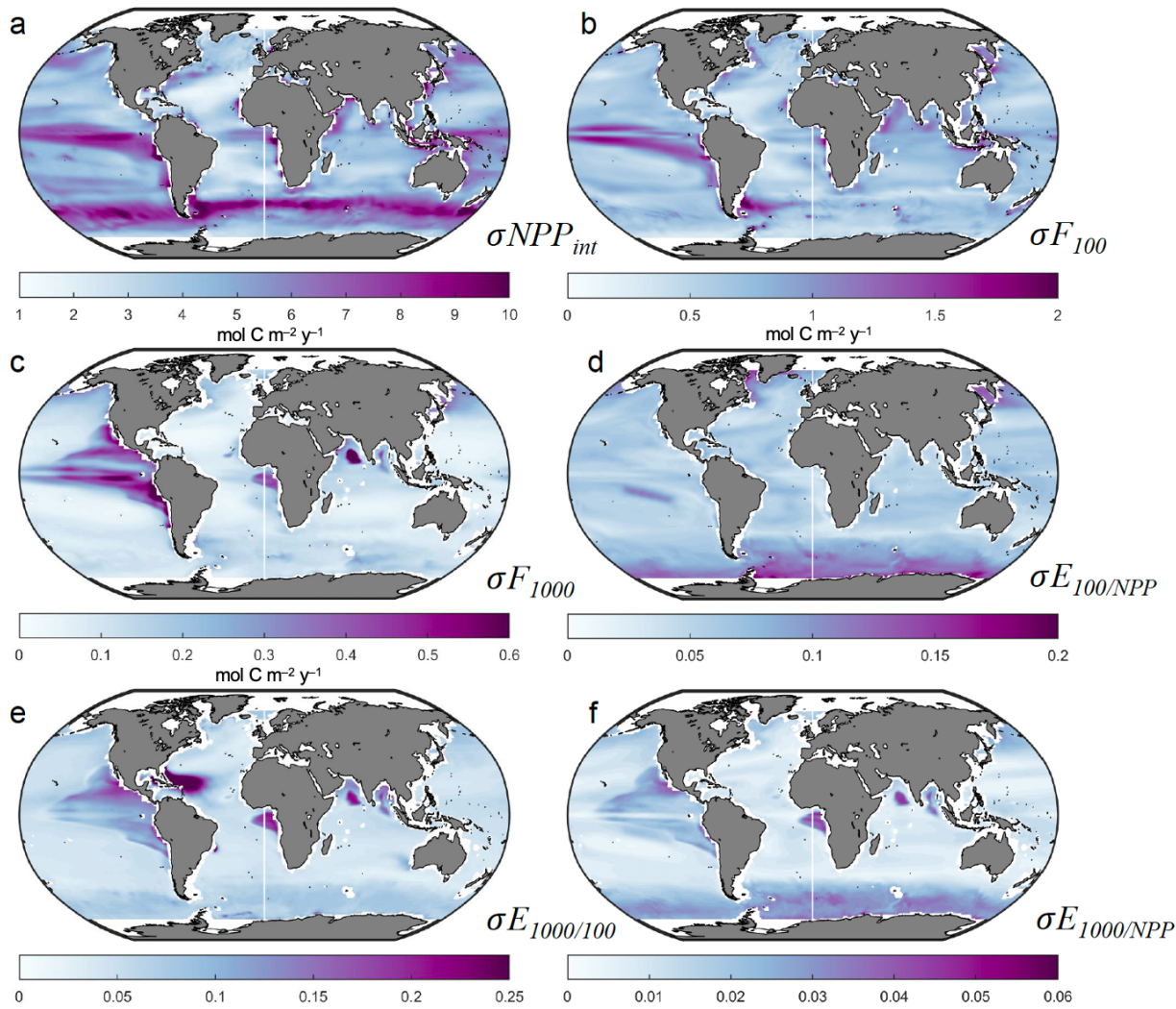
1414     The REgional Carbon Cycle Assessment and Processes (RECCAP) project is a coordinated, international  
1415     effort to constrain contemporary ocean carbon air-sea fluxes and interior storage trends using a combination  
1416     of field observations, inverse model products, and ocean biogeochemical hindcast simulations. The second  
1417     phase, RECCAP2, extends the original synthesis using additional years of ocean observational data and  
1418     updated numerical results (DeVries et al., 2023) as well as expanding the scope of the observational and model  
1419     analysis, in this case into the biological carbon pump magnitude and efficiency.

1420

1421     **Supplement Figures**

1422

1423



1424

1425

1426

1427

**Figure S1.** Maps of within-ensemble standard deviation of biological pump parameters. Standard deviations across model ensemble members are computed relative to the average model ensemble presented in Figure 1 for: (a) vertically integrated primary productivity  $\sigma_{NPP}$ , (b) particulate organic carbon export fluxes at 100 m  $\sigma F_{100}$ , and (c) 1000 m  $\sigma F_{1000}$ , all in moles C m<sup>-2</sup> y<sup>-1</sup>, and (d) surface export efficiency ratio  $E_{100/NPP} = F_{100}/NPP$ , (e) mesopelagic transfer efficiency at 1000 m  $E_{1000/100} = F_{1000}/F_{100}$ , and (f) export efficiency to the deep ocean  $E_{1000/NPP} = F_{1000}/NPP$ , all ratios unitless.

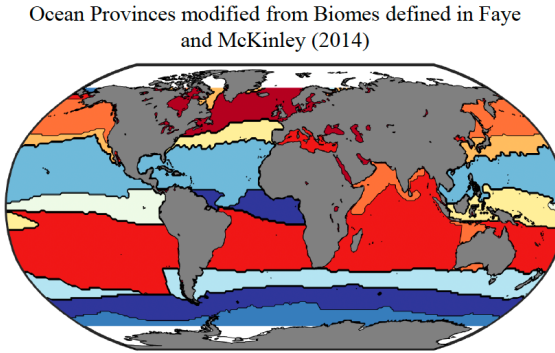
1434

1435

1436

1437

1438



Biome Number	Biome Acronym	Biome Description
18	SOSPSS	Southern Ocean Subpolar Seasonally Stratified
17	NaAEQU	N. Atlantic Equatorial
16	SOICE	Southern Ocean Ice
15	NPICE	North Pacific Ice
14	NPSTPS	N. Pacific Subtropical Permanently Stratified
13	NaSTPS	N. Atlantic Subtropical Seasonally Stratified
12	SOSTSS	Southern Ocean Subtropical Seasonally Stratified
11	BARENTS	Barents Sea
10	PEQUE	Eastern Equatorial Pacific
9	PEQUW	Western Equatorial Pacific
8	NAICE	N. Atlantic Ice
7	NaSTSS	N. Atlantic Subtropical Seasonally Stratified
6	NPSTSS	N. Pacific Subtropical Seasonally Stratified
5	NPSPSS	N. Pacific Subpolar Seasonally Stratified
4	INDSTPS	Indian Ocean Subtropical Permanently Stratified
3	MED	Mediterranean Sea
2	SASTPS	S. Atlantic Subtropical Permanently Stratified
1	NaSPSS	N. Atlantic Subpolar Seasonally Stratified

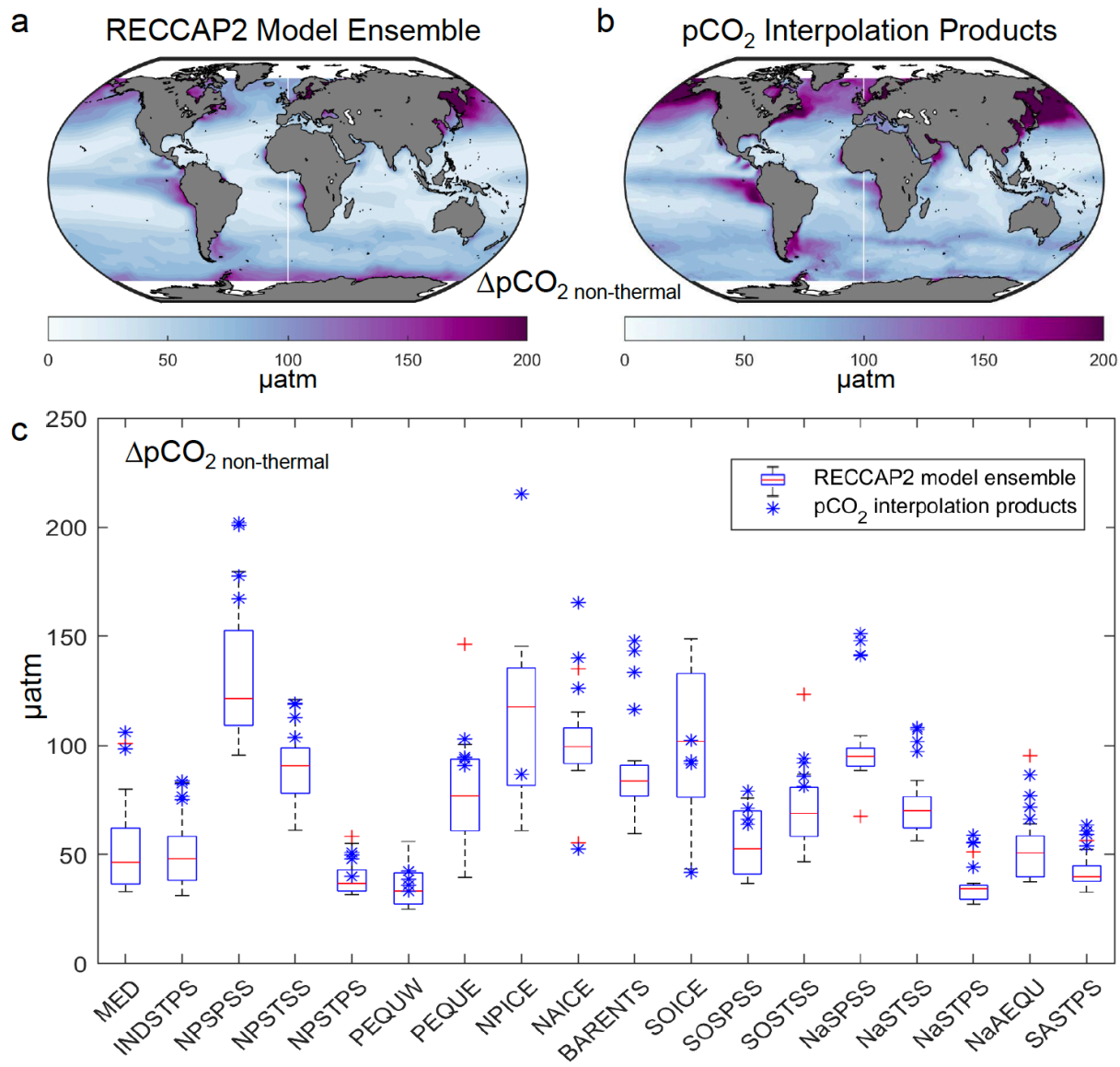
1439

1440

1441 **Figure S2.** Map of standard RECCAP2 biomes by ocean basin (Fay and McKinley, 2014). The  
 1442 biomes include polar (ICE), subpolar seasonally-stratified (SPSS), subtropical seasonally stratified  
 1443 (STSS), subtropical permanently stratified (STPS), and equatorial regions (EQU); note the  
 1444 equatorial Pacific is divided into western and eastern sub-basins. The equatorial eastern Pacific  
 1445 and Atlantic, monsoon-influenced Indian, and seasonally-stratified biomes generally exhibited  
 1446 relatively high NPP,  $F_{100}$ , and  $F_{1000}$ . Polar and sub-polar biomes exhibited relatively high  $E_{100}$ .

1447

1448

1449  
1450

1451 **Figure S3.** Analysis of the seasonal cycle of non-thermal  $\Delta pCO_2$  non-thermal (a) spatial map of  
 1452 RECCAP2 multi-model ensemble average, (b) spatial map from pCO<sub>2</sub> observational data products,  
 1453 and (c) box-whisker plot of RECCAP2 multi-model ensemble medians, interquartile ranges, and  
 1454 outliers pooled into Fay and McKinley biomes (Figure S2).  
 1455

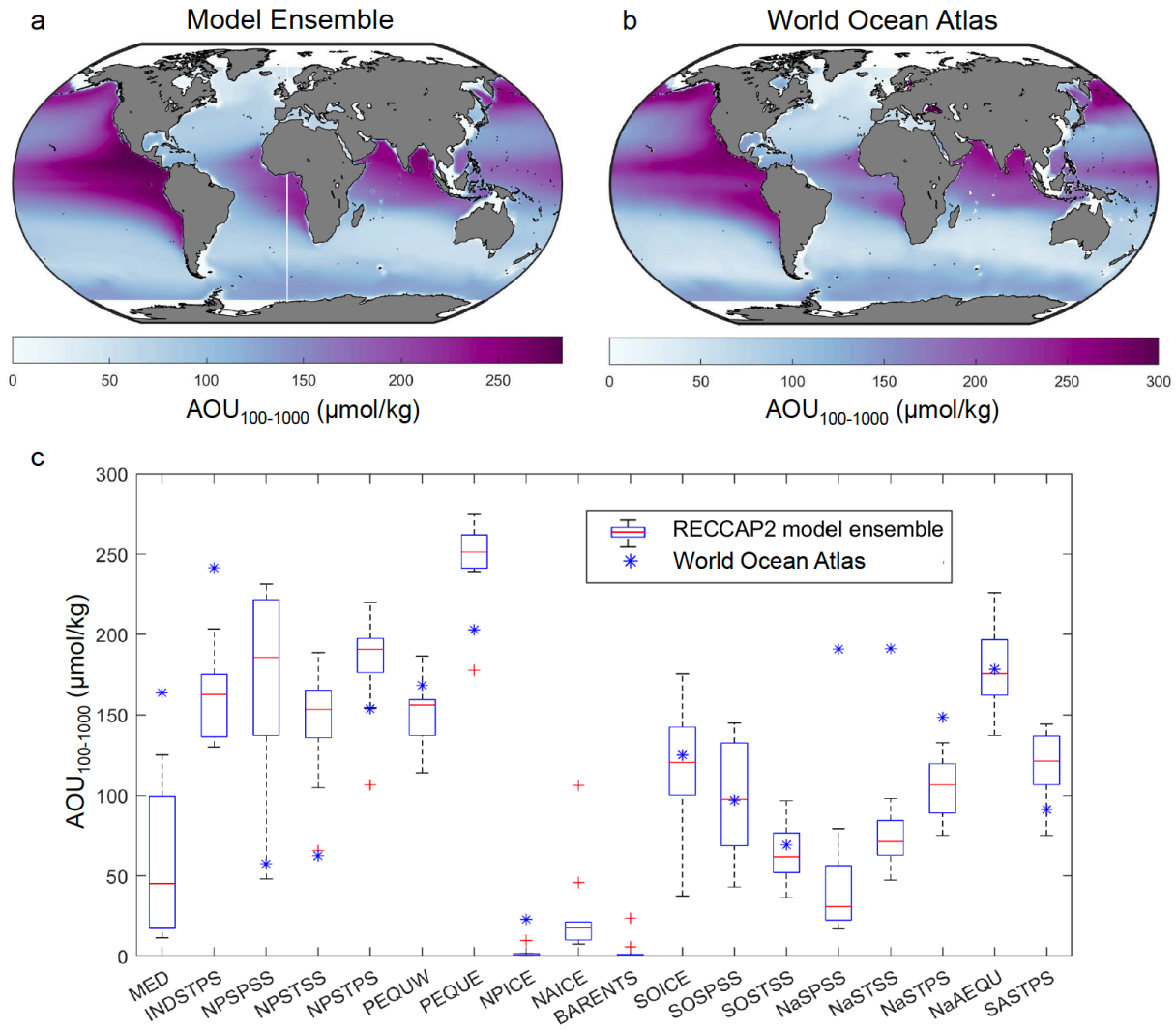


**Figure S4.** Analysis of apparent oxygen utilization (AOU) vertically averaged over the mesopelagic zone (100-1000 m) (a) spatial map of RECCAP2 multi-model ensemble average, and (b) spatial map from WOA observational data set, and (c) box-whisker plot of RECCAP2 multi-model ensemble medians, interquartile ranges, and outliers pooled into Fay and McKinley biomes (Figure S2).

#### Supporting Information Tables

1467 **Table S1.** Interannual variability (1985-2018) for the RECCAP2 simulations (simulation A) for  
 1468 global-integrated, annual-mean variables: vertically integrated net primary productivity *NPP* and  
 1469 particulate organic carbon export fluxes at 100 m  $F_{100}$  and 1000 m depth  $F_{1000}$ . Interannual  
 1470 variability (standard deviation) are in Pg C  $y^{-1}$ .

1471

	CCSM- WHOI	CESM- ETHZ	CNRM- ESM2	ECCO- Darwin	EC- Earth3	FESOM - RECoM _LR	MOM6- Princeto n	MPIOM - HAMO CC	MRI- ESM2-0	Nor_ES M- OC1.2	ORCA1 -LIM3- PISCES	PlankT OM12
NPP	0.1914	0.3743	0.2000	0.7272	0.2194	0.3878	0.3204	1.5377	0.4127	0.3518	0.2286	0.3655
F100	0.0352	0.0491	0.0304	0.1966	0.0412	0.1079	0.0383	0.2004	0.0736	0.0717	0.0484	0.1447
F1000	0.0024	0.0140	0.0000	0.1107	0.0000	0.0143	0.0000	0.0419	0.0103	0.0283	0.0000	0.0000

1472

1473 **Table S2.** Long-term temporal trends (1985-2018) for the RECCAP2 simulations (simulation A)  
 1474 for global-integrated, annual-mean variables: vertically integrated net primary productivity *NPP*  
 1475 and particulate organic carbon export fluxes at 100 m  $F_{100}$  and 1000 m depth  $F_{1000}$ . Trends are in  
 1476 Pg C  $y^{-1}/year$ ,

1477

	CCSM- WHOI	CESM- ETHZ	CNRM- ESM2	ECCO- Darwin	EC- Earth3	FESOM - RECoM _LR	MOM6- Princeto n	MPIOM - HAMO CC	MRI- ESM2-0	Nor_ES M- OC1.2	ORCA1 -LIM3- PISCES	PlankT OM12
NPP	-0.0140	-0.0172	0.0005	-0.0727	0.0017	-0.0094	0.0102	0.0028	-0.0047	0.0009	0.0190	0.0184
F100	-0.0031	-0.0020	0.0000	-0.0209	0.0000	0.0013	0.0010	0.0001	0.0002	0.0017	0.0029	0.0237
F1000	-0.0002	-0.0002	0.0000	-0.0117	0.0000	0.0004	0.0000	0.0013	0.0000	-0.0001	0.0000	0.0000

1478

1479

1  
2 **Observational and numerical modeling constraints on the global ocean biological**  
3 **carbon pump**

4  
5 **Scott C. Doney<sup>1</sup>, Kayla A. Mitchell<sup>1,2</sup>, Stephanie A. Henson<sup>3</sup>, Emma Cavan<sup>4</sup>, Tim DeVries<sup>5</sup>,**  
6 **Nicolas Gruber<sup>6</sup>, Judith Hauck<sup>7</sup>, Colleen B. Mouw<sup>8</sup>, Jens D. Müller<sup>6</sup>, and Francois W.**  
7 **Primeau<sup>2</sup>**

8  
9 **Submitted, March 4<sup>th</sup>, 2024**

10  
11 <sup>1</sup> Department of Environmental Sciences, University of Virginia, Charlottesville, VA, USA,

12 <sup>2</sup> Department of Earth System Science, University of California, Irvine, Irvine, CA, USA,

13 <sup>3</sup> National Oceanography Centre, Southampton, UK,

14 <sup>4</sup> Department of Life Sciences, Silwood Park Campus, Imperial College London, Berkshire, UK,

15 <sup>5</sup> Earth Research Institute and Department of Geography, University of California, Santa

16 Barbara, Santa Barbara, CA, USA,

17 <sup>6</sup> Environmental Physics, Institute of Biogeochemistry and Pollutant Dynamics, ETH Zurich,  
18 Zürich, Switzerland

19 <sup>7</sup> Alfred-Wegener-Institut, Helmholtz-Zentrum für Polar- und Meeresforschung, Bremerhaven,  
20 Germany

21 <sup>8</sup> Graduate School of Oceanography, University of Rhode Island, Narragansett, RI, USA.

22

23 Corresponding author: Scott Doney ([sdoney@virginia.edu](mailto:sdoney@virginia.edu)) ORCID: 0000-0002-3683-2437

24

25 **Key Points:**

26

- 27 • Global-scale, ocean biogeochemical simulations are compared with observation-based  
estimates of the marine biological carbon pump.
- 28 • A multi-model ensemble exhibits relatively good agreement with observation-based  
metrics for carbon export flux and transfer efficiency.
- 30 • Based on identified model-observation and inter-model differences, we provide guidance  
31 for future model evaluations and development.

32

33 **Abstract**

34 This study characterized ocean biological carbon pump metrics in the second iteration of  
35 the REgional Carbon Cycle Assessment and Processes (RECCAP2) project, a coordinated,  
36 international effort to constrain contemporary ocean carbon air-sea fluxes and interior carbon  
37 storage trends using a combination of observation-based estimates, inverse models, and global  
38 ocean biogeochemical models. The analysis here focused on comparisons of global and biome-  
39 scale regional patterns in particulate organic carbon production and sinking flux from the  
40 RECCAP2 model ensemble against observational products derived from satellite remote sensing,  
41 sediment traps, and geochemical methods. There was generally encouraging model-data  
42 agreement in large-scale spatial patterns, though with substantial spread across the model ensemble  
43 and observational products. The global-integrated, model ensemble-mean export production, taken  
44 as the sinking particulate organic carbon flux at 100 m ( $6.41 \pm 1.52 \text{ Pg C yr}^{-1}$ ), and export ratio  
45 defined as sinking flux divided by net primary production ( $0.154 \pm 0.026$ ) both fell at the lower end  
46 of observational estimates. Comparison with observational constraints also suggested that the  
47 model ensemble may have underestimated regional biological CO<sub>2</sub> drawdown and air-sea CO<sub>2</sub> flux  
48 in high productivity regions. Reasonable model-data agreement was found for global-integrated,  
49 ensemble-mean sinking particulate organic carbon flux into the deep ocean at 1000 m ( $0.95 \pm 0.64$   
50 Pg C yr<sup>-1</sup>) and the transfer efficiency defined as flux at 1000m divided by flux at 100m ( $0.121 \pm$   
51 0.035), with both variables exhibiting considerable regional variability. Future modeling studies  
52 are needed to improve system-level simulation of interaction between model ocean physics and  
53 biogeochemical response.

54

55 **Plain Language Summary**

56 Phytoplankton in the surface ocean create each year an amount of organic carbon  
57 approximately equivalent to all the annual photosynthesis by plants on land. A small fraction of  
58 this newly formed organic carbon is exported below the surface layer, and an even smaller amount  
59 makes it all the way to the deep ocean. The transport of organic carbon to the sub-surface ocean,  
60 called the biological carbon pump, influences the global-scale distributions of ocean nutrients,  
61 oxygen, and inorganic carbon as well as the amount of carbon dioxide in the atmosphere. The  
62 global rates and geographic patterns of photosynthesis and carbon flux out of the surface ocean  
63 have previously been constructed from ship measurements and satellite remote sensing. Here, we  
64 compare these observation-based estimates to a suite of three-dimensional, numerical ocean  
65 models and find broadly similar results. The model simulations also capture aspects of the  
66 biological carbon pump deeper in the water column, where there are fewer direct constraints from  
67 field observations. Our comparison of observations and simulations identifies some deficiencies  
68 in the models that should be corrected in order to better simulate climate change impacts on the  
69 biological carbon pump.

70

71 **1 Introduction**

72 Marine biogeochemical processes play a central role in the global Earth System,  
73 modulating the distribution of inorganic carbon, oxygen, and nutrients within the ocean and the  
74 partitioning of carbon between ocean and atmosphere reservoirs (Broecker and Peng, 1982;  
75 Sarmiento and Gruber, 2002; Devries, 2022; Iversen, 2023; Siegel et al., 2023). Because of the

76 strong oceanic influence on atmospheric CO<sub>2</sub> concentration and thus planetary climate, there is  
77 considerable scientific focus on quantifying both the baseline and trends in ocean carbon storage  
78 and fluxes arising from the uptake of anthropogenic CO<sub>2</sub> and climate change impacts on marine  
79 biogeochemical and physical dynamics (Henson et al., 2016; DeVries et al., 2019; Hauck et al.,  
80 2020; Canadell et al., 2021; Crisp et al., 2022; Wilson et al., 2022; Gruber et al., 2023). The  
81 REgional Carbon Cycle Assessment and Processes (RECCAP) project is a coordinated,  
82 international effort to constrain contemporary ocean carbon air-sea fluxes and interior storage  
83 trends using a combination of observation-based estimates, inverse models, and global ocean  
84 biogeochemical models (GOBMs) (Wanninkhof et al., 2013; Khatiwala et al., 2013). The second  
85 phase, RECCAP2, extends the original synthesis using additional years of ocean observations and  
86 updated methodology and numerical results (DeVries et al., 2023; Hauck et al., 2023) as well as  
87 expanding the scope of the analysis, in this case into biological carbon pump magnitude and  
88 efficiency.

89 In a simple 1-D form, the marine biological carbon pump can be viewed as the net  
90 production of particulate organic carbon (POC) and inorganic carbon (PIC) in the surface ocean,  
91 downward vertical transport of particulate carbon into the thermocline and deep sea, and  
92 subsequent respiration and remineralization of particulate carbon back into dissolved inorganic  
93 carbon (DIC) (Volk and Hoffert, 1985). The downward organic carbon transport, or export flux,  
94 drives subsurface marine biogeochemistry, fuels deep-ocean ecosystems, and influences ocean  
95 carbon storage and atmospheric CO<sub>2</sub>. The biological pump accentuates the vertical gradient in DIC  
96 already established from CO<sub>2</sub> system thermal solubility and temperature gradients, and deep-ocean  
97 carbon storage reflects a net balance between the biological carbon pump source and physical  
98 ocean circulation processes that return elevated deep-ocean DIC waters back to the surface ocean  
99 via upwelling and vertical mixing (Sarmiento and Gruber, 2006). The relationship between ocean  
100 carbon storage and the strength of the biological pump is not necessarily straightforward because  
101 of physical-biological interactions; for example, stronger overturning circulation can enhance both  
102 biological export through increased nutrient supply and the physical return of high-DIC deep-  
103 ocean waters to the surface (Doney et al., 2006). The vertical structure of the biological carbon  
104 pump is also important. Sinking POC fluxes decline rapidly in the thermocline (0 to ~1000 m  
105 depth), with only a fraction of surface export flux reaching the deep ocean below 1000 m (Martin  
106 et al., 1987; Lutz et al., 2007; Lima et al., 2014; Dinauer et al., 2022). Deeper remineralization  
107 depths, that is the transport of a greater fraction of POC into the lower thermocline or deep ocean  
108 prior to respiration, enhances ocean carbon storage because of generally reduced physical return  
109 rates to the surface ocean for deeper waters, and therefore longer retention times for the  
110 remineralized DIC, although with substantial regional variations associated with circulation  
111 pathways and rates (Kwon et al., 2009; Siegel et al., 2021).

112 Net primary production (NPP) by surface ocean phytoplankton generates POC and  
113 dissolved organic carbon (DOC), and most marine NPP is converted rapidly back to DIC through  
114 zooplankton grazing of living biomass and detritus or through the microbial loop involving  
115 consumption of POC and DOC pools. Export fluxes require an excess of community production  
116 of organic carbon over respiration that in turn must be supported by an external supply of new  
117 nutrients over sufficient time and space scales (Ducklow and Doney, 2013). The fraction of NPP  
118 that is exported (export ratio = export flux/NPP), is modulated by the magnitude and seasonality  
119 of NPP, environmental conditions, and phytoplankton and zooplankton community composition  
120 (Laufkötter et al., 2016). Export flux from the euphotic zone occurs through multiple pathways  
121 including gravitational sinking of POC (e.g., living and dead cells; fecal pellets; marine snow),

122 physical subduction and mixing of POC and DOC below the surface layer, and active biological  
123 transport by vertically migrating organisms (Siegel et al., 2016). Contemporary models capture,  
124 with varying levels of sophistication and skill, biological processes involved in NPP and export  
125 flux from the upper ocean (Fennel et al., 2022), though models tend to focus on gravitational  
126 particle sinking and many do not incorporate all of the relevant export pathways (Boyd et al., 2019;  
127 Henson et al., 2022) or dynamics governing vertical carbon fluxes from the surface to the deep sea  
128 (Burd, 2024). Here we focus on simulated export via gravitational particle sinking, which is  
129 incorporated in virtually all global ocean biogeochemical models in some form. Observation-based  
130 estimates of the global export flux have a large range ( $\sim 5\text{--}12 \text{ Pg C yr}^{-1}$ ; Siegel et al., 2016), which  
131 is almost identical to the range in export estimates for the modern-day era simulated by coupled  
132 climate models ( $4.5\text{--}12 \text{ Pg C yr}^{-1}$ ; Henson et al., 2022), i.e. the observations-based estimates of  
133 export flux provide a poor constraint for biogeochemical models. Because of differences in model  
134 climate responses and parameterizations of the ocean biological carbon pump, substantial  
135 uncertainties also plague projections of future changes in export flux in response to climate change.  
136 For example, Henson et al. (2022) found a large inter-model spread in projected changes in export  
137 flux by 2100 of between  $+0.16$  and  $-1.98 \text{ Pg C yr}^{-1}$  ( $+1.8$  to  $-41\%$ ) under the high-emission SSP5-  
138 8.5 scenario.

139 Much of the export flux of organic carbon from the euphotic zone, taken here as the  
140 downward flux through 100m ( $F_{100}$ ), is consumed by respiration in the mesopelagic zone (100 –  
141 1000 m). The diverse mechanisms for vertical transport and remineralization of organic matter in  
142 the mesopelagic are only partially captured in models (Fennel et al., 2022). A steep decline with  
143 depth in the gravitational sinking flux of particles is well documented from mid-depth sediment  
144 traps (e.g., Lutz et al., 2007; Lima et al., 2014; Dinauer et al., 2022), but the exact processes  
145 involved are less well quantified and may include physical and biological particle fragmentation  
146 (Briggs et al., 2020) as well as particle consumption and repackaging by zooplankton (Stukel et  
147 al., 2019). Particle fluxes and the depth-scale of remineralization are affected by particle  
148 composition, size, density, and sinking speeds. Particles can vary widely from small, slowly  
149 sinking dead cells and detrital material, to large marine snow aggregates with enhanced sinking  
150 speeds from captured ballast material, to large rapidly sinking fecal pellets (Lam et al., 2011;  
151 Omand et al., 2020). Vertical migrators transport organic carbon downward from the euphotic  
152 zone into the mesopelagic, respiring  $\text{CO}_2$  and releasing fecal pellets at depth (Archibald et al.,  
153 2019). Sinking particle fluxes and mesopelagic biological processes typically are not modeled in  
154 great mechanistic detail in contemporary global ocean biogeochemical models, and often relatively  
155 simplistic empirical relationships such as variants of the Martin power-law flux curve (Martin et  
156 al., 1987) are used in place of explicit representation of the processes controlling mesopelagic flux  
157 attenuation.

158 The proportion of sinking exported POC that survives remineralization in the mesopelagic  
159 zone to reach depths  $> 1000$  meters is referred to as the transfer efficiency, given here as the ratio  
160 of sinking fluxes at 100 and 1000 meters ( $E_{1000/100}$ ). POC reaching 1000m depth is remineralized  
161 below the main thermocline and is likely sequestered on timescales of  $>100$  years, thus  
162 contributing to the long-term ocean carbon sink (Siegel et al., 2021). There is currently little  
163 consensus on the global magnitude or spatial patterns of transfer efficiency, with some approaches  
164 suggesting that  $E_{1000/100}$  is high at high latitudes and low at low latitudes (Marsay et al., 2015;  
165 Weber et al., 2016; DeVries and Weber, 2017), whilst others imply the opposite pattern (Lam et  
166 al., 2011; Henson et al., 2012; Guidi et al., 2015; Mouw et al., 2016b; Dinauer et al. 2022). A  
167 variety of approaches have been used to generate these estimates, including paired in situ

168 observations of  $^{234}\text{Th}$ -derived export flux and deep sediment trap flux (Henson et al. 2012), vertical  
169 profiles of flux from drifting sediment traps (Marsay et al., 2015) or inverting the observed nutrient  
170 and/or oxygen distributions using an inverse model (Weber et al., 2016; Devries and Weber, 2017;  
171 Cram et al., 2018). The differing approaches, and differing time and space scales that they integrate  
172 over, are likely a significant source of the uncertainty in global  $E_{1000/100}$  patterns. In CMIP6  
173 models, there are substantial differences in both the preindustrial mean  $E_{1000/100}$  (varying from 3%  
174 to 25% across models) and its response to 21<sup>st</sup> century climate change, with projections showing  
175 both increases and decreases in  $E_{1000/100}$  over time (Wilson et al., 2022).

176 Early model skill assessments relied heavily on model-data comparisons to transient  
177 tracers, ocean physics, and sub-surface nutrient and oxygen fields that reflect the imprint of  
178 biological pump fluxes and ocean circulation (e.g., Matsumoto et al., 2004; Doney et al. 2004;  
179 Najjar et al. 2007). However, observational constraints on the ocean biological carbon pump have  
180 advanced considerably since the early global 3-D ocean biogeochemical modelling efforts (e.g.,  
181 Bacastow and Maier-Reimer, 1990; Maier-Reimer, 1993). Global-scale data compilations of  
182 primary production, surface export and mesopelagic sinking carbon fluxes are now available based  
183 on a wealth of satellite remote sensing, sediment traps, and geochemical methods (e.g., Henson et  
184 al. 2012; Mouw et al., 2016a). Past model-data skill assessments using multi-model ensembles  
185 have highlighted differences in simulated ocean biological carbon pump patterns, magnitudes, and  
186 mechanisms and identified model biases relative to admittedly imperfect observational estimates  
187 (Laufkötter et al., 2015; Laufkötter et al., 2016). This study expands on these past assessment  
188 efforts of the ocean biological carbon pump to include the current generation of global ocean  
189 biogeochemical models compiled for RECCAP2 (DeVries et al., 2023).

190 The objective of this study is to characterize the global-scale biological carbon pump from  
191 RECCAP2 models and compare the simulation results with observation-based metrics. The focus  
192 is on the spatial patterns and global-integrated rates from the multi-model ensemble mean taking  
193 into consideration inter-model spread. Key metrics include export of sinking POC from the surface  
194 euphotic zone and the efficiency of POC transfer through the mesopelagic ocean, both of which  
195 are central to ocean carbon storage. Based on identified model-observation and inter-model  
196 differences, we also provide guidance for future global ocean biogeochemical model evaluations  
197 and development that could include targeted, more detailed analyses of dynamics and biases within  
198 individual RECCAP models.

199

## 200 **2 Methods and Data**

### 201 **2.1 RECCAP2 model simulations and observational data products**

202 This study leveraged a collection of ocean simulation and observational data sets, outlined  
203 in Table 1, assembled for RECCAP2 following standardized protocols and data reporting for  
204 numerical and observation-based pCO<sub>2</sub> products (RECCAP2 Ocean Science Team, 2022; DeVries  
205 et al., 2023; Müller, 2023). The RECCAP2 ocean data sets included monthly surface and annual  
206 ocean interior output for the contemporary period from more than a dozen global ocean  
207 biogeochemical model hindcast simulations, including both forward and data-assimilated models,  
208 along with observation-based surface ocean pCO<sub>2</sub> interpolation products. Many of the models  
209 included in the RECCAP2 suite have been used in the Global Carbon Project to assess the ocean  
210 carbon sink (Hauck et al., 2020; Friedlingstein et al., 2022). Here, we present model results for

1985 to 2018 from RECCAP2 simulation A, which was forced with historical atmospheric reanalysis data and increasing atmospheric CO<sub>2</sub>, and hence represents both steady-state and variable climate processes and both natural, pre-industrial carbon fluxes and anthropogenic carbon fluxes caused by rising atmospheric CO<sub>2</sub> (DeVries et al., 2023).

215

**Table 1.** Description of RECCAP2 global ocean biogeochemical hindcast models, global data-assimilated models, and observation-based products used in this study. For more details see Tables S1 and S2 in DeVries et al. (2023). The World Ocean Atlas (WOA) data set was also used in the model-data evaluation.

220

221 <b>Global hindcast models</b>	222 <b>Data range</b>	223 <b>References</b>
222 CCSM-WHOI	223 1958-2017	224 Doney et al. (2009)
223 CESM-ETHZ	224 1980-2018	225 Lindsay et al. (2014); Yang and Gruber (2016)
224 CNRM-ESM2 -1	225 1980-2018	226 Séférian et al. (2019; 2020); Berthet et al. (2019)
225 EC-Earth3	226 1980-2018	227 Döscher et al. (2021)
226 FESOM-RECoM-LR	227 1980-2018	228 Hauck et al. (2020)
227 MPIOM-HAMOCC	228 1980-2018	229 Ilyina et al. (2013); Mauritzen et al. (2019)
228 MOM6-Princeton	229 1980-2018	230 Liao et al. (2020); Stock et al. (2020)
229 MRI-ESM2-1	230 1980-2018	231 Urakawa et al. (2020); Tsujino et al. (2017)
230 NorESM-OC1.2	231 1980-2018	232 Swinger et al. (2016)
231 NEMO-PlankTOM12.1	232 1980-2018	233 Le Quéré et al. (2016); Wright et al. (2021)
232 ORCA1-LIM3-PISCES	233 1980-2018	234 Aumont et al. (2015)

233

#### 234 **Data-assimilated models**

235 ECCO-Darwin	236 1995-2018	237 Carroll et al. (2020; 2022)
236 SIMPLE-TRIM	237 Climatology	238 DeVries and Weber (2017)

237

#### 238 **pCO<sub>2</sub> interpolation products**

239 CMEMS-LSCE-FFNN	240 1985-2018	241 Chau et al. (2022)
240 JenaMLS	241 1985-2018	242 Rödenbeck et al. (2013); Rödenbeck et al. (2022)
241 MPI-SOMFFN	242 1982-2018	243 Landschützer et al. (2016)
242 NIES-ML3	243 1980-2020	244 Zeng et al. (2022)
243 OceanSODA-ETHZ	244 1985-2018	245 Gregor and Gruber (2021)
244 LDEO_HPD	245 1985-2018	246 Gloege et al. (2022)
245 UOEX_Wat20	246 1985-2019	247 Watson et al. (2020)

246

#### 247 **World Ocean Atlas**

248 Oxygen and AOU	249 Climatology	250 Garcia et al. (2019)
--------------------	-----------------	--------------------------

249

#### 250 **Biological carbon pump metrics**

251 net primary production, export production,	252 and sinking POC flux	253 Climatology	254 Mouw et al. (2016a; 2016b)
--	--------------------------	-----------------	--------------------------------

253

254

255 Spatial 2D model output and pCO<sub>2</sub> interpolation products were provided to RECCAP2  
256 with 1° x 1° resolution at monthly time steps, and 3D model output was resolved at annual time

257 steps. All estimates derived in this study were computed on the  $1^\circ \times 1^\circ$  grid. Global multi-model  
 258 ensembles, spatial integrals and averages were computed as needed from the gridded results. For  
 259 the aggregation to sub-basin ocean regions, ocean biomes based on Fay and McKinley (2014) were  
 260 used in most instances to facilitate consistent regional intercomparison across RECCAP2 studies  
 261 (e.g., Hauck et al., 2023). Longhurst provinces (Supplement Figure S1; Reygondeau et al., 2013)  
 262 were additionally used in some of the biological pump model-observational comparisons to be  
 263 consistent with one of the key observational data synthesis products (Mouw et al., 2016a). The  
 264 notation and units for the biological, chemical and physical variables used in this study are  
 265 described in Table 2. More details on the RECCAP2 ocean data sets can be found in DeVries et  
 266 al. (2023).

267 We also used an observational compilation of surface ocean export production and sinking  
 268 POC flux combined with satellite ocean color data products for primary production synthesized in  
 269 Mouw et al. (2016a) and as aggregated to Longhurst regional provinces in Mouw et al. (2016b).  
 270 The full dataset includes over 15000 individual sediment trap and  $^{234}\text{Th}$  POC flux measurements  
 271 at 673 locations, combined with satellite-derived estimates of NPP. Chlorophyll measurements  
 272 collected from the SeaWiFS sensor on the OrbView-2 ocean color satellite, spanning from August  
 273 1997 to December 2010, were used to derive NPP using the vertically generalized production  
 274 model (VGPM) (Behrenfeld and Falkowski, 1997) on an equal-area grid with 9-km resolution.  
 275 The climatology in Mouw et al. (2016a) used an interpolation approach to combine the satellite  
 276 timeseries and short-deployment (<30 days trap cup intervals) sediment trap POC flux  
 277 measurements at overlapping locations. Over 43% of the POC flux measurements were collected  
 278 after 1997, overlapping with the satellite record. For each POC flux location, median monthly  
 279 values are computed and binned into biogeochemical Longhurst provinces for the climatology.  
 280 The POC flux climatology also has a depth dimension, with depth bins centered at 20 m for a near-  
 281 surface layer, in 50 m intervals in the upper thermocline, and in 200 m intervals from 500 m to  
 282 5000 m.

283  
 284 **Table 2.** Glossary and description of modeled, observed, and derived variables including  
 285 notation and units.  
 286

Variable Name	Units	Output frequency	Description
<b>2D or surface ocean properties</b>			
$p\text{CO}_2$	$\mu\text{atm}$	monthly	Surface ocean $p\text{CO}_2$
$NPP$	$\text{mol C m}^{-2} \text{yr}^{-1}$	monthly	Vertically-integrated net primary production of organic carbon
$F_{100}$	$\text{mol C m}^{-2} \text{yr}^{-1}$	monthly	POC sinking flux at 100 m
$F_{1000}$	$\text{mol C m}^{-2} \text{yr}^{-1}$	monthly	POC sinking flux at 1000 m
<b>3D or Interior Ocean Properties</b>			
T	$^\circ\text{C}$	annual	Seawater potential temperature
S	-	annual	Salinity (PSS-78)
$F_{3D}$	$\text{mol C m}^{-2} \text{yr}^{-1}$	annual	3D field of POC sinking flux

O <sub>2</sub>	mol O <sub>2</sub> m <sup>-3</sup>	annual	Dissolved oxygen concentration
<b>Derived Variables</b>			
$E_{100/NPP} = F_{100}/NPP$	-	monthly	Surface Export Ratio
$E_{1000/100} = F_{1000}/F_{100}$	-	monthly	Mesopelagic Transfer Efficiency
$E_{1000/NPP} = F_{1000}/NPP$	-	monthly	Surface to Deep-sea Export Efficiency
AOU	μmol kg <sup>-1</sup>	monthly	Apparent oxygen utilization

287

288

289 **2.2 Ocean biological pump and biogeochemical metrics**

290 Our analysis utilized biogeochemical model estimates of vertically integrated NPP and  
 291 export fluxes of sinking POC flux across a shallow surface at the approximate base of the euphotic  
 292 zone (100 m,  $F_{100}$ ) and at the base of the main thermocline (1000 m,  $F_{1000}$ ). Note that the 1000 m  
 293 fluxes were not provided for all models (see Figure 2c), and therefore the ensemble means for  $F_{100}$   
 294 and  $F_{1000}$  were constructed from different subsets of RECCAP2 simulations. The export ratio,  
 295  $E_{100/NPP}$ , was computed as the ratio of POC sinking flux at 100 m divided by net integrated primary  
 296 production:

$$297 \quad E_{100/NPP} = \frac{F_{100}}{NPP} \quad (1)$$

298 The transfer efficiency across the 1000 m depth horizon,  $E_{1000/100}$ , was similarly computed as the  
 299 ratio of sinking POC fluxes at 100 m and 1000 m:

$$301 \quad E_{1000/100} = \frac{F_{1000}}{F_{100}} \quad (2)$$

303 A depth of 1000 m is taken as an approximate boundary between the main thermocline with  
 304 ventilation timescales of years to decades and the deep ocean with time-scales of a century and  
 305 longer (Siegel et al., 2021).

306 The relationship between the biological pump and the inorganic CO<sub>2</sub> system was examined  
 307 by partitioning the seasonal variability in surface seawater pCO<sub>2</sub> into thermal and non-thermal  
 308 components following Takahashi et al. (2002). We refer readers interested in a thorough analysis  
 309 of RECCAP2 CO<sub>2</sub> system seasonality to Rodgers et al. (2023). The temperature effect on pCO<sub>2</sub>  
 310 was calculated for isochemical seawater using the approximation  $\frac{\partial(\ln(pCO_2))}{\partial T} = 0.0423 ({}^\circ C^{-1})$  from  
 311 the experimental value from Takahashi et al. (1993). The seasonal cycle in monthly surface  
 312 temperature anomalies relative to the annual mean surface temperature generated a corresponding  
 313 seasonal variation in the thermal (temperature-dependent) pCO<sub>2</sub> component about the pCO<sub>2</sub> annual  
 314 mean:

$$315 \quad pCO_2^{thermal} = (pCO_2)_{mean} \times \exp[0.0423(T_{monthly} - T_{mean})] \quad (3)$$

316

317 Ocean hindcast simulations typically capture quite well the seasonal cycle of sea surface  
318 temperature because the ocean models are forced by atmospheric reanalysis products and heat flux  
319 boundary conditions that effectively contain information on the observed temperature record  
320 (Doney et al., 2007); the same model-data agreement transfers to the thermal pCO<sub>2</sub> seasonal  
321 component. The non-thermal pCO<sub>2</sub> component was computed by subtracting the thermal  
322 component from the monthly pCO<sub>2</sub> values, and the seasonal amplitude  $\Delta pCO_2, \text{non-thermal}$  was  
323 calculated as the seasonal peak-to-trough difference. The non-thermal pCO<sub>2</sub> component reflects  
324 seasonal variations in DIC and alkalinity from biological organic and inorganic carbon production  
325 and remineralization, air-sea CO<sub>2</sub> gas exchange, and physical transport and mixing. Note that the  
326 seasonal phasing of the non-thermal pCO<sub>2</sub> component can be distinct from the phasing of the total  
327 pCO<sub>2</sub> cycle. This is especially the case in the low latitudes, where the thermal component  
328 dominates the seasonal cycle (Takahashi et al., 1993; Landschützer et al., 2018; Rodgers et al.,  
329 2023).

330 We also computed apparent oxygen utilization (AOU) using modeled dissolved oxygen,  
331 salinity, and potential temperature fields. Modeled average AOU at 100 m (AOU<sub>100</sub>) and 1000 m  
332 depth (AOU<sub>1000</sub>) were found using nearest depth bins in model products (bins centered within 50  
333 m of depths). The simulated AOU fields are compared against the World Ocean Atlas (WOA) data  
334 product (Garcia et al., 2019).

335

### 336 3 Results

#### 337 3.1 Simulated ocean biological carbon pump metrics

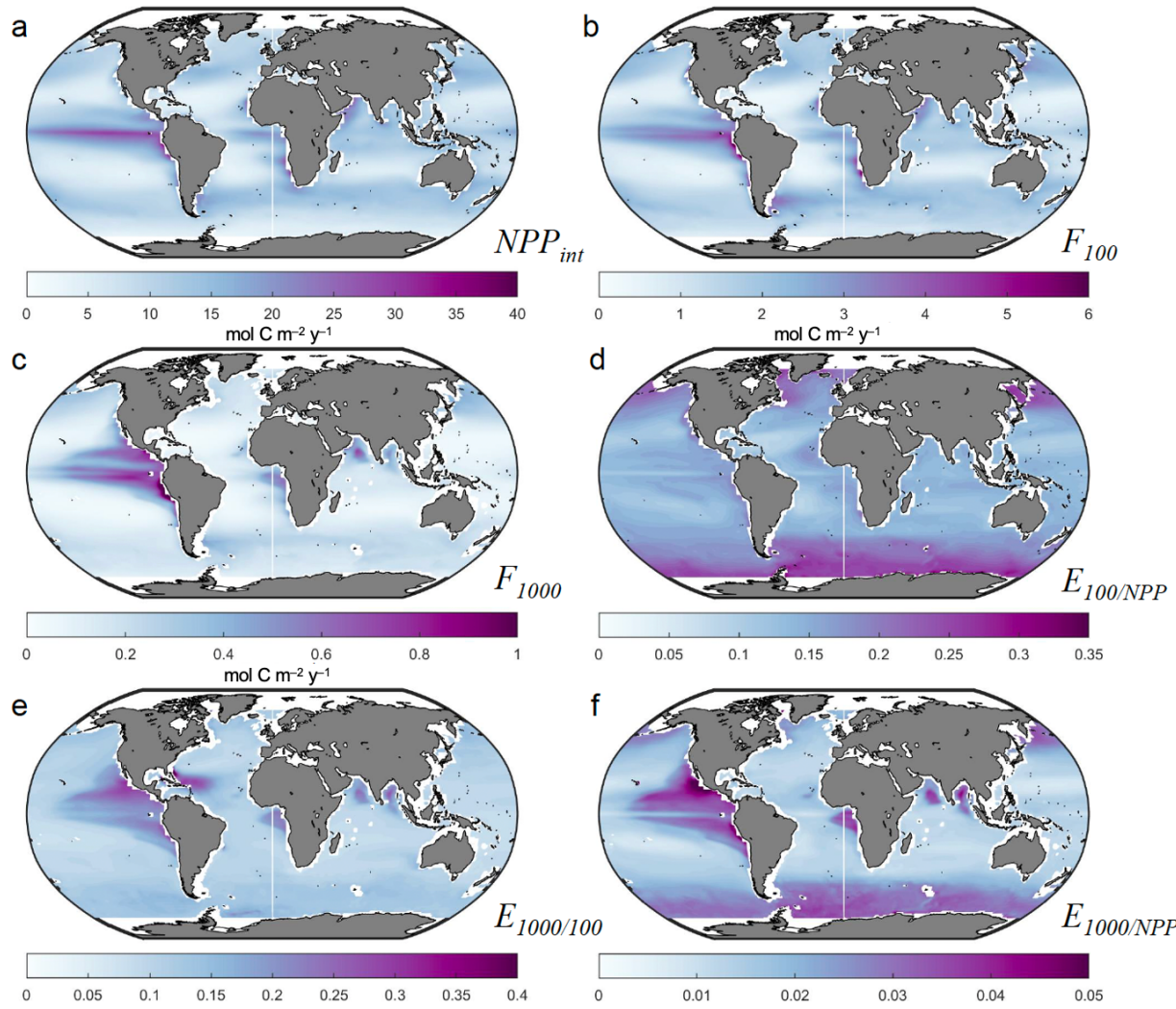
338 Global spatial fields of present-day biological carbon pump variables are displayed in  
339 Figure 1 for the RECCAP2 model ensemble mean with the corresponding ensemble standard  
340 deviation in Figure S1. Biome-scale ensemble-mean averages and within-ensemble standard  
341 deviation values for the biological pump metrics are reported in Table 3 using the standard  
342 RECCAP2 biomes by ocean basin (Figure S2; Fay and McKinley, 2014).

343 The magnitude and spatial patterns of simulated annual mean NPP and export flux from  
344 sinking POC ( $F_{100}$ ) (Figure 1a and 1b) are broadly similar to observational estimates (Section 3.2).  
345 Simulated upper-ocean biological pump variables showed large geographic variations with annual-  
346 mean NPP ranging on biome scales (Table 3) from 8 to 21 mol C m<sup>-2</sup> yr<sup>-1</sup> and  $F_{100}$  ranging from  
347 1.1 to 2.9 mol C m<sup>-2</sup> yr<sup>-1</sup>. The simulated spatial patterns reflect euphotic zone temperature, nutrient  
348 supply, and grazing and loss rates that govern phytoplankton standing stock in the models  
349 (Falkowski et al., 1998; Laufkötter et al., 2015; Laufkötter et al., 2016). The imprint of nutrient  
350 supply was particularly evident in the elevated NPP and export fluxes found in equatorial and  
351 coastal upwelling regions, western boundary currents, and mid-latitude bands of deep seasonal  
352 mixing. Within-ensemble standard deviations ( $\sigma$ ) of NPP and  $F_{100}$  were elevated in the equatorial  
353 band, and high  $\sigma_{NPP}$  values were found also in the Southern Ocean indicating substantial model  
354 disagreement within the ensemble (Figure S1a and S1b). Biome-scale  $\sigma_{NPP}$  values ranged from 2.1  
355 to 6.6 mol C m<sup>-2</sup> yr<sup>-1</sup> (from as low as 0.22 to nearly 0.72 times the ensemble mean in parts of the  
356 Southern Ocean); biome-scale  $\sigma_{F100}$  values varied from 0.4 to >1.0 mol C m<sup>-2</sup> yr<sup>-1</sup> with the largest  
357 absolute and fractional within-ensemble variation of >0.7 times the ensemble mean occurring in  
358 the western equatorial Pacific.

359 The local POC sinking flux at the base of the mesopelagic ( $F_{1000}$ ) ranged at biome scale  
360 from 0.09 to 0.54 mol C m<sup>-2</sup> yr<sup>-1</sup> with broadly similar patterns to  $F_{100}$ , though with some notable  
361 exceptions such as the high  $F_{1000}$  values in tropical low-oxygen zones in the eastern tropical Pacific  
362 and Arabian Sea (Figure 1c). Note the roughly half to full order of magnitude decline in scale in  
363 Figure 1 from NPP to  $F_{100}$  and then  $F_{100}$  to  $F_{1000}$ . This indicates first that the bulk of simulated  
364 NPP is recycled within the euphotic zone above 100 m, rather than exported as sinking POC flux,  
365 and second that most of the sinking POC flux at 100 m is remineralized in the mesopelagic, rather  
366 than reaching the deep ocean below 1000 m. As for NPP and  $F_{100}$ , some correspondence was found  
367 for the spatial patterns of ensemble-mean  $F_{1000}$  and  $\sigma_{F1000}$ . Highest biome-scale  $\sigma_{F1000}$  values of  
368 0.26 to 0.29 mol C m<sup>-2</sup> yr<sup>-1</sup> occurred in the North Pacific and eastern equatorial Pacific, equal to  
369 0.85 and 0.53 times the ensemble-mean  $F_{1000}$  for those biomes; biome-scale  $\sigma_{F1000}$  values of ~0.5  
370 or more of the ensemble-mean were common, with even higher fractional values locally such as in  
371 the eastern subtropical North Pacific (Figure S1c; Table 3).

372 The fraction of NPP exported across 100 m, or export ratio ( $E_{100/NPP}$ , Figure 1d; Table 3)  
373 varies at the biome scale in the ensemble mean from 0.12 to 0.21 with elevated values in high  
374 latitudes. The spatial patterns for within-ensemble  $E_{100/NPP}$  standard deviation (Figure S1d) mirror  
375 that of the mean  $E_{100/NPP}$  with biome-mean standard deviations of 0.035 to 0.050 in most biomes  
376 and up to 0.091 in the sub-polar Southern Ocean biome where there is more within-ensemble  
377 model spread.

378  
379  
380

381  
382

383 **Figure 1.** Multi-model ensemble averages of biological pump parameters from 1985 to 2018  
 384 across all RECCAP2 model simulations (simulation A). Maps of annual mean (a) integrated net  
 385 primary productivity  $NPP$ , (b) particulate organic carbon export fluxes at 100 m  $F_{100}$ , and (c) 1000  
 386 m depth  $F_{1000}$ , all in  $\text{mol C m}^{-2} \text{ yr}^{-1}$ . Ensemble mean (d) surface export efficiency ratio  $E_{100/NPP} =$   
 387  $F_{100}/NPP$  (Eq. 1), (e) mesopelagic transfer efficiency at 1000 m  $E_{1000/100} = F_{1000}/F_{100}$  (Eq. 2), and  
 388 (f) export efficiency to the deep ocean  $E_{1000/NPP} = F_{1000}/NPP$ , all ratios unitless.

389

390 The ensemble-mean transfer efficiency through the mesopelagic,  $E_{1000/100}$  (Figure 1e; Table  
 391 3), exhibited background levels at the biome-scale of 0.09-0.14 for most biomes and ranging as  
 392 high as 0.18 in the eastern equatorial Pacific biome; sub-biome regional values up to 0.3 occurred  
 393 in the eastern tropical Pacific, western and eastern tropical Atlantic, and Arabian Sea and Bay of  
 394 Bengal. Some ocean biogeochemical models reduce sub-surface POC remineralization in low-  
 395 oxygen zones, using a parameterization based on local oxygen concentrations, driving higher  
 396  $E_{1000/100}$  values in low-oxygen regions such as the eastern tropical Pacific, Arabian Sea and Bay of  
 397 Bengal. Furthermore, POC flux mineral ballasting from Saharan dust deposition, prescribed as an

398 external forcing, is likely an important contributor in at least some models (CCSM-WHOI and  
 399 CESM-ETHZ) to high  $E_{1000/100}$  in the western tropical Atlantic (Lima et al., 2014). The ensemble  
 400  $E_{1000/100}$  standard deviation (Figure S1e) generally followed  $E_{1000/100}$  with particularly large  
 401  $\sigma E_{1000/100}$  values up to 0.3 in the western tropical Atlantic reflecting differences across models in  
 402 the parameterization of POC sinking in the presence of desert dust. The metric  $E_{1000/NPP}$  (Figure  
 403 1f), combining surface export and mesopelagic transfer efficiencies, had generally similar spatial  
 404 patterns to  $E_{1000/100}$  but with lower values, reflecting the small fraction of NPP that sinks below  
 405 1000 m and is sequestered in the deep ocean. More than a factor of two variation was found for  
 406 metric  $E_{1000/NPP}$  across biomes (0.012 to 0.027) with large within-ensemble variation for some  
 407 biomes where the standard deviation approached or exceeded the ensemble mean.

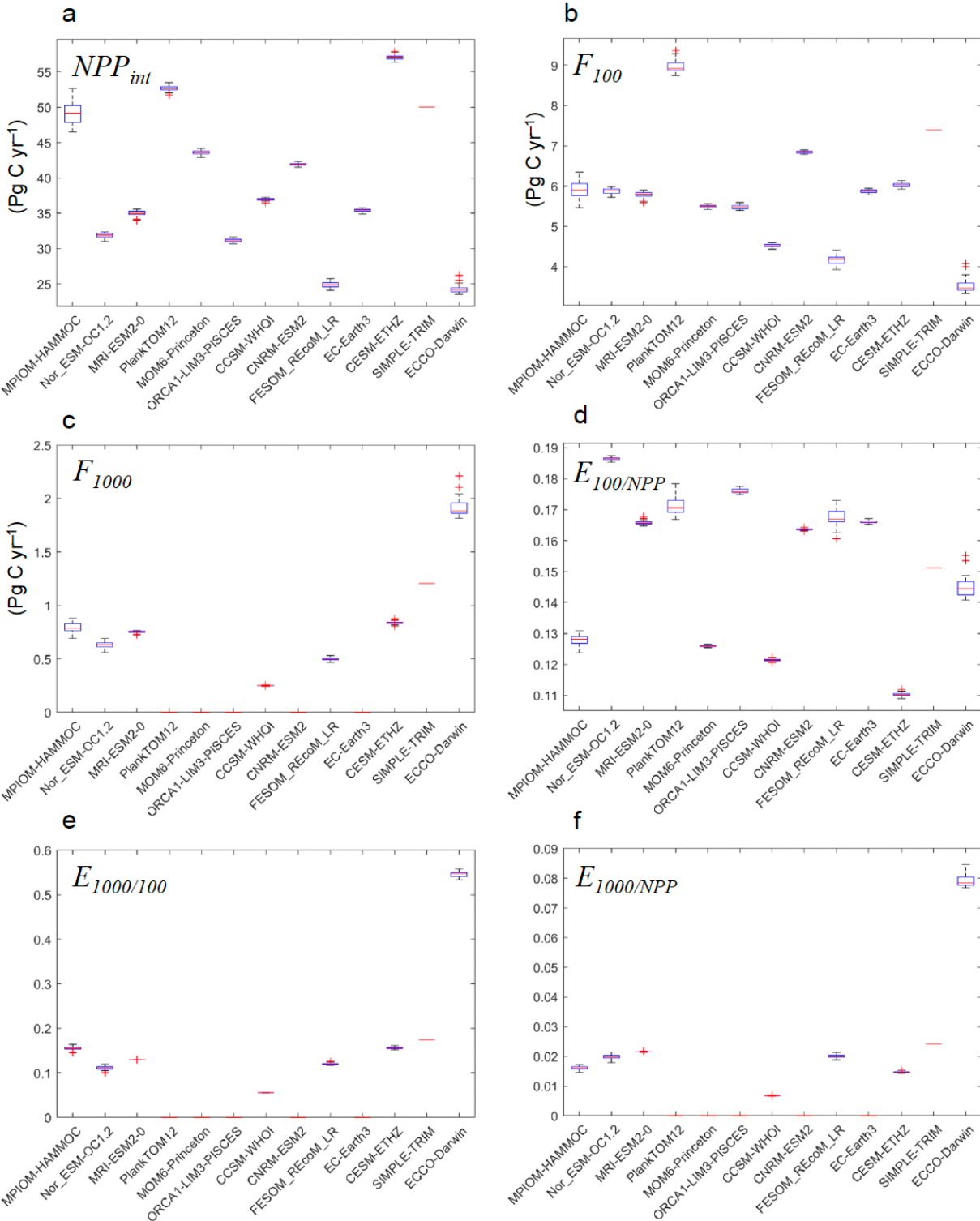
408  
 409 **Table 3.** Model ensemble averages and standard deviations of biological pump parameters by  
 410 RECCAP2 regional biomes (Figure S2) (see also Figure 1) grouped as Sub-Polar Seasonally  
 411 Stratified (SPSS), Sub-Tropical Seasonally Stratified (STSS), Sub-Tropical Permanently Stratified  
 412 (STPS), Equatorial (EQU), and Mediterranean (MED). Table includes annual means and standard  
 413 deviations for vertically integrated net primary productivity  $NPP$ , particulate organic carbon export  
 414 fluxes at 100 m  $F_{100}$ , and 1000 m depth  $F_{1000}$ , all in mol C m<sup>-2</sup> yr<sup>-1</sup>, and average surface export  
 415 efficiency ratio  $E_{100/NPP} = F_{100}/NPP$ , mesopelagic transfer efficiency at 1000 m  $E_{1000/100} =$   
 416  $F_{1000}/F_{100}$ , and export efficiency to the deep ocean  $E_{1000/NPP} = F_{1000}/NPP$ , all ratios unitless.  
 417 Ensemble were not computed for the small, high-latitude polar ice biomes due to noisy and/or  
 418 missing data across the full ensemble.  
 419

	$NPP$	$F_{100}$	$F_{1000}$	$E_{100/NPP}$	$E_{1000/100}$	$E_{1000/NPP}$
<b>SPSS</b>						
N. PACIFIC	11.89±4.81	2.21±0.65	0.307±0.263	0.206±0.076	0.124±0.071	0.018±0.012
N. ATLANTIC	9.30±3.00	1.77±0.65	0.177±0.156	0.211±0.075	0.116±0.060	0.014±0.009
SOUTHERN	9.24±6.64	1.59±0.60	0.197±0.119	0.213±0.091	0.132±0.071	0.023±0.025
<b>STSS</b>						
N. PACIFIC	13.53±3.68	2.04±0.70	0.206±0.117	0.161±0.040	0.114±0.049	0.014±0.006
N. ATLANTIC	12.98±3.28	1.93±0.54	0.165±0.069	0.162±0.049	0.099±0.036	0.014±0.006
SOUTHERN	13.91±5.02	2.12±0.39	0.222±0.087	0.173±0.053	0.109±0.040	0.016±0.009
<b>STPS</b>						
N. PACIFIC	8.92±3.24	1.18±0.61	0.177±0.102	0.131±0.047	0.132±0.049	0.017±0.010
N. ATLANTIC	7.70±2.37	0.97±0.44	0.092±0.057	0.121±0.051	0.140±0.097	0.013±0.008
S. ATLANTIC	9.78±2.16	1.33±0.41	0.138±0.090	0.130±0.043	0.104±0.040	0.012±0.008
INDIAN	16.67±4.75	2.25±0.85	0.284±0.162	0.143±0.035	0.130±0.063	0.016±0.008
<b>EQU</b>						
W. PACIFIC	11.03±5.31	1.44±1.06	0.10±0.078	0.134±0.059	0.089±0.050	0.013±0.011
E. PACIFIC	21.16±5.16	2.91±0.74	0.542±0.288	0.151±0.043	0.178±0.086	0.027±0.015
ATLANTIC	14.33±4.71	1.94±0.65	0.272±0.137	0.145±0.039	0.140±0.043	0.019±0.010
<b>MED</b>	9.21±3.71	1.34±0.79	0.074±0.062	0.141±0.060	0.119±0.107	0.011±0.008

420

421 To illustrate differences among the models making up the RECCAP2 multi-model  
422 ensemble, global integrals of the annual average biological pump metrics are displayed in Figure  
423 2. A box-whisker plot is shown for each model ensemble member quantifying the interannual  
424 variability for each model for the RECCAP2 reporting period (1985-2018). Note that some  
425 RECCAP2 models did not report  $F_{1000}$ , resulting in missing estimates for  $E_{1000/100}$  and  $E_{1000/NPP}$ .  
426 Some models stood out as either anomalously low (e.g. FESOM-REcom-LR for NPP) or high  
427 (e.g. NEMO-PlankTOM12.1 for  $F_{100}$ ) relative to the other RECCAP2 ensemble members, though  
428 inter-model agreement alone was not necessarily a robust indicator of model skill (see Section  
429 3.2). For global  $E_{100/NPP}$ , the models were roughly split into low (0.10-0.12) and high (0.16-0.19)  
430 groups (Figure 2d). Global  $F_{1000}$ ,  $E_{1000/100}$ , and  $E_{1000/NPP}$  varied widely for the smaller number of  
431 available models (Figure 2c, 2e, and 2f).

432

433  
434

435 **Figure 2.** Boxplots showing median values (1985-2018), interannual interquartile ranges, and  
 436 outliers of biological pump metrics across model products in RECCAP2 ensemble (simulation A).  
 437 Globally integrated, annual (a) net primary productivity  $NPP$ , (b) particulate organic carbon export  
 438 fluxes at 100 m  $F_{100}$ , and (c) 1000 m depth  $F_{1000}$ , all in  $\text{Pg C yr}^{-1}$ . Global and annual average (d)

439 surface export efficiency ratio  $E_{100/NPP} = F_{100}/NPP$  (Eq. 1), (e) mesopelagic transfer efficiency at  
 440 1000 m  $E_{1000/100} = F_{1000}/F_{100}$  (Eq. 2), and (f) export efficiency to the deep ocean  $E_{1000/NPP} =$   
 441  $F_{1000}/NPP$ , all ratios unitless. CCSM-WHOI output does not include the year 2018 and SIMPLE-  
 442 TRIM does not simulate interannual variability. Efficiency ratios are not given in panels d, e, and  
 443 f for models lacking the corresponding  $NPP$ ,  $F_{100}$ , or  $F_{1000}$ .  
 444

### 445 3.2 Model-observational comparisons

446 The global ocean biological carbon pump metrics from the RECCAP2 multi-model  
 447 ensemble were compared against corresponding literature values in Table 4 and Figure 3. The  
 448 RECCAP2 multi-model ensemble global-integrated NPP value,  $42.7 \pm 10.9 \text{ Pg C yr}^{-1}$ , was at the  
 449 lower end of literature estimates (43.5-68 Pg C yr $^{-1}$ ), and the inter-quartiles have limited overlap.  
 450 Similarly, global-integrated  $F_{100}$  from the multi-model ensemble of  $6.41 \pm 1.52 \text{ Pg C yr}^{-1}$  was  
 451 lower than the mean of the literature estimates of sinking POC flux ( $\sim 8 \text{ Pg C yr}^{-1}$ , range 4-13 Pg  
 452 C yr $^{-1}$ ), though the inter-quartiles overlapped substantially because of the large range in  
 453 observation-based estimates. The global-integrated model ensemble  $F_{1000}$  value of  $0.95 \pm 0.64 \text{ Pg}$   
 454 C yr $^{-1}$  fell between one low estimate of  $0.66 \text{ Pg C yr}^{-1}$  (Henson et al., 2012) and two other literature  
 455 estimates of  $1.1 \text{ Pg C yr}^{-1}$ . The global multi-model ensemble-mean export and transfer efficiencies,  
 456  $E_{100/NPP}$  ( $0.15 \pm 0.03$ ) and  $E_{1000/100}$  ( $0.12 \pm 0.04$ ), were within the range of literature values after  
 457 removing the high  $E_{100}$  values (0.3 and 0.38) from Laws et al. (2000) and acknowledging one low  
 458 outlier model for global  $E_{1000/100}$  ( $\sim 0.05$ ; CCSM-WHOI; Figure 2e).

459 The wide range of literature estimates reflects differences in measurement methodologies,  
 460 biases, and uncertainties in the datasets used for biological carbon pump metric estimation, as well  
 461 as uncertainties introduced by data sampling biases, aggregation, time/space interpolation and  
 462 modeling approaches. At global scales, in situ observational sampling for some variables remains  
 463 sparse and regionally patchy, and satellites, empirical relationships, and numerical models have  
 464 been used to gap-fill for global-scale product generation. For example, even with field data sets  
 465 available for ocean NPP based on  $^{14}\text{C}$  uptake incubation studies, satellite remote sensing has been  
 466 required to create uniform global NPP products, which have been calibrated/validated against  $^{14}\text{C}$   
 467 NPP field data. A variety of in situ methods have been used to estimate surface ocean export flux  
 468 estimates ( $\sim F_{100}$ ) – drifting sediment traps,  $^{234}\text{Th}$  deficit, etc. To derive global-scale fields of  
 469 export, extrapolation from the limited in situ data is required which generates uncertainties in the  
 470 derived estimates due to the underlying data sparsity (Henson et al., 2024). Typically, satellite data  
 471 is used to build an empirical relationship between flux and readily derived variables, such as sea  
 472 surface temperature or chlorophyll concentration. Other approaches include merging satellite data  
 473 with food-web models (e.g., Siegel et al., 2014). Observation-based global  $F_{1000}$  estimates have  
 474 been generated from sediment trap data (Mouw et al., 2016a), and estimates of both global  $F_{100}$   
 475 and  $F_{1000}$  have been derived from inverse and data-assimilation ocean models (e.g., Devries and  
 476 Weber, 2017; Nowicki et al., 2022).  
 477

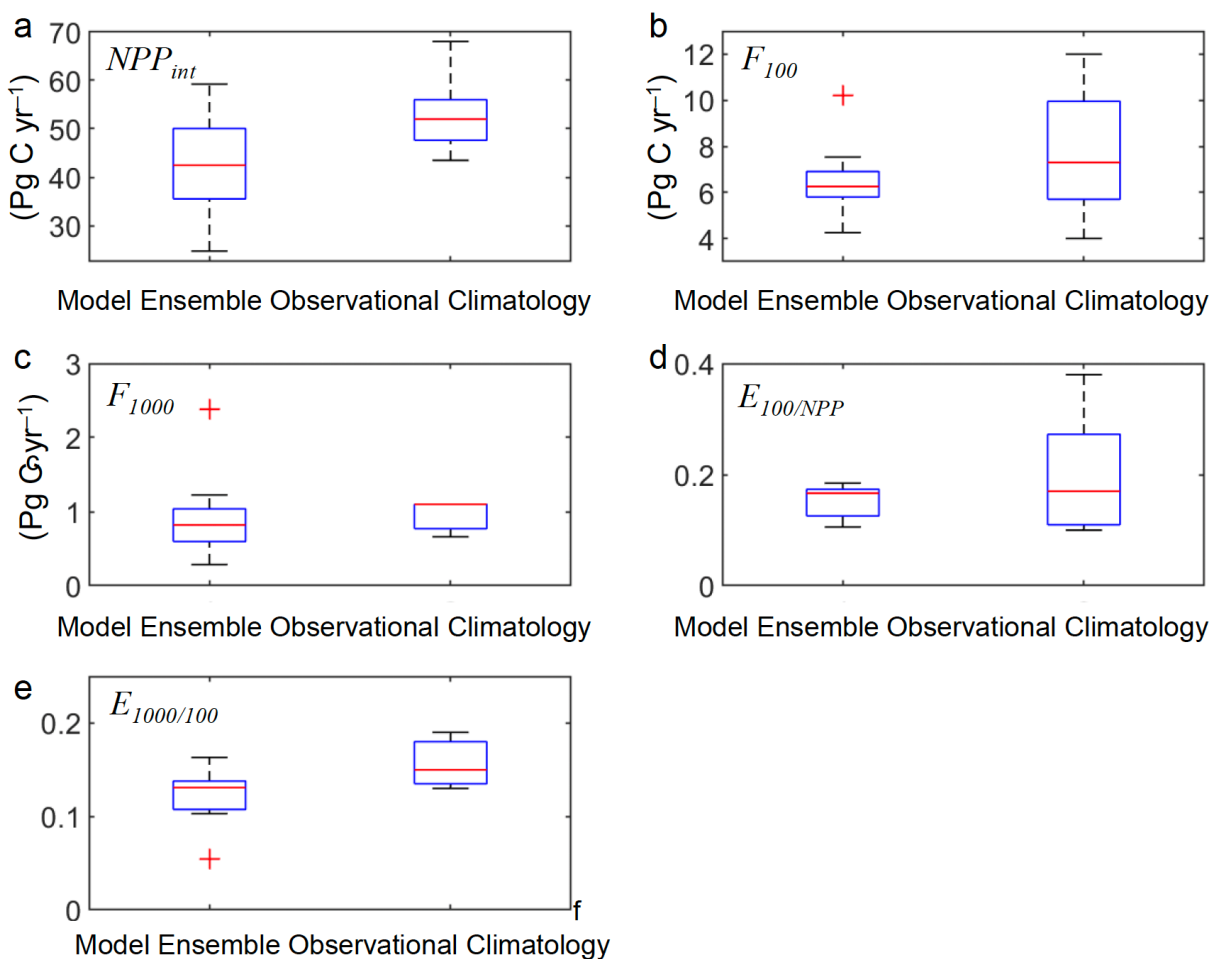
478 **Table 4.** Comparison of literature-based, global observation-based ocean biological carbon pump  
 479 metrics with the RECCAP2 model ensemble means and within-ensemble standard deviations.  
 480 Note that SIMPLE-TRIM data assimilation results from Devries and Weber (2017) are also  
 481 included in the RECCAP-2 model ensemble.

482

Net Primary Production $NPP$ (Pg C $yr^{-1}$ )	References
43.5	VGPM Behrenfeld & Falkowski (1997)
52	CAFÉ Silsbe et al. 2016
68	Carr (2002) & Carr et al. 2006
49	Marra et al. (2003)
52	CbPM2 Behrenfeld et al. 2005
<b>42.7 ± 10.9</b>	<b>RECCAP2 model ensemble mean and STD</b>
POC Export $\sim F_{100}$ (Pg C $yr^{-1}$ )	
4	Henson et al. (2012)
9.6	Dunne et al. (2007)
11.1-12.9	Laws et al. (2000)
5.7	Siegel et al. (2014)
9.6	Schlitzer (2000); inversion
9-13	Laws et al. (2011)
8.8 (7.3 at 100 m)	DeVries & Weber (2017); data assimilating
7.3 (6.4 at 100 m)	Nowicki et al. (2022)
<b>6.41 ± 1.52</b>	<b>RECCAP2 model ensemble-mean and STD</b>
POC Flux 1000 m $F_{1000}$ (Pg C $yr^{-1}$ )	
0.66	Henson et al. (2012)
1.1	DeVries & Weber (2017)
1.1	Nowicki et al. (2022)
<b>0.95 ± 0.64</b>	<b>RECCAP2 model ensemble mean and STD</b>
Export Ratio $\sim E_{100/NPP}$	
0.1	Henson et al. (2012)
0.19	Dunne et al. (2007)
0.3	Laws et al. (2000); food web
0.38	Laws et al. (2000); empirical
0.103	Siegel et al. (2014)
0.17	DeVries & Weber (2017)

0.13 (for POC only)	Nowicki et al. (2022)
0.18 (for POC + DOC + vertical migration)	
<b>0.154 ± 0.026</b>	<b>RECCAP2 model ensemble mean and STD</b>
<b>Transfer Flux Efficiency <math>E_{1000/100}</math></b>	
0.19	Henson et al. (2012)
0.13	DeVries & Weber (2017)
0.15	Nowicki et al. (2022)
<b>0.121 ± 0.035</b>	<b>RECCAP2 model ensemble mean</b>

483



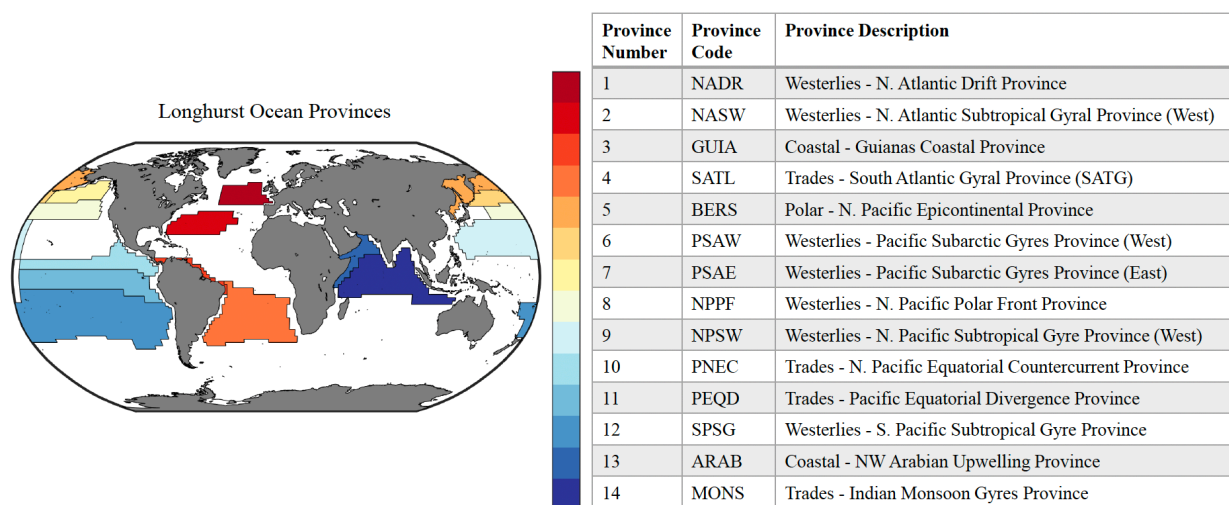
484

485

486 **Figure 3.** Box-whisker plots showing median values and interquartile ranges of biological pump  
 487 parameters from 1985-2018 averaged across model products in RECCAP2 ensemble (simulation  
 488 A). Global integrated, annual (a) net primary productivity  $NPP$ , (b) particulate organic carbon  
 489 export fluxes at 100 m  $F_{100}$ , and (c) 1000 m depth  $F_{1000}$ , all in Pg C yr<sup>-1</sup> (note that the median line  
 490 for  $F_{1000}$  is also the upper interquartile because two of the three observational estimates match).

491 Global and annual average surface export efficiency ratio (d)  $E_{100/NPP} = F_{100}/NPP$  (Eq. 1), and (e)  
492 mesopelagic transfer efficiency at 1000 m  $E_{1000/100} = F_{1000}/F_{100}$  (Eq. 2), all ratios unitless.

493

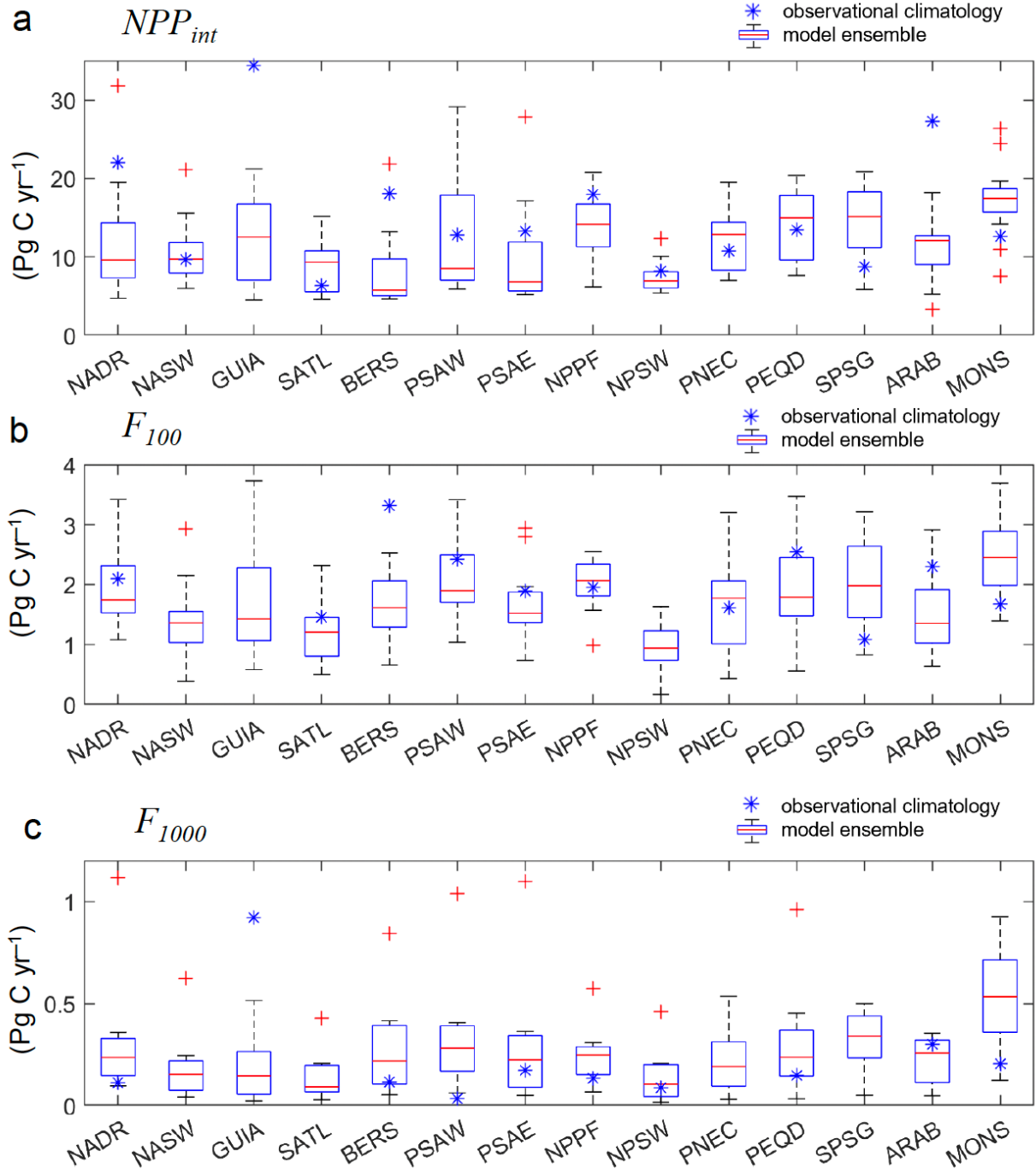


494

495

496 **Figure 4.** Map of Longhurst provinces (Reygondeau et al., 2013) used in analysis of biological  
 497 pump field observations and model results (Mouw et al., 2016a).

498

499  
500

501 **Figure 5.** Box-whisker plot of RECCAP2 multi-model ensemble medians, interquartile ranges,  
 502 and outliers for annual-mean (a) vertical integrated primary production ( $NPP_{int}$ ), (b)  
 503 sinking POC fluxes at 100m ( $F_{100}$ ), and (c) sinking POC flux at 1000m ( $F_{1000}$ ), all in  $\text{Pg C yr}^{-1}$ , pooled into  
 504 biogeochemical Longhurst ocean provinces (Figure 4) and compared to the observational  
 505 climatology for the same provinces constructed by Mouw et al. (2016b). Robust uncertainty  
 506 estimates are not available for the observational climatology which averages available data that is

507 often spatially sparse and/or concentrated in brief time intervals. Note that only provinces with  
 508 sufficient observational data are plotted (see Figure 4).

509

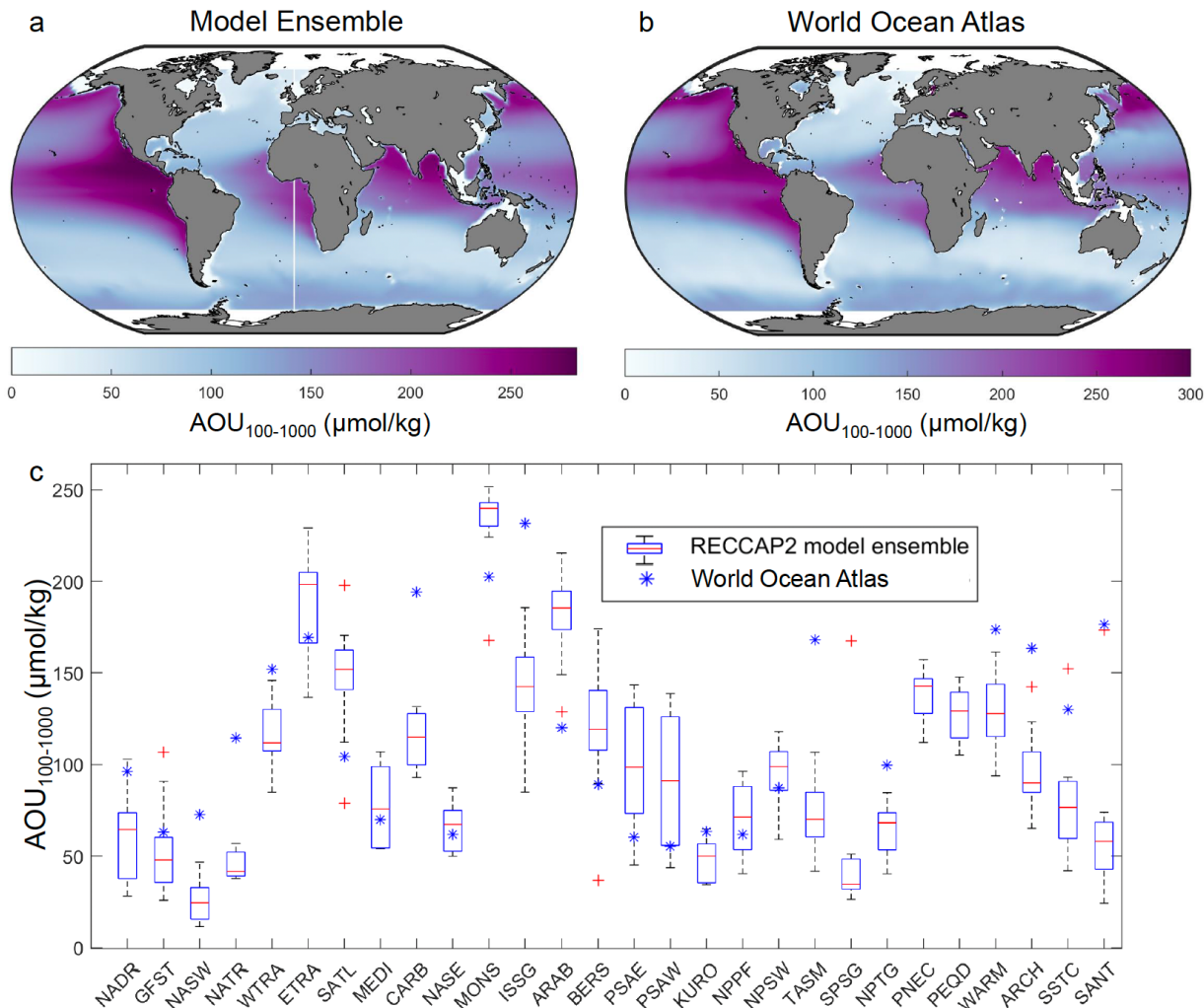
510 The biological carbon pump model comparison to observation-based estimates was  
 511 extended in Figure 5 to a regional level using the observational data of Mouw et al. (2016a) as  
 512 aggregated by Mouw et al. (2016b) into monthly climatological values for Longhurst  
 513 biogeographic provinces (Figure 4). The Mouw et al. (2016a) date set aggregates the limited  
 514 available field data that is often spatially sparse and locally high frequency with considerable  
 515 mesoscale variability, some of which may be aliased into monthly and province scale averages.  
 516 Therefore, robust uncertainty estimates are not available for the Mouw et al. (2016b) observational  
 517 climatology. The variations across the RECCAP2 models are displayed as box-whisker plots. The  
 518 members of the model ensemble exhibited a wide range of NPP,  $F_{100}$  and  $F_{1000}$  values for many  
 519 provinces, but still the observational climatology falls within the multi-model ensemble inter-  
 520 quartiles for only about half of the provinces. The substantial model-observational offsets indicate  
 521 recurring regional differences consistent across multiple models in the RECCAP2 ensemble; these  
 522 disagreements could be targets for future ocean biogeochemical model development and analyses  
 523 of observational sampling biases. The model ensemble members also exhibited extreme model-  
 524 data differences in some provinces where the observational climatology value falls outside the  
 525 simulated range including model outliers. The RECCAP2 models consistently underestimated the  
 526 strength of biological carbon pump metrics, relative to the observational climatology, in polar and  
 527 sub-polar provinces in the North Pacific (N. Pacific epicontinental sea, BERS, low NPP and  $F_{100}$ )  
 528 and North Atlantic (N. Atlantic Drift, NADR, low NPP); and in equatorial provinces in the Indian  
 529 (Northwest Arabian Sea upwelling, ARAB, low NPP), Pacific (Trades-Pacific Equatorial  
 530 Divergence, PEQD, low  $F_{100}$ ) and Atlantic (Guianas coast, GUIA, low  $F_{1000}$ ; note, the observed  
 531 high Guianas coast value reflects a small, productive region that may not be well represented in  
 532 global-scale models). In other provinces, the model ensemble overestimated the biological pump  
 533 in the South Pacific gyre (SPSG, high NPP and  $F_{100}$ ), Indian monsoon gyre (MONS, high NPP  
 534 and  $F_{100}$ ), and Western Pacific subarctic gyres (PSAW, high  $F_{1000}$ ).

535

### 536 **3.3 Biological pump imprint on ocean CO<sub>2</sub> system and biogeochemistry**

537 The ocean biological carbon pump imprints on surface and sub-surface biogeochemistry  
 538 (see Introduction), and these effects are simulated in the RECCAP2 models. A strong positive  
 539 mesopelagic AOU signal is generated by cumulative biological O<sub>2</sub> consumption along the  
 540 ventilation paths of subsurface waters (Najjar et al., 2007). AOU fields thus integrate non-local,  
 541 large-scale biogeochemical dynamics and physical resupply of O<sub>2</sub> from the surface. A key  
 542 contributor to AOU is the remineralization of sinking POC flux in the mesopelagic, quantified by  
 543 the large decline between  $F_{100}$  and  $F_{1000}$  and low transfer efficiency through the mesopelagic  
 544  $E_{1000/100}$  (Figures 1–3; Tables 3 and 4). For the RECCAP2 model ensemble, there was generally  
 545 good model-data agreement in the geographic pattern in AOU averaged over the mesopelagic  
 546 (100–1000 m) (Figure 6). The model ensemble captured the regional AOU variation of <50 to  
 547 >250  $\mu\text{mol kg}^{-1}$ , though substantial disagreement arose on the scale of Longhurst provinces where  
 548 the model-ensemble interquartile spans the observational data for only a handful of provinces  
 549 (Figure 6c). The RECCAP2 models did not exhibit a strong inter-model relationship between  
 550 global mean AOU and  $F_{100}$  (not shown). The weak relationship between AOU and  $F_{100}$  across  
 551 models likely highlights the influence on AOU of substantial variations in the strength of model

552 thermocline ventilation rates that could also influence simulated anthropogenic CO<sub>2</sub> uptake (e.g.,  
 553 Dutay et al., 2002; Matsumoto et al., 2004). Model deep-ocean AOU was not evaluated because  
 554 model spin-up time scales were too short for the simulations to reach steady-state (Séférian et al.,  
 555 2019), an issue that also would affect simulated deep-ocean preindustrial DIC (Mikaloff Fletcher  
 556 et al., 2007). Some imprint of the observational fields used for model initial conditions could also  
 557 be retained in the simulated mesopelagic AOU depending on the model spin-up procedure.  
 558

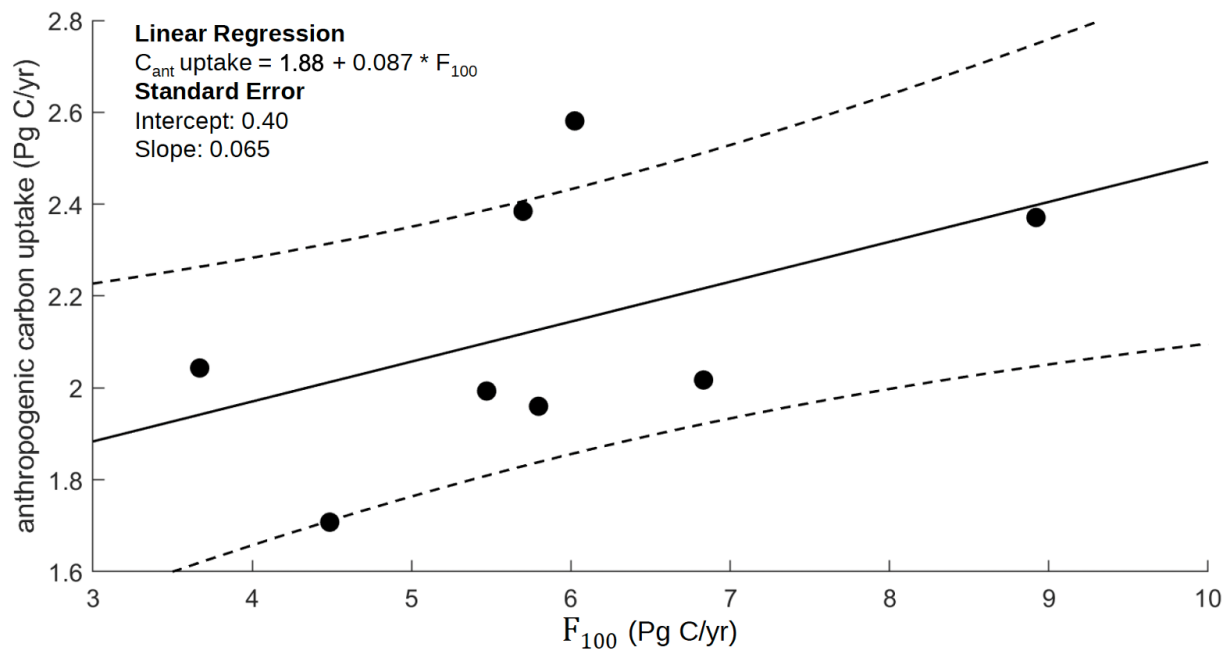


559  
 560  
 561 **Figure 6.** Analysis of apparent oxygen utilization (AOU,  $\mu\text{mol kg}^{-1}$ ) vertically averaged over the  
 562 mesopelagic zone (100-1000 m): (a) spatial map of RECCAP2 multi-model ensemble average,  
 563 and (b) spatial map from WOA observational data set, and (c) box-whisker plot of RECCAP2  
 564 multi-model ensemble medians, interquartile ranges, and outliers pooled into biogeochemical  
 565 Longhurst ocean provinces (Figure 4).  
 566

567 The simulated regional patterns and global integrated surface POC export  $F_{100}$  (Figures 1  
 568 –3; Tables 3 and 4) must be balanced on appropriate time and space scales by new production and  
 569 external nutrient supply, largely from physical upwelling and mixing for most ocean regions

570 (Ducklow and Doney, 2013). As an indicator of physical controls on export associated with  
 571 nutrient supply, the individual RECCAP2 model, global-integrated  $F_{100}$  values exhibited a positive  
 572 correlation with global-ocean anthropogenic CO<sub>2</sub> uptake (Figure 7) (DeVries et al., 2023). This is  
 573 consistent with findings from previous model intercomparison exercises where models with  
 574 stronger thermocline ventilation had both larger export flux and anthropogenic CO<sub>2</sub> uptake (Najjar  
 575 et al., 2007). The  $F_{100}$ –anthropogenic CO<sub>2</sub> uptake correlation, therefore, is indirect through a  
 576 common underlying physical mechanism whereby stronger ventilation enhances both the  
 577 downward transport of anthropogenic CO<sub>2</sub> correlation and the upward transport of nutrients and  
 578 thus  $F_{100}$ . The physical-chemical solubility mechanisms controlling ocean anthropogenic CO<sub>2</sub>  
 579 uptake are well documented, and there is no evidence of any significant role for biogeochemical  
 580 processes, though climate-change biogeochemical feedbacks on ocean carbon storage may become  
 581 more important in the future (Canadell et al., 2021).

582



583

584

585 **Figure 7.** Scatter plot of global-integrated ocean anthropogenic CO<sub>2</sub> uptake (mean of 1985–2018)  
 586 (Pg C yr<sup>-1</sup>) versus particulate organic carbon (POC) export flux ( $F_{100}$ , Pg C yr<sup>-1</sup>) for individual  
 587 RECCAP2 models. Anthropogenic CO<sub>2</sub> uptake for the same RECCAP2 models was taken from  
 588 DeVries et al. (2023). A linear regression and confidence intervals for the regression are overlain.  
 589 The  $F_{100}$ –anthropogenic CO<sub>2</sub> uptake correlation was indirect through a common underlying  
 590 physical mechanism whereby stronger ventilation enhances both the downward transport of  
 591 anthropogenic CO<sub>2</sub> correlation and the upward transport of nutrients and thus  $F_{100}$ .

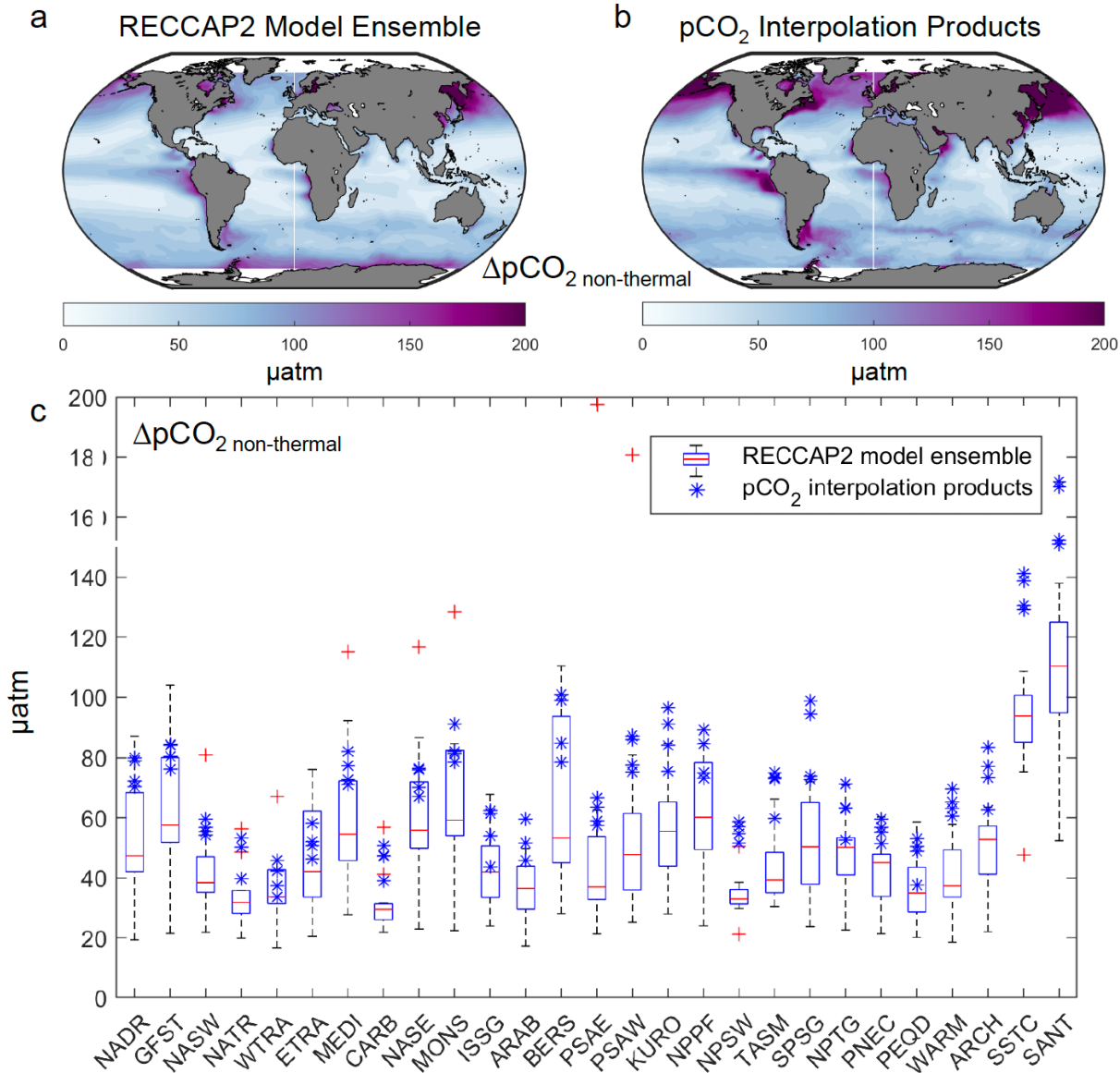
592

593

594 Seasonal variations in upper-ocean biogeochemistry were used as a metric of the physical  
 595 controls associated with seasonal mixing and nutrient supply, which are reflected in simulated  
 596 POC export. By correcting for seasonal thermal variations in pCO<sub>2</sub> (Equation 3), we used model  
 597 monthly pCO<sub>2</sub> fields to quantify the combined effects of seasonal biogeochemical, gas-exchange  
 598 and physical processes through the seasonal amplitude of non-thermal pCO<sub>2</sub>,  $\Delta p\text{CO}_{2,\text{non-thermal}}$   
 (Takahashi et al., 2002). The geographic pattern of  $\Delta p\text{CO}_{2,\text{non-thermal}}$  from the RECCAP2 model

599 ensemble was similar to the pattern from the mean of the  $\text{pCO}_2$  observational products (Figure 8a  
600 and 8b). Both the model ensemble and observational products exhibited regional variations of  
601  $\Delta\text{pCO}_{2,\text{non-thermal}}$  that ranged from 30 to  $>150 \mu\text{atm}$  with elevated values in mid- to high latitudes  
602 as well as equatorial and eastern boundary current upwelling regions. However, the magnitude of  
603  $\Delta\text{pCO}_{2,\text{non-thermal}}$  in the model ensemble was considerably lower in the mid- to high latitude northern  
604 hemisphere, eastern tropical Pacific, and Brazil-Malvinas convergence region, suggesting a  
605 generally weaker modeled seasonal cycling of DIC. The same low bias in the RECCAP2 models  
606 was evident on the scale of Longhurst provinces where the observational products fell at the top  
607 end or well above the model-ensemble interquartile (Figure 8c). In many ocean regions, strong  
608 seasonality in mixed layer depth modulates vertical nutrient supply and annual-mean biological  
609 productivity. The weaker model ensemble  $\Delta\text{pCO}_{2,\text{non-thermal}}$  values (Figure 8), therefore, may be  
610 linked to regional patterns of lower NPP and  $F_{100}$  relative to observations (Figure 5) in the North  
611 Pacific (BERS province), North Atlantic (NADR province), eastern equatorial Pacific (PEQD),  
612 and Brazil-Malvinas convergence (western part of SATL province).

613

614  
615

616 **Figure 8.** Analysis characterizing the combined effects of seasonal biogeochemical, gas-exchange  
617 and physical processes using the seasonal amplitude of non-thermal  $\Delta pCO_{2,non-thermal}$  (a) spatial  
618 map of RECCAP2 multi-model ensemble average, (b) spatial map from pCO<sub>2</sub> observational data  
619 products, and (c) box-whisker plot of RECCAP2 multi-model ensemble medians, interquartile  
620 ranges, and outliers pooled into biogeochemical Longhurst ocean provinces (Figure 4). The  
621 province means from each observational product are plotted in panel (c) as individual points rather  
622 than as box-whiskers because of the limited number of observational products.  
623

#### 624 4 Discussion and Conclusions

625 Our analysis of the ocean biological carbon pump fields from the RECCAP2 multi-model  
626 ensemble revealed generally encouraging agreement with many aspects of observed patterns.

627 Global-integrated NPP and surface export flux ( $F_{100}$ ) from the RECCAP2 models tended to fall at  
 628 the lower end of observational estimates (Figure 3 and Table 4), and geographic patterns in NPP  
 629 were generally consistent with observational data products (Figures 1 and 5). Similar to previous  
 630 model intercomparison studies (Laufkötter et al., 2015; Laufkötter et al., 2016), we found  
 631 substantial within-ensemble variation in global biological carbon pump metrics, including the  
 632 presence of model outliers (Figure 3), indicating that these aspect of biogeochemical models have  
 633 not necessarily converged with time.

634 Regional patterns in the RECCAP2 model-mean ensemble included elevated NPP, surface  
 635 export flux ( $F_{100}$ ) and export efficiency ( $E_{100}$ ) in high-latitudes and coastal and equatorial  
 636 upwelling regions, with lower values in more oligotrophic regions. These results are in line with  
 637 previous studies that found that a substantial proportion of NPP in nutrient-rich regions is driven  
 638 by large phytoplankton such as diatoms and, combined with an active zooplankton population, this  
 639 can generate a significant export flux in the form of both dense aggregates and fecal pellets. High-  
 640 latitude elevated biomass, colder temperatures (Dunne et al., 2005), and strong seasonality also  
 641 have been implicated in observations of higher POC export fluxes in spring and/or summer months  
 642 contributing to the annual mean (Buesseler et al., 2001; Lampitt et al., 2001; Bol et al., 2018;  
 643 Henson et al., 2023). In low nutrient regimes, such as the lower latitude oligotrophic gyres,  
 644 previous studies report export flux to be low (Henson et al., 2012) but relatively constant  
 645 throughout the year with small seasonal increases in fluxes (Karl et al., 2012). Future studies of  
 646 the RECCAP2 ensemble could investigate in more detail the seasonality in NPP,  $F_{100}$ , and  $E_{100}$ ,  
 647 exploring, for example, the seasonal variability in export ratio that can be substantial due in part  
 648 to the time lag between NPP and export flux (Henson et al., 2015; Giering et al., 2017; Laws and  
 649 Maiti, 2019; Henson et al., 2015).

650 The sinking POC flux into the deep ocean ( $F_{1000}$ ) and mesopelagic transfer efficiency  
 651 across the mesopelagic zone ( $E_{1000/100}$ ) in the RECCAP2 multi-model ensemble (Figures 1 and 5)  
 652 exhibited different spatial patterns than found for surface export, similar to findings of previous  
 653 studies (e.g., Henson et al., 2012). Simulated  $F_{1000}$  and  $E_{1000/100}$  were greater in the tropical eastern  
 654 Pacific, eastern Atlantic, and Arabian Sea, and  $E_{1000/100}$  was also elevated in the western tropical  
 655 North Atlantic and, to a lesser extent, Southern Ocean. Previous model studies have also found  
 656 substantial regional variations due to particle size and composition effects (Lima et al., 2014) that  
 657 modify empirical power curves used for modeling POC sinking and remineralization (Martin et  
 658 al., 1987). Model parameterizations tend to increase the effective remineralization length scales  
 659 and thus transfer to depth in regions with high mineral fluxes (e.g., dust,  $\text{CaCO}_3$ , silica) (Armstrong  
 660 et al., 2002) or in tropical oxygen minimum zones (Laufkötter et al., 2017; Dinauer et al., 2022).  
 661 The RECCAP2 regional variations in mesopelagic transfer efficiency, modulated with basin-scale  
 662 variations in physical circulation-driven sequestration time-scale (Siegel et al., 2021), influence  
 663 the effect of the biological pump on ocean carbon storage (Kwon et al., 2009).

664 While we focused primarily on long-term mean NPP and export fluxes, the RECCAP2  
 665 models also exhibited year-to-year variability (Table S1), though typically much lower than  
 666 within-ensemble model differences (Figure 2), and small long-term temporal trends (Table S2).  
 667 No consistent positive or negative trend was observed across the models in simulated NPP and  
 668 sinking POC fluxes at 100m and 1000m, with NPP trends of order  $\pm 0.01 \text{ Pg C yr}^{-1}/\text{year}$  over the  
 669 33 years of the time series (1985-2018). Although these trends could contain a signal from climate  
 670 change, the relatively short duration of the RECCAP2 analysis period resulted in large signal to  
 671 noise due to interannual variability. Previous modeling studies indicate that chlorophyll and NPP

672 time series of 30-40 years length are needed to distinguish climate change trends from natural  
 673 variability (Henson et al., 2010). Hence, the RECCAP2 analysis period may indeed not be long  
 674 enough to separate trends from interannual variability. While a recent study suggests that climate-  
 675 change trends can emerge more rapidly in ocean color remote-sensing reflectance (Cael et al.,  
 676 2023), any actual climate change signal in models may be masked by temporal biases associated  
 677 with incomplete model spin-up and resulting temporal drift (Séférian et al., 2016).

678 Our analysis of the biological carbon pump was relevant in several ways to the primary  
 679 focus of the RECCAP2 ocean project on air-sea CO<sub>2</sub> fluxes and ocean uptake of anthropogenic  
 680 CO<sub>2</sub> (DeVries et al., 2023). Biological net CO<sub>2</sub> uptake and carbon export modulate the background,  
 681 pre-industrial and contemporary spatial and seasonal patterns of surface ocean pCO<sub>2</sub> and sea-air  
 682 CO<sub>2</sub> flux that must be accounted for to determine anthropogenic CO<sub>2</sub> perturbations. The low model  
 683  $F_{100}$  values globally (Figure 3) and for mid- to high-latitude Northern Hemisphere and eastern  
 684 equatorial Pacific provinces (Figure 5), relative to observations, suggested that the RECCAP2  
 685 model ensemble may have underestimated biological CO<sub>2</sub> drawdown in high productivity regions.  
 686 Potential issues were also identified in simulated seasonal biogeochemical, gas-exchange and  
 687 physical dynamics as captured in the seasonal amplitude of non-thermal pCO<sub>2</sub> variations, with  
 688 weaker  $\Delta pCO_{2,non-thermal}$  values found at mid- to high-latitudes and in the eastern equatorial Pacific  
 689 in the model ensemble relative to observations (Figure 8). Future work with more detailed model  
 690 diagnostics could explore the connections between regional biases in simulated annual-mean and  
 691 seasonal export production and biases in air-sea CO<sub>2</sub> flux as observed in other RECCAP2 studies  
 692 (DeVries et al., 2023; Hauck et al., 2023).

693 Ocean circulation modulates biological export flux on basin to global scales (Najjar et al.,  
 694 2007), and the range in RECCAP2 global-integrated  $F_{100}$  values indicated that substantial  
 695 differences exist in simulated ocean physics within the RECCAP2 marine biogeochemical models  
 696 (Doney et al., 2004). The same ocean circulation variations also likely influenced the  
 697 anthropogenic CO<sub>2</sub> uptake estimates from DeVries et al. (2023) as indicated by the positive  
 698 correlation between anthropogenic CO<sub>2</sub> uptake and  $F_{100}$  across individual RECCAP2 models  
 699 (Figure 7). This is supported by further analysis of the RECCAP2 models demonstrating that the  
 700 rate of ocean overturning circulation is strongly correlated with anthropogenic CO<sub>2</sub> uptake in the  
 701 models (Terhaar et al., 2023). Variations in model export could also be compared against metrics  
 702 of physical stratification (Fu et al., 2022). The substantial inter-model spread in both physical and  
 703 biogeochemical metrics likely reflects common factors resulting from differences in simulated  
 704 thermocline ventilation and exchange between the surface and mid-depth ocean.

705 A set of additional model development recommendations emerge from our analyses. One  
 706 path forward would leverage independent model skill evaluation for inert chemical tracers (e.g.,  
 707 CFC-11, CFC-12, SF<sub>6</sub>) using standard ocean model intercomparison protocols (e.g., CMIP6 Ocean  
 708 Model Intercomparison Project; Orr et al., 2017). The transient tracer simulations would help  
 709 decipher the physical-biological factors controlling simulated AOU (Figure 6). Remineralization  
 710 of sinking biological organic matter structures sub-surface ocean dissolved inorganic carbon, O<sub>2</sub>,  
 711 and nutrient fields, a signal that must be addressed in observational estimates of anthropogenic  
 712 CO<sub>2</sub>. While the predominant pathway for ocean anthropogenic CO<sub>2</sub> uptake involves physical-  
 713 chemical dynamics, rather than biological dynamics, the same physical circulation and mixing  
 714 processes influence biogeochemical rates such as nutrient supply. Therefore, evaluation and  
 715 improvement of the ocean biological pump may provide additional insight.

716 The substantial variation in biological pump metrics shown here highlighted the need to  
717 reconcile inter-model and model-observational differences. Challenges arise for model  
718 improvement because there is limited agreement on the appropriate parameterizations for many  
719 key processes of biological carbon export (Henson et al., 2022), subsurface particle sinking, and  
720 remineralization. Many global models include detailed representation of euphotic zone processes  
721 but rather more simplistic representation of mesopelagic processes. Thus, the simulated global-  
722 scale biological carbon pump responses to interannual variability, let alone decadal climate  
723 change, remain poorly constrained (Henson et al., 2016). Following the mechanistic approach  
724 reported in previous model intercomparison studies for primary production (Laufkötter et al.,  
725 2015) and export production (Laufkötter et al., 2016), future studies could emphasize how overall  
726 model behavior reflects differences in model parameterizations, functional equations, and  
727 parameter values in both the euphotic and mesopelagic zones.

728 Opportunities exist to leverage process-level information from lab and field studies to  
729 improve model treatment of POC production, sinking POC flux and extension of export pathways  
730 beyond POC gravitational sinking, for example physical subduction and active migration by  
731 organisms (Boyd et al., 2019; Siegel et al., 2016; Henson et al., 2022; Siegel et al., 2023).  
732 Phytoplankton community structure, captured to some degree in many models, influences  
733 magnitude and composition of export flux from the euphotic zone, the heterotrophic consumers of  
734 sinking POC and zooplankton community structure (Boyd and Newton, 1995; Cavan et al., 2019).  
735 Model treatments could be improved for grazers, such as zooplankton, that act to decrease particle  
736 flux by consuming phytoplankton and sinking POC, while also increasing flux by packaging POC  
737 into fecal pellets with a wide range of sinking speeds (Turner, 2015; Steinberg and Landry, 2017).  
738 Grazer diel vertical migration may also need to be incorporated as a carbon shunt below the depth  
739 horizons of most intense heterotrophic activity (i.e., upper mesopelagic zone), consuming POC in  
740 the surface ocean and respiring it at grazer resident daytime depth (Bianchi et al., 2013). More  
741 mechanistic treatment of particle dynamics may also be feasible. Particle disaggregation,  
742 physically through shear or biologically through fragmentation by grazers, likely contributes  
743 substantially to the decline in POC flux with depth while also providing a POC source for  
744 mesopelagic microbes (Laurenceau-Cornec et al., 2020; Briggs et al., 2020). Microbes also can  
745 reduce POC flux directly, as they constantly attach and detach from sinking POC (Kiørboe et al.,  
746 2002; Kiørboe et al., 2003), hydrolyzing and respiring the POC. While variable particle sinking  
747 speed is included in some model parameterizations, large meta-analyses of empirical data have  
748 struggled to find a strong link between sinking rate and size of particles, because of the vast  
749 variability in particle type, methods used to measure sinking rate, and environment the particles  
750 were collected from (Cael et al., 2021).

751 Many of these process-level insights are already driving progress on mechanistic  
752 parameterizations for sinking particle flux (e.g., Dinauer et al., 2022), vertical migration (e.g.,  
753 Archibald et al., 2019), and other key factors in the marine biological pump. Together with global-  
754 scale ocean biogeochemical data compilations and syntheses (e.g., Mouw et al., 2016a; Mouw et  
755 al., 2016b, Clements et al., 2023) there are now promising new opportunities to evaluate, constrain,  
756 and improve ocean biological carbon pump simulations. Based on the model-data analysis  
757 presented here, the RECCAP2 multi-model ensemble exhibited relatively good agreement with  
758 observed biological carbon pump metrics, where there is sufficient data. The analysis also  
759 identified model-data biases and substantial differences among some of the models included in  
760 RECCAP2. These biases should be used to guide directions for future model development.

761  
762  
763

#### 764 **Funding**

765 S.C. Doney and K.A. Mitchell acknowledge support from the U.S. National Science Foundation  
766 via the Center for Chemical Currencies of a Microbial Planet (NSF 2019589). S.A. Henson  
767 received support from a European Research Council Consolidator grant (GOCART, agreement  
768 number 724416). S. Henson and J. Hauck received support from the European Union's Horizon  
769 2020 research and innovation programme under grant agreement no. 820989 (COMFORT), and  
770 the European Union's Horizon Europe research and innovation programme under grant agreement  
771 no. 101083922 (OceanICU). Funding to J. Hauck was provided by the Initiative and Networking  
772 Fund of the Helmholtz Association (Helmholtz Young Investigator Group Marine Carbon and  
773 Ecosystem Feedbacks in the Earth System, MarESys, Grant VH-NG-1301). J.D. Müller and N.  
774 Gruber acknowledge support from the European Union's Horizon 2020 research and innovation  
775 programme under grant agreement no. 821003 (project 4C) and no. 820989 (project COMFORT).  
776 T. DeVries acknowledges support from NSF grant OCE-1958955. E.L. Cavan was funded by an  
777 Imperial College Research Fellowship.

778

#### 779 **Acknowledgements**

780 Conceptualization (Ideas; formulation or evolution of overarching research goals and aims):  
781 S.C.D, S.A.H.

782 Data curation (Management activities to annotate (produce metadata), scrub data and maintain  
783 research data (including software code, where it is necessary for interpreting the data itself) for  
784 initial use and later re-use): K.A.M, J.D.M.

785 Formal analysis (Application of statistical, mathematical, computational, or other formal  
786 techniques to analyze or synthesize study data): S.C.D., K.A.M., S.A.H.

787 Funding acquisition (Acquisition of the financial support for the project leading to this  
788 publication): S.C.D, S.A.H.

789 Investigation (Conducting a research and investigation process, specifically performing the  
790 experiments, or data/evidence collection): All co-authors

791 Methodology (Development or design of methodology; creation of models): S.C.D., K.A.M.,  
792 S.A.H.

793 Project administration (Management and coordination responsibility for the research activity  
794 planning and execution): S.C.D., S.A.H., J.D.M.

795 Software (Programming, software development; designing computer programs; implementation  
796 of the computer code and supporting algorithms; testing of existing code components): K.A.M.,  
797 J.D.M.

798 Supervision (Oversight and leadership responsibility for the research activity planning and  
799 execution, including mentorship external to the core team): S.C.D, S.A.H., J.D.M.

800 Visualization (Preparation, creation and/or presentation of the published work, specifically  
801 visualization/data presentation): S.C.D., K.A.M.

802 Writing – original draft (Preparation, creation and/or presentation of the published work,  
803 specifically writing the initial draft (including substantive translation)): S.C.D., K.A.M., S.A.H.,  
804 E.C.

805 Writing – review and editing (Preparation, creation and/or presentation of the published work by  
806 those from the original research group, specifically critical review, commentary or revision –  
807 including pre- or post-publication stages): All co-authors

808

## 809 **Open Research**

810 The RECCAP2 ocean data collection can be found in Müller (2023).

811 Müller, Jens Daniel. (2023). RECCAP2-ocean data collection [Data set]. Zenodo.

812 1631 <https://doi.org/10.5281/zenodo.7990823>

813

## 814 **References**

815

816 Archibald, K., Siegel, D. A., & Doney, S. C. (2019) Modeling the impact of zooplankton diel  
817 vertical migration on the carbon export flux of the biological pump. *Global Biogeochemical  
818 Cycles*, 33, 181–199. <https://doi.org/10.1029/2018GB005983>

819

820 Armstrong, R. A., Lee, C., Hedges, J. I., Honjo, S., & Wakeham, S. G. (2001). A new, mechanistic  
821 model for organic carbon fluxes in the ocean based on the quantitative association of POC with  
822 ballast minerals, *Deep Sea Research Part II*, 49, 219–236. [https://doi.org/10.1016/S0967-0645\(01\)00101-1](https://doi.org/10.1016/S0967-<br/>823 0645(01)00101-1)

824

825 Aumont, O., Ethé, C., Tagliabue, A., Bopp, L., & Gehlen, M. (2015). PISCES-v2: An ocean  
826 biogeochemical model for carbon and ecosystem studies. *Geoscientific Model Development*, 8,  
827 2465–2513. <https://doi.org/10.5194/gmd-8-2465-2015>

828

829 Bacastow, R., & Maier-Reimer, E. (1990). Ocean-circulation model of the carbon cycle. *Climate  
830 Dynamics*, 4, 95–125. <https://doi.org/10.1007/BF00208905>

831

832 Behrenfeld, M. J., & Falkowski, P. G. (1997). Photosynthetic rates derived from satellite-based  
833 chlorophyll concentration. *Limnology and Oceanography*, 42, 1–20.  
834 <https://doi.org/10.4319/lo.1997.42.1.0001>

835

836 Behrenfeld, M. J., Boss, E., Siegel, D. A., & Shea, D. M. (2005). Carbon-based ocean  
837 productivity and phytoplankton physiology from space, *Global Biogeochemical Cycles*, 19,  
838 GB1006. <https://doi.org/10.1029/2004GB002299>.

839

840 Berthet, S., Séférian, R., Bricaud, C., Chevallier, M., Volodire, A., & Ethé, C. (2019). Evaluation  
841 of an online grid-coarsening algorithm in a global eddy-admitting ocean-biogeochemical model.  
842 *Journal of Advances in Modeling Earth Systems*, 11(6), 1759–1783.  
843 <https://doi.org/10.1029/2019ms001644>

844

845 Bianchi, D., Stock, C., Galbraith, E. D., & Sarmiento, J. L. (2013). Diel vertical migration:  
846 Ecological controls and impacts on the biological pump in a one-dimensional ocean model.  
847 *Global Biogeochemical Cycles*, 27, 478–491. <https://doi.org/10.1002/gbc.20031>

848

849 Bol, R., Henson, S. A., Rumyantseva, A., & Briggs, N. (2018). High-frequency variability of  
850 small-particle carbon export flux in the Northeast Atlantic. *Global Biogeochemical Cycles*, 32,  
851 1803–1814. <https://doi.org/10.1029/2018GB005963>

852

853 Boyd, P., & Newton, P. (1995). Evidence of the potential influence of planktonic community  
854 structure on the interannual variability of particulate organic carbon flux, *Deep Sea Research*  
855 Part I, 42, 619–639. [https://doi.org/10.1016/0967-0637\(95\)00017-Z](https://doi.org/10.1016/0967-0637(95)00017-Z)

856

857 Boyd, P.W., Claustre, H., Levy, M., Siegel, D. A., & Weber, T. (2019). Multi-faceted particle  
858 pumps drive carbon sequestration in the ocean. *Nature*, 568, 327–335.  
859 <https://doi.org/10.1038/s41586-019-1098-2>

860

861 Briggs, N., Dall'Olmo, G., & Claustre, H. (2020). Major role of particle fragmentation in  
862 regulating biological sequestration of CO<sub>2</sub> by the oceans, *Science*, 367, 791–793.  
863 <https://doi.org/10.1126/science.aay1790>

864

865 Broecker, W. S. and T. H. Peng (1982). *Tracers in the Sea*, Eldigio Press, Palisades, NY, 690 pp.  
866 [https://www.ideo.columbia.edu/~broecker/Home\\_files/TracersInTheSea\\_searchable.pdf](https://www.ideo.columbia.edu/~broecker/Home_files/TracersInTheSea_searchable.pdf)

867

868 Buesseler, K. O., Ball, K. O. L., Andrews, J., Cochran, J. K., Hirschberg, D. J., Bacon, M. P., et  
869 al. (2001). Upper ocean export of particulate organic carbon and biogenic silica in the Southern  
870 Ocean along 170°W, *Deep Sea Research Part II*, 48, 4275–4297. [https://doi.org/10.1016/S0967-0645\(01\)00089-3](https://doi.org/10.1016/S0967-0645(01)00089-3)

872

873 Burd, A. B. (2024). Modeling the vertical flux of organic carbon in the global ocean, *Annual  
874 Review of Marine Science*, 16, 135–161, <https://doi.org/10.1146/annurev-marine-022123-102516>

875

876 Cael, B. B., Cavan, E. L., & Britten, G. L. (2021). Reconciling the size-dependence of marine  
877 particle sinking speed. *Geophysical Research Letters*, 48, e2020GL091771.  
878 <https://doi.org/10.1029/2020GL091771>

879

880 Cael, B. B., Bisson, K., Boss, E., Dutkiewicz, S., & Henson. S. (2023). Global climate-change  
881 trends detected in indicators of ocean ecology. *Nature*, 619, 551–554.  
882 <https://doi.org/10.1038/s41586-023-06321-z>

883

884 Canadell, J. G., Monteiro, P. M. S., Costa, M. H., Cotrim da Cunha, L., Cox, P. M., Eliseev, A.  
885 V., et al. (2021). Global Carbon and other Biogeochemical Cycles and Feedbacks. In *Climate  
886 Change 2021: The Physical Science Basis. Contribution of Working Group I to the Sixth  
887 Assessment Report of the Intergovernmental Panel on Climate Change* [Masson-Delmotte, V., P.  
888 Zhai, A. Pirani, S.L. Connors, C. Péan, S. Berger, N. Caud, Y. Chen, L. Goldfarb, M.I. Gomis,  
889 M. Huang, K. Leitzell, E. Lonnoy, J.B.R. Matthews, T.K. Maycock, T. Waterfield, O. Yelekçi,  
890 R. Yu, and B. Zhou (eds.)]. Cambridge University Press, Cambridge, United Kingdom and New  
891 York, NY, USA, pp. 673–816. <https://doi.org/10.1017/9781009157896.007>

892

893 Carroll, D., Menemenlis, D., Adkins, J. F., Bowman, K. W., Brix, H., Dutkiewicz, S., et al.  
894 (2020). The ECCO-Darwin data-assimilative global ocean biogeochemistry model: Estimates of

895 seasonal to multidecadal surface ocean pCO<sub>2</sub> and air-sea CO<sub>2</sub> flux. *Journal of Advances in*  
896 *Modeling Earth Systems*, 12(10), e2019MS001888.

897

898 Carroll, D., Menemenlis, D., Dutkiewicz, S., Lauderdale, J. M., Adkins, J. F., Bowman, K. W., et  
899 al. (2022). Attribution of space-time variability in global-ocean dissolved inorganic carbon.  
900 *Global Biogeochemical Cycles*, 36(3), e2021GB007162.

901

902 Carr, M. E. (2002). Estimation of potential productivity in Eastern Boundary Currents using  
903 remote sensing, *Deep Sea Research Part II*, 49(1–3), 59–80.

904

905 Carr, M., Friedrichs, M., Schmeltz, M., Noguchiaita, M., Antoine, D., Arrigo, K., & et al. (2006).  
906 A comparison of global estimates of marine primary production from ocean color. *Deep-Sea*  
907 *Research Part II*, 53, 741–770. <https://doi.org/10.1016/j.dsr2.2006.01.028>

908

909 Cavan, E. L., Laurenceau-Cornec, E. C., Bressac, M., Boyd, P. W. (2019). Exploring the ecology  
910 of the mesopelagic biological pump. *Progress in Oceanography*, 176, 102125.  
911 <https://doi.org/10.1016/j.pocean.2019.102125>

912

913 Chau, T. T. T., Gehlen, M., & Chevallier, F. (2022). A seamless ensemble-based reconstruction of  
914 surface ocean pCO<sub>2</sub> and air-sea CO<sub>2</sub> fluxes over the global coastal and open oceans.  
915 *Biogeosciences*, 19(4), 1087–1109. <https://doi.org/10.5194/bg-19-1087-2022>

916

917 Clements, D. J., Yang, S., Weber, T., McDonnell, A. M. P., Kiko, R., Stemmann, L., Bianchi, D.  
918 (2023). New estimate of organic carbon export from optical measurements reveals the role of

919 particle size distribution and export horizon. *Global Biogeochemical Cycles*, 37,  
920 e2022GB007633. <https://doi.org/10.1029/2022GB007633>

921

922 Cram, J. A., Weber, T., Leung, S. W., McDonnell, A. M. P., Liang, J.-H., & Deutsch, C. (2018).  
923 The role of particle size, ballast, temperature, and oxygen in the sinking flux to the deep sea.  
924 *Global Biogeochemical Cycles*, 32, 858–876. <https://doi.org/10.1029/2017GB005710>

925

926 Crisp, D., Dolman, H., Tanhua, T., McKinley, G. A., Hauck, J., Bastos, A., et al. (2022). How  
927 well do we understand the land-ocean-atmosphere carbon cycle? *Reviews of Geophysics*, 60,  
928 e2021RG000736. <https://doi.org/10.1029/2021RG000736>

929

930 DeVries, T. (2022). The ocean carbon cycle, *Annual Review of Environment and Resources*, 47,  
931 317–341. <https://doi.org/10.1146/annurev-environ-120920-111307>

932

933 DeVries, T., & Weber, T. (2017). The export and fate of organic matter in the ocean: New  
934 constraints from combining satellite and oceanographic tracer observations. *Global  
935 Biogeochemical Cycles*, 31, 535–555. <https://doi.org/10.1002/2016GB005551>

936

937 DeVries, T., Le Quéré, C., Andrews, O., Berthet, S., Hauck, J., Ilyina, T., et al. (2019). Decadal  
938 trends in the ocean carbon sink. *Proceedings of the National Academy of Sciences*, 116(24),  
939 11646–11651. <https://doi.org/10.1073/pnas.1900371116>

940

941 DeVries, T., Yamamoto, K., Wanninkhof, R., Gruber, N., Hauck, J., Müller, J. D., et al. (2023).  
942 Magnitude, trends, and variability of the global ocean carbon sink from 1985–2018, *Global  
943 Biogeochemical Cycles*, 37 e2023GB007780. <https://doi.org/10.1029/2023GB007780>

944

945 Dinauer, A., Laufkötter, C., Doney, S. C., & Joos, F. (2022). What controls the large-scale  
946 efficiency of carbon transfer through the ocean's mesopelagic zone? Insights from a new,  
947 mechanistic model (MSPACMAM). *Global Biogeochemical Cycles*, 36, e2021GB007131.  
948 <https://doi.org/10.1029/2021GB007131>

949

950 Doney, S. C., Lindsay, K., Caldeira, K., Campin, J.-M., Drange, H., Dutay, J. C., et al. (2004).  
951 Evaluating global ocean carbon models: The importance of realistic physics. *Global  
952 Biogeochemical Cycles*, 18(3), GB3017. <https://doi.org/10.1029/2003GB002150>

953

954 Doney, S. C., Lindsay, K., Fung, I., J. John, J. (2006). Natural variability in a stable 1000 year  
955 coupled climate-carbon cycle simulation. *Journal of Climate*, 19(13), 3033–3054.  
956 <https://doi.org/10.1175/JCLI3783.1>

957

958 Doney, S. C., Yeager, S., Danabasoglu, G., Large, W. G., McWilliams, J. C. (2007). Mechanisms  
959 governing interannual variability of upper ocean temperature in a global hindcast simulation.  
960 *Journal of Physical Oceanography*, 37, 1918–1938. <https://doi.org/10.1175/JPO3089.1>

961

962 Doney, S. C., Lima, I., Feely, R. A., Glover, D. M., Lindsay, K., Mahowald, N., Moore, J. K.,  
963 Wanninkhof, R. (2009): Mechanisms governing interannual variability in upper-ocean inorganic  
964 carbon system and air-sea CO<sub>2</sub> fluxes: Physical climate and atmospheric dust. *Deep Sea*

965 *Research Part II: Topical Studies in Oceanography*, 56(8–10) 640–655.  
966 <https://doi.org/10.1016/j.dsr2.2008.12.006>

967

968 Döscher, R., Acosta, M., Alessandri, A., Anthoni, P., Arsouze, T., Bergman, T., et al. (2022). The  
969 EC-Earth3 Earth system model for the Coupled Model Intercomparison Project 6. *Geoscientific  
970 Model Development*, 15(7), 2973–3020. <https://doi.org/10.5194/gmd-15-2973-2022>

971

972 Ducklow, H. W., & Doney, S. C. (2013). What is the metabolic state of the oligotrophic ocean? A  
973 debate. *Annual Review of Marine Science*, 5, 525–533. <https://doi.org/10.1146/annurev-marine-121211-172331>

974

975

976 Dunne, J. P., Armstrong, R. A., Gnanadesikan, A., & Sarmiento, J. L. (2005). Empirical and  
977 mechanistic models for the particle export ratio, *Global Biogeochemical Cycles*, 19, GB4026.  
978 <https://doi.org/10.1029/2004GB002390>.

979

980 Dunne, J. P., Sarmiento, J. L., & Gnanadesikan, A. (2007). A synthesis of global particle export  
981 from the surface ocean and cycling through the ocean interior and on the seafloor. *Global  
982 Biogeochemical Cycles*, 21, GB4006. <https://doi.org/10.1029/2006GB002907>

983

984 Dutay, J.-C., Bullister, J. L., Doney, S. C., Orr, J. C., Najjar, R., Caldeira, K., et al. (2002).  
985 Evaluation of ocean model ventilation with CFC-11: comparison of 13 global ocean models.  
986 *Ocean Modelling*, 4, 89–120. [https://doi.org/10.1016/S1463-5003\(01\)00013-0](https://doi.org/10.1016/S1463-5003(01)00013-0)

987

988 Falkowski, P. G., Barber, R. T., & Smetacek, V. (1998). Biogeochemical controls and feedbacks  
989 on ocean primary production. *Science*, 281(5374), 200–206.  
990 <https://doi.org/10.1126/science.281.5374.200>

991

992 Fay, A. R., & McKinley, G. A. (2014). Global open-ocean biomes: mean and temporal  
993 variability. *Earth System Science Data*, 6, 273–284. <https://doi.org/10.5194/essd-6-273-2014>.

994

995 Fennel, K., Mattern, J. P., Doney, S. C., Bopp, L., Moore, A. M., Wang, B., & Yu, L. (2022).  
996 Ocean biogeochemical modelling. *Nature Reviews Methods Primers*, 2, 76.  
997 <https://doi.org/10.1038/s43586-022-00154-2>

998

999 Friedlingstein, P., O’Sullivan, M., Jones, M. W., Andrew, R. M., Gregor, L., Hauck, J., et al.  
1000 (2022). Global carbon budget 2022. *Earth System Science Data*, 14, 4811–4900.  
1001 <https://doi.org/10.5194/essd-14-4811-2022>

1002

1003 Fu, W., Moore, J. K., Primeau, F., Collier, N., Ogunro, O. O., Hoffman, F. M., & Randerson, J. T.  
1004 (2022). Evaluation of ocean biogeochemistry and carbon cycling in CMIP earth system models  
1005 with the International Ocean Model Benchmarking (IOMB) software system. *Journal of  
1006 Geophysical Research: Oceans*, 127, e2022JC018965. <https://doi.org/10.1029/2022JC018965>

1007

1008 Garcia, H. E., Weathers, K., Paver, C. R., Smolyar, I., Boyer, T. P., Locarnini, R. A., et al. (2019).  
1009 World Ocean Atlas 2018, Volume 3: Dissolved Oxygen, Apparent Oxygen Utilization, and

1010 Oxygen Saturation. A. Mishonov Technical Ed., *NOAA Atlas NESDIS 83*, 38pp.  
1011 [https://www.ncei.noaa.gov/sites/default/files/2020-04/woa18\\_vol3.pdf](https://www.ncei.noaa.gov/sites/default/files/2020-04/woa18_vol3.pdf)

1012

1013 Giering, S., Sanders, R., Lampitt, R., Anderson, T. R., Tamburini, C., Boutrif, M., et al. (2014).  
1014 Reconciliation of the carbon budget in the ocean's twilight zone. *Nature*, 507, 480–483.  
1015 <https://doi.org/10.1038/nature13123>

1016

1017 Giering, S. L. C., Sanders, R., Martin, A. P., Henson, S. A., Riley, J. S., Marsay, C. M., & Johns,  
1018 D. G. (2017). Particle flux in the oceans: Challenging the steady state assumption, *Global*  
1019 *Biogeochemical Cycles*, 31, 159–171. <https://doi.org/10.1002/2016GB005424>

1020

1021 Gloege, L., Yan, M., Zheng, T., & McKinley, G. A. (2022). Improved quantification of ocean  
1022 carbon uptake by using machine learning to merge global models and pCO<sub>2</sub> data. *Journal of*  
1023 *Advances in Modeling Earth Systems*, 14(2), e2021MS002620.  
1024 <https://doi.org/10.1029/2021ms002620>

1025

1026 Glover, D. M., Jenkins, W. J., & Doney, S. C. (2011). *Modeling Methods for Marine Science*.  
1027 Cambridge, United Kingdom: Cambridge University Press.  
1028 <https://doi.org/10.1017/CBO9780511975721>

1029

1030 Gregor, L., & Gruber, N. (2021). OceanSODA-ETHZ: A global gridded data set of the surface  
1031 ocean carbonate system for seasonal to decadal studies of ocean acidification. *Earth System*  
1032 *Science Data*, 13(2), 777–808. <https://doi.org/10.5194/essd-13-777-2021>

1033

1034 Gruber, N., Bakker, D.C.E., DeVries, T., Gregor, L., Hauck, J., Landschützer, P., McKinley, G.  
1035 A., & Müller, J. D. (2023). Trends and variability in the ocean carbon sink. *Nature Reviews Earth*  
1036 *and Environment*, 4, 119–134. <https://doi.org/10.1038/s43017-022-00381-x>

1037

1038 Guidi, L., Legendre, L., Reygondeau, G., Uitz, J., Stemmann, L., & Henson, S. A. (2015). A new  
1039 look at ocean carbon remineralization for estimating deep water sequestration. *Global*  
1040 *Biogeochemical Cycles*, 29, 1044–1059. <https://doi.org/10.1002/2014GB005063>

1041

1042 Hauck, J., Zeising, M., Le Quéré, C., Gruber, N., Bakker, D. C. E., Bopp, L., et al. (2020).  
1043 Consistency and challenges in the ocean carbon sink estimate for the global carbon budget.  
1044 *Frontiers in Marine Science*, 7, 571720. <https://doi.org/10.3389/fmars.2020.571720>

1045

1046 Hauck, J., Gregor, L., Nissen, C., Patara, L., Hague, M., Mongwe, P., et al. (2023). The Southern  
1047 Ocean carbon cycle 1985–2018: Mean, seasonal cycle, trends, and storage. *Global*  
1048 *Biogeochemical Cycles*, 37, e2023GB007848. <https://doi.org/10.1029/2023GB007848>

1049

1050 Henson, S. A., Sarmiento, J. L., Dunne, J. P., Bopp, L., Lima, I., Doney, S. C., et al. (2010).  
1051 Detection of anthropogenic climate change in satellite records of ocean chlorophyll and  
1052 productivity. *Biogeosciences*, 7, 621–640. <https://doi.org/10.5194/bg-7-621-2010>

1053

1054 Henson, S. A., Sanders, R., & Madsen, E. (2012). Global patterns in efficiency of particulate  
1055 organic carbon export and transfer to the deep ocean. *Global Biogeochemical Cycles*, 26,  
1056 GB1028. <https://doi.org/10.1029/2011GB004099>

1057

1058 Henson, S. A., Yool, A., & Sanders, R. (2015). Variability in efficiency of particulate organic  
1059 carbon export: A model study, *Global Biogeochemical Cycles*, 29, 33–45.  
1060 doi:10.1002/2014GB004965

1061

1062 Henson, S. A., Beaulieu, C., & Lampitt, R. (2016). Observing climate change trends in ocean  
1063 biogeochemistry: When and where. *Global Change Biology*, 22(4), 1561–1571.  
1064 <https://doi.org/10.1111/gcb.13152>

1065

1066 Henson, S. A., Laufkötter, C., Leung, S. Giering, S. L. C., Palevsky, H. I., & Cavan, E. L. (2022).  
1067 Uncertain response of ocean biological carbon export in a changing world. *Nature Geoscience*,  
1068 15, 248–254. <https://doi.org/10.1038/s41561-022-00927-0>

1069

1070 Henson, S. A., Briggs, N., Carvalho, F., Manno, C., Mignot, A., Thomalla, S. (2023). A seasonal  
1071 transition in biological carbon pump efficiency in the northern Scotia Sea, Southern Ocean. *Deep  
1072 Sea Research Part II*, 208, 105274. <https://doi.org/10.1016/j.dsr2.2023.105274>

1073

1074 Henson, S. A., Kelsey Bisson, K., Hammond, M. L., Martin, A., Mouw, C., Yool, A. (2024).  
1075 Effect of sampling bias on global estimates of ocean carbon export. *Environmental Research  
1076 Letters*, 19, 024009. <http://dx.doi.org/10.1088/1748-9326/ad1e7f>

1077

1078 Ilyina, T., Six, K. D., Segschneider, J., Maier-Reimer, E., Li, H., & Núñez-Riboni, I. (2013).  
1079 Global ocean biogeochemistry model HAMOCC: Model architecture and performance as  
1080 component of the MPI-Earth system model in different CMIP5 experimental realizations.  
1081 *Journal of Advances in Modeling Earth Systems*, 5(2), 287–315.  
1082 <https://doi.org/10.1029/2012ms000178>

1083

1084 Iversen, M. H. (2023). Carbon export in the ocean: a biologist's perspective. *Annual Review of  
1085 Marine Science*, 15, 357–381. <https://doi.org/10.1146/annurev-marine-032122-035153>

1086

1087 Karl, D. M., Church, M. J., Dore, J. E., Letelier, R., & Mahaffey, C. (2012). Predictable and  
1088 efficient carbon sequestration in the North Pacific Ocean supported by symbiotic nitrogen  
1089 fixation, *Proceedings of the National Academy of Sciences USA*, 109, 1842–1849.  
1090 <https://doi.org/10.1073/pnas.1120312109>

1091

1092 Khatiwala, S., Tanhua, T., Mikaloff Fletcher, S., Gerber, M., Doney, S. C., Graven, H. D., et al.  
1093 (2013). Global ocean storage of anthropogenic carbon, *Biogeosciences*, 10, 2169–2191.  
1094 <https://doi.org/10.5194/bg-10-2169-2013>

1095

1096 Kiørboe, T., Grossart, H.-P., Ploug, H., & Tang, K. (2002). Mechanisms and rates of bacterial  
1097 colonization of sinking aggregates, *Applied and Environmental Microbiology*, 68, 3996–4006.  
1098 <https://doi.org/10.1128/AEM.68.8.3996-4006.2002>

1099

1100 Kiørboe, T., Tang, K., Grossart, H.-P., & Ploug, H. (2003). Dynamics of microbial communities  
1101 on marine snow aggregates: colonization, growth, detachment, and grazing mortality of attached  
1102 bacteria, *Applied and Environmental Microbiology*, 69, 3036–3047.  
1103 <https://doi.org/10.1128/AEM.69.6.3036-3047.2003>

1104

1105 Kwon, E., Primeau, F., & Sarmiento, J. (2009). The impact of remineralization depth on the air–  
1106 sea carbon balance, *Nature Geoscience*, 2, 630–635. <https://doi.org/10.1038/ngeo612>

1107

1108 Lam, P. J., Doney, S. C., & Bishop, J. K. B. (2011). The dynamic ocean biological pump:  
1109 Insights from a global compilation of particulate organic carbon, CaCO<sub>3</sub>, and opal concentration  
1110 profiles from the mesopelagic. *Global Biogeochemical Cycles*, 25, GB3009.  
1111 <https://doi.org/10.1029/2010GB003868>.

1112

1113 Lampitt, R. S., Bett, B. J., Kiriakoulakis, K., Popova, E. E., Ragueneau, O., Vangriesheim, A., &  
1114 Wolff, G. A. (2001). Material supply to the abyssal seafloor in the Northeast Atlantic, *Progress in  
1115 Oceanography*, 50, 27–63. [https://doi.org/10.1016/S0079-6611\(01\)00047-7](https://doi.org/10.1016/S0079-6611(01)00047-7)

1116

1117 Landschützer, P., Gruber, N., & Bakker, D. C. (2016). Decadal variations and trends of the global  
1118 ocean carbon sink. *Global Biogeochemical Cycles*, 30(10), 1396–1417.  
1119 <https://doi.org/10.1002/2015gb005359>

1120

1121 Landschützer, P., Gruber, N., Bakker, D. C. E., Stemmler, I., Six, K. D. (2018). Strengthening  
1122 seasonal marine CO<sub>2</sub> variations due to increasing atmospheric CO<sub>2</sub>. *Nature Climate Change*, 8,  
1123 146–150. <https://doi.org/10.1038/s41558-017-0057-x>

1124

1125 Laufkötter, C., Vogt, M., Gruber, N., Aita-Noguchi, M., Aumont, O., Bopp, L., et al. (2015).  
1126 Drivers and uncertainties of future global marine primary production in marine ecosystem  
1127 models. *Biogeosciences*, 12(23), 6955–6984. <https://doi.org/10.5194/bg-12-6955-2015>

1128

1129 Laufkötter, C., Vogt, M., Gruber, N., Aumont, O., Bopp, L., Doney, S. C., et al. (2016). Projected  
1130 decreases in future marine export production: The role of the carbon flux through the upper  
1131 ocean ecosystem. *Biogeosciences*, 13, 4023–4047. <https://doi.org/10.5194/bg-13-4023-2016>

1132

1133 Laufkötter, C., John, J. G., Stock, C. A., & Dunne, J. P. (2017). Temperature and oxygen  
1134 dependence of the remineralization of organic matter. *Global Biogeochemical Cycles*, 31, 1038–  
1135 1050. <https://doi.org/10.1002/2017GB005643>

1136

1137 Laurenceau-Cornec, E. C., Le Moigne, F. A. C., Gallinari, M., Moriceau, B., Toullec, J., Iversen,  
1138 M. I., Engel, A., & De La Rocha, C. L. (2020). New guidelines for the application of Stokes'  
1139 models to the sinking velocity of marine aggregates, *Limnology and Oceanography*, 65, 1264–  
1140 1285. <https://doi.org/10.1002/lno.11388>

1141

1142 Laws, E. A., Falkowski, P. G., Smith Jr, W. O., Ducklow, H., & McCarthy, J. J. (2000).  
1143 Temperature effects on export production in the open ocean. *Global Biogeochemical Cycles*, 14,  
1144 1231–1246. <https://doi.org/10.1029/1999GB001229>

1145

1146 Laws, E. A., & Maiti, K. (2019). The relationship between primary production and export  
1147 production in the ocean: Effects of time lags and temporal variability, *Deep Sea Research Part I*,  
1148 148, 100–107. <https://doi.org/10.1016/j.dsr.2019.05.006>

1149

1150 Laws, E. A., D'sa, E., & Naik, P. (2011). Simple equations to estimate ratios of new or export  
1151 production to total production from satellite-derived estimates of sea surface temperature and  
1152 primary production. *Limnology and Oceanography: Methods*, 9(12), 593–601.  
1153 <https://doi.org/10.4319/lom.2011.9.593>

1154

1155 Le Quéré, C., Buitenhuis, E. T., Moriarty, R., Alvain, S., Aumont, O., Bopp, L., et al. (2016).  
1156 Role of zooplankton dynamics for Southern Ocean phytoplankton biomass and global  
1157 biogeochemical cycles. *Biogeosciences*, 13(14), 4111–4133. <https://doi.org/10.5194/bg-13-4111-2016>

1159

1160 Liao, E., Resplandy, L., Liu, J., & Bowman, K. W. (2020). Amplification of the ocean carbon  
1161 sink during El Niños: Role of poleward Ekman transport and influence on atmospheric CO<sub>2</sub>.  
1162 *Global Biogeochemical Cycles*, 34(9), e2020GB006574. <https://doi.org/10.1029/2020gb006574>

1163

1164 Lima, I. D., Lam, P. J., & Doney, S. C. (2014). Dynamics of particulate organic carbon flux in a  
1165 global ocean model, *Biogeosciences*, 11, 1177–1198. <https://doi.org/10.5194/bg-11-1177-2014>

1166

1167 Lindsay, K., Bonan, G. B., Doney, S. C., Hoffman, F. M., Lawrence, D. M., Long, M. C., et al.  
1168 (2014). Preindustrial-control and twentieth-century carbon cycle experiments with the Earth  
1169 System Model CESM1(BGC). *Journal of Climate*, 27(24), 8981–9005. <https://doi.org/10.1175/jcli-d-12-00565.1>

1171

1172 Lutz, M. J., Caldeira, K., Dunbar, R. B., & Behrenfeld, M. J. (2007). Seasonal rhythms of net  
1173 primary production and particulate organic carbon flux to depth describe the efficiency of  
1174 biological pump in the global ocean. *Journal of Geophysical Research Oceans*, 112, C10011.  
1175 <https://doi.org/10.1029/2006JC003706>

1176

1177 Maier-Reimer, E. (1993). Geochemical cycles in an ocean general circulation model.  
1178 Preindustrial tracer distributions, *Global Biogeochemical Cycles*, 7, 645–677.  
1179 <https://doi.org/10.1029/93GB01355>

1180

1181 Marinov, I., Gnanadesikan, A., Sarmiento, J. L., Toggweiler, J. R., Follows, M., & Mignone, B.  
1182 K. (2008). Impact of oceanic circulation on biological carbon storage in the ocean and  
1183 atmospheric pCO<sub>2</sub>, *Global Biogeochemical Cycles*, 22, GB3007.  
1184 <https://doi.org/10.1029/2007GB002958>

1185

1186 Marra, J., Ho, C., & Trees, C. C. (2003). An alternative algorithm for the calculation of primary  
1187 production from remote sensing data, Rep. LDEO 2003–1, Lamont-Doherty Earth Observatory,  
1188 Palisades, New York. <https://www.ledo.columbia.edu/~marra/MarraAlgorithm.pdf> (Accessed  
1189 August, 2022).

1190

1191 Marsay, C. M., Sanders, R. J., Henson, S. A., Pabortsava, K., Achterberg, E. P., & Lampitt, R. S.  
1192 (2015). Attenuation of sinking particulate organic carbon flux through the mesopelagic ocean,  
1193 *Proceedings of the National Academy of Sciences USA*, 112(4) 1089–1094.  
1194 <https://doi.org/10.1073/pnas.1415311112>

1195

1196 Martin, J. H., Knauer, G. A., Karl, D. M., & Broenkow, W. W. (1987). VERTEX: carbon cycling  
1197 in the northeast Pacific, *Deep-Sea Research*, 34, 267–285. [https://doi.org/10.1016/0198-0149\(87\)90086-0](https://doi.org/10.1016/0198-0149(87)90086-0)

1198

1199

1200 Matsumoto, K., Sarmiento, J. L., Key, R. M., Bullister, J. L., Caldeira, K., Campin, J.-M., et al.  
1201 (2004). Evaluation of ocean carbon cycle models with data-based metrics, *Geophysical Research  
Letters*, 31, L07303. <https://doi.org/10.1029/2003GL018970>

1202

1203

1204 Mauritsen, T., Bader, J., Becker, T., Behrens, J., Bittner, M., Brokopf, R., et al. (2019).  
1205 Developments in the MPI-M Earth system model version 1.2 (MPI-ESM1. 2) and its response to  
1206 increasing CO<sub>2</sub>. *Journal of Advances in Modeling Earth Systems*, 11(4), 998–1038.  
1207 <https://doi.org/10.1029/2018ms001400>

1208

1209 Mayor, D. J., Sanders, R., Giering, S. L. C., & Anderson, T. R. (2014). Microbial gardening in  
1210 the ocean's twilight zone: Detritivorous metazoans benefit from fragmenting, rather than  
1211 ingesting, sinking detritus, *BioEssays*, 36, 1132–1137. <https://doi.org/10.1002/bies.201400100>

1212

1213 Mikaloff Fletcher, S. E., Gruber, N., Jacobson, A. R., Gloor, M., Doney, S. C., Dutkiewicz, S., et  
1214 al. (2007). Inverse estimates of the oceanic sources and sinks of natural CO<sub>2</sub> and their implied  
1215 oceanic transport. *Global Biogeochemical Cycles*, 21, GB1010.  
1216 <https://doi.org/10.1029/2006GB002751>

1217

1218 Mouw, C. B., Barnett, A., McKinley, G. A., Gloege, L., & Pilcher, D. (2016a). Global ocean  
1219 particulate organic carbon flux merged with satellite parameters, *Earth System Science Data*, 8,  
1220 531–541. <https://doi.org/10.5194/essd-8-531-2016>

1221

1222 Mouw, C. B., Barnett, A., McKinley, G. A., Gloege, L., & Pilcher, D. (2016b). Phytoplankton  
1223 size impact on export flux in the global ocean, *Global Biogeochemical Cycles*, 30, 1542–1562.  
1224 <https://doi.org/10.1002/2015GB005355>

1225

1226 Müller, Jens Daniel. (2023). RECCAP2-ocean data collection [Data set]. Zenodo. 1631.  
1227 <https://doi.org/10.5281/zenodo.7990823>

1228

1229 Najjar, R. G., X. Jin, F. Louanchi, O. Aumont, K. Caldeira, S.C. Doney, et al. (2007). Impact of  
1230 circulation on export production, dissolved organic matter and dissolved oxygen in the ocean:  
1231 Results from Phase II of the Ocean Carbon-cycle Model Intercomparison Project (OCMIP-2),  
1232 *Global Biogeochemical Cycles*, 21, GB3007. <https://doi.org/10.1029/2006GB002857>.

1233

1234 Nowicki, M., DeVries, T., & Siegel, D. A. (2022). Quantifying the carbon export and  
1235 sequestration pathways of the ocean's biological carbon pump. *Global Biogeochemical Cycles*,  
1236 36, e2021GB007083. <https://doi.org/10.1029/2021GB007083>

1237

1238 Omand, M. M., Govindarajan, R., He, J., & Mahadevan, A. (2020). Sinking flux of particulate  
1239 organic matter in the oceans: Sensitivity to particle characteristics. *Scientific Reports*, 10, 5582.  
1240 <https://doi.org/10.1038/s41598-020-60424-5>

1241

1242 Orr, J. C., R.G. Najjar, O. Aumont, L. Bopp, J.L. Bullister, G. Danabasoglu, et al. (2017).  
1243 Biogeochemical protocols and diagnostics for the CMIP6 Ocean Model Intercomparison Project  
1244 (OMIP). *Geoscientific Model Development*, 10, 2169–2199. <https://doi.org/10.5194/gmd-10-2169-2017>

1245

1246

1247 RECCAP2 Ocean Science Team (2022). RECCAP2 Ocean Protocols, accessed August 3<sup>rd</sup>, 2022.  
1248 <https://reccap2-ocean.github.io/protocols/>

1249

1250 Reygondeau, G., Longhurst, A., Martinez, E., Beaugrand, G., Antoine, D., & Maury, O. (2013),  
1251 Dynamic biogeochemical provinces in the global ocean, *Global Biogeochemical Cycles*, 27,  
1252 1046–1058. <https://doi.org/10.1002/gbc.20089>

1253

1254 Rödenbeck, C., DeVries, T., Hauck, J., Le Quéré, C., & Keeling, R. F. (2022). Data-based  
1255 estimates of interannual sea–air CO<sub>2</sub> flux variations 1957–2020 and their relation to  
1256 environmental drivers. *Biogeosciences*, 19(10), 2627–2652. <https://doi.org/10.5194/bg-19-2627-2022>

1257

1258

1259 Rödenbeck, C., Keeling, R. F., Bakker, D. C., Metzl, N., Olsen, A., Sabine, C., & Heimann, M.  
1260 (2013). Global surface-ocean pCO<sub>2</sub> and sea–air CO<sub>2</sub> flux variability from an observation-driven  
1261 ocean mixed-layer scheme. *Ocean Science*, 9(2), 193–216. <https://doi.org/10.5194/os-9-193-2013>

1262

1263

1264 Rodgers, K. B., Schwinger, J., Fassbender, A. J., Landschützer, P., Yamaguchi, R., Frenzel, H., et  
1265 al. (2023). Seasonal variability of the surface ocean carbon cycle: A synthesis. *Global  
1266 Biogeochemical Cycles*, 37, e2023GB007798. <https://doi.org/10.1029/2023GB007798>

1267

1268 Sarmiento, J. L., & Gruber, N. (2002). Anthropogenic carbon sinks. *Physics Today*, 55(8), 30–36.  
1269 <https://doi.org/10.1063/1.1510279>

1270

1271 Sarmiento, J. L., & Gruber, N. (2006). *Ocean Biogeochemical Dynamics*. Princeton University  
1272 Press. <https://doi.org/10.1017/S0016756807003755>

1273

1274 Schlitzer, R. (2000). Applying the adjoint method for biogeochemical modeling: Export of  
1275 particulate organic matter in the World Ocean, *Inverse methods in biogeochemical cycles*, ed. P.  
1276 Kasibhata, AGU Monograph 114, pp. 107–124.

1277

1278 Schwinger, J., Goris, N., Tjiputra, J. F., Kriest, I., Bentsen, M., Bethke, I., et al. (2016).  
1279 Evaluation of NorESM-OC (versions 1 and 1.2), the ocean carbon-cycle stand-alone  
1280 configuration of the Norwegian Earth System Model (NorESM1). *Geoscientific Model  
1281 Development*, 9(8), 2589–2622. <https://doi.org/10.5194/gmd-9-2589-2016>

1282

1283 Séférian, R., Gehlen, M., Bopp, L., Resplandy, L., Orr, J. C., Marti, O., et al. (2016). Inconsistent  
1284 strategies to spin up models in CMIP5: implications for ocean biogeochemical model  
1285 performance assessment, *Geoscientific Model Development*, 9, 1827–1851.  
1286 <https://doi.org/10.5194/gmd-9-1827-2016>

1287

1288 Séférian, R., Berthet, S., Yool, A., Palmiéri, J., Bopp, L., Tagliabue, A., et al. (2020). Tracking  
1289 improvement in simulated marine biogeochemistry between CMIP5 and CMIP6. *Current*  
1290 *Climate Change Reports*, 6(3), 95–119. <https://doi.org/10.1007/s40641-020-00160-0>

1291

1292 Séférian, R., Nabat, P., Michou, M., Saint-Martin, D., Volodire, A., Colin, J., et al. (2019).  
1293 Evaluation of CNRM Earth-System model, CNRM-ESM2-1: Role of Earth system processes in  
1294 present-day and future climate. *Journal of Advances in Modeling Earth Systems*, 11(12),  
1295 4182–4227. <https://doi.org/10.1029/2019ms001791>

1296

1297 Siegel, D. A., Buesseler, K. O., Doney, S. C., Sailley, S. F., Behrenfeld, M. J., & Boyd, P. W.  
1298 (2014). Global assessment of ocean carbon export by combining satellite observations and food-  
1299 web models. *Global Biogeochemical Cycles*, 28(3), 181–196.  
1300 <https://doi.org/10.1002/2013gb004743>

1301

1302 Siegel, D. A., Buesseler, K. O., Behrenfeld, M. J., Benitez-Nelson, C. R., Boss, E., Brzezinski,  
1303 M. A., et al. (2016). Prediction of the export and fate of global ocean net primary production: the  
1304 EXPORTS science plan, *Frontiers in Marine Science*, 3, 22.  
1305 <http://doi.org/10.3389/fmars.2016.00022>

1306

1307 Siegel, D. A., DeVries, T., Doney, S. C., & T. Bell, T. (2021). Assessing the sequestration time  
1308 scales of some ocean-based carbon dioxide reduction strategies, *Environmental Research Letters*,  
1309 16, 104003. <https://doi.org/10.1088/1748-9326/ac0be0>

1310

1311 Siegel, D. A., DeVries, T., Cetinić, I., & K Bisson, K. M. (2023). Quantifying the ocean's  
1312 biological pump and Its carbon cycle impacts on global scales, *Annual Review of Marine*  
1313 *Science*, 15, 329–356. <https://doi.org/10.1146/annurev-marine-040722-115226>

1314

1315 Silsbe, G. M., Behrenfeld, M. J., Halsey, K. H., Milligan, A. J., & Westberry, T. K. (2016). The  
1316 CAFE model: A net production model for global ocean phytoplankton, *Global Biogeochemical*  
1317 *Cycles*, 30, 1756–1777. doi:10.1002/2016GB005521

1318

1319 Steinberg, D. K., & M.R. Landry, M. R. (2017). Zooplankton and the ocean carbon cycle, *Annual*  
1320 *Review of Marine Science*, 9, 413–444. <https://doi.org/10.1146/annurev-marine-010814-015924>

1321

1322 Stock, C. A., Dunne, J. P., Fan, S., Ginoux, P., John, J., Krasting, J. P., et al. (2020). Ocean  
1323 biogeochemistry in GFDL's Earth system model 4.1 and its response to increasing atmospheric  
1324 CO<sub>2</sub>. *Journal of Advances in Modeling Earth Systems*, 12(10), e2019MS002043. <https://doi.org/10.1029/2019ms002043>

1325

1326

1327 Stukel, M. R., Ohman, M. D., Kelly, T. B., & Biard, T. (2019). The roles of suspension-feeding  
1328 and flux-feeding zooplankton as gatekeepers of particle flux into the mesopelagic ocean in the  
1329 Northeast Pacific. *Frontiers in Marine Science*, 6, 397. <https://doi.org/10.3389/fmars.2019.00397>  
1330

1331 Takahashi, T., Olafsson, J., Goddard, J. G., Chipman, D. W., & Sutherland, S. C. (1993).  
1332 Seasonal variation of CO<sub>2</sub> and nutrients in the high-latitude surface oceans: A comparative study,  
1333 *Global Biogeochemical Cycles*, 7(4), 843–878. <https://doi.org/10.1029/93GB02263>  
1334

1335 Takahashi, T., Sutherland, S. C., Sweeney, C., Poisson, A., Metzl, N., Tilbrook, B., et al. (2002).  
1336 Global sea-air CO<sub>2</sub> flux based on climatological surface ocean pCO<sub>2</sub>, and seasonal biological  
1337 and temperature effects. *Deep Sea Research Part II: Topical Studies in Oceanography*, 49(9–10),  
1338 1601–1622. [https://doi.org/10.1016/S0967-0645\(02\)00003-6](https://doi.org/10.1016/S0967-0645(02)00003-6)  
1339

1340 Terhaar, T., Goris, N., Müller, J. D., DeVries, T., Gruber, N., Hauck, J., et al. (2023). Assessment  
1341 of global ocean biogeochemistry models for ocean carbon sink estimates in RECCAP2 and  
1342 recommendations for future studies. *ESS Open Archive*.  
1343 <https://doi.org/10.22541/essoar.168394734.41886821/v1>  
1344

1345 Turner, J. T. (2015). Zooplankton fecal pellets, marine snow, phytodetritus and the ocean's  
1346 biological pump, *Progress in Oceanography*, 130, 205–248.  
1347 <https://doi.org/10.1016/j.pocean.2014.08.005>  
1348

1349 Tsujino, H., Nakano, H., Sakamoto, K., Urakawa, S., Hirabara, M., Ishizaki, H., & Yamanaka, G.  
1350 (2017). Reference manual for the meteorological research institute community ocean model  
1351 version 4 (MRI. COMv4) (Vol. 80, p. 306). Technical Reports of the Meteorological Research  
1352 Institute.  
1353

1354 Urakawa, L. S., Tsujino, H., Nakano, H., Sakamoto, K., Yamanaka, G., & Toyoda, T. (2020). The  
1355 sensitivity of a depth-coordinate model to diapycnal mixing induced by practical  
1356 implementations of the isopycnal tracer diffusion scheme. *Ocean Modelling*, 154, 101693.  
1357 <https://doi.org/10.1016/j.ocemod.2020.101693>  
1358

1359 Volk, T., & Hoffert, M. I. (1985). Ocean carbon pumps: Analysis of relative strengths and  
1360 efficiencies in ocean-driven atmospheric CO<sub>2</sub> changes. In E. Sundquist & W. Broecker (Eds.),  
1361 *The carbon cycle and atmospheric CO<sub>2</sub>: Natural variations archean to present* (Vol. 32, pp. 99–  
1362 110). American Geophysical Union (AGU). <https://doi.org/10.1029/GM032P0099>  
1363

1364 Wanninkhof, R., Park, G.-H., Takahashi, T., Sweeney, C., Feely, R., Nojiri, Y., et al. (2013).  
1365 Global ocean carbon uptake: magnitude, variability and trends, *Biogeosciences*, 10, 1983–2000.  
1366 <https://doi.org/10.5194/bg-10-1983-2013>  
1367

1368 Watson, A. J., Schuster, U., Shutler, J. D., Holding, T., Ashton, I. G., Landschützer, P., et al.  
1369 (2020). Revised estimates of ocean-atmosphere CO<sub>2</sub> flux are consistent with ocean carbon  
1370 inventory. *Nature Communications*, 11(1), 1–6. <https://doi.org/10.1038/s41467-020-18203-3>  
1371

1372 Weber, T., Cram, J. A., Leung, S. W., DeVries, T., & Deutsch, C. (2016). Deep ocean nutrients  
1373 imply large latitudinal variation in particle transfer efficiency, *Proceedings of the National  
1374 Academy of Sciences*, 113, 8606–8611. <https://doi.org/10.1073/pnas.1604414113>

1375

1376 Wilson, J. D., Andrews, O., Katavouta, A., de Melo Viríssimo, F., Death, R. M., Adloff, M., et al.  
1377 (2022). The biological carbon pump in CMIP6 models: 21st century trends and uncertainties.  
1378 *Proceedings of the National Academy of Sciences USA*, 119(29), e2204369119.  
1379 <https://doi.org/10.1073/pnas.2204369119>

1380

1381 Wright, R. M., Le Quéré, C., Buitenhuis, E., Pitois, S., & Gibbons, M. J. (2021). Role of jellyfish  
1382 in the plankton ecosystem revealed using a global ocean biogeochemical model. *Biogeosciences*,  
1383 18(4), 1291–1320. <https://doi.org/10.5194/bg-18-1291-2021>

1384

1385 Yang, S., & Gruber, N. (2016). The anthropogenic perturbation of the marine nitrogen cycle by  
1386 atmospheric deposition: Nitrogen cycle feedbacks and the  $^{15}\text{N}$  Haber-Bosch effect. *Global  
1387 Biogeochemical Cycles*, 30(10), 1418–1440. <https://doi.org/10.1002/2016gb005421>

1388

1389 Zeng, J., Iida, Y., Matsunaga, T., & Shirai, T. (2022). Surface ocean  $\text{CO}_2$  concentration and air-  
1390 sea flux estimate by machine learning with modelled variable trends. *Frontiers in Marine  
1391 Science*, 9, 989233. <https://doi.org/10.3389/fmars.2022.989233>

1392

1393

**Supporting Information:**

1394     **Observational and numerical modeling constraints on the global ocean biological carbon pump**

1395

1396     **Scott C. Doney<sup>1</sup>, Kayla A. Mitchell<sup>1,2</sup>, Stephanie A. Henson<sup>3</sup>, Emma Cavan<sup>4</sup>, Tim DeVries<sup>5</sup>,**  
1397     **Nicolas Gruber<sup>6</sup>, Judith Hauck<sup>7</sup>, Colleen B. Mouw<sup>8</sup>, Jens D. Müller<sup>6</sup>, and Francois W.**  
1398     **Primeau<sup>2</sup>**

1399

1400     **February 4<sup>th</sup>, 2024**

1401

1402     <sup>1</sup> Department of Environmental Sciences, University of Virginia, Charlottesville, VA, USA,

1403     <sup>2</sup> Department of Earth System Science, University of California, Irvine, Irvine, CA, USA,

1404     <sup>3</sup> National Oceanography Centre, Southampton, UK,

1405     <sup>4</sup> Department of Life Sciences, Silwood Park Campus, Imperial College London, Berkshire, UK,

1406     <sup>5</sup> Earth Research Institute and Department of Geography, University of California, Santa  
1407     Barbara, Santa Barbara, CA, USA,

1408     <sup>6</sup> Environmental Physics, Institute of Biogeochemistry and Pollutant Dynamics, ETH Zurich,  
1409     Zürich, Switzerland

1410     <sup>7</sup> Alfred-Wegener-Institut, Helmholtz-Zentrum für Polar- und Meeresforschung, Bremerhaven,  
1411     Germany

1412     <sup>8</sup> Graduate School of Oceanography, University of Rhode Island, Narragansett, RI, USA.

1413

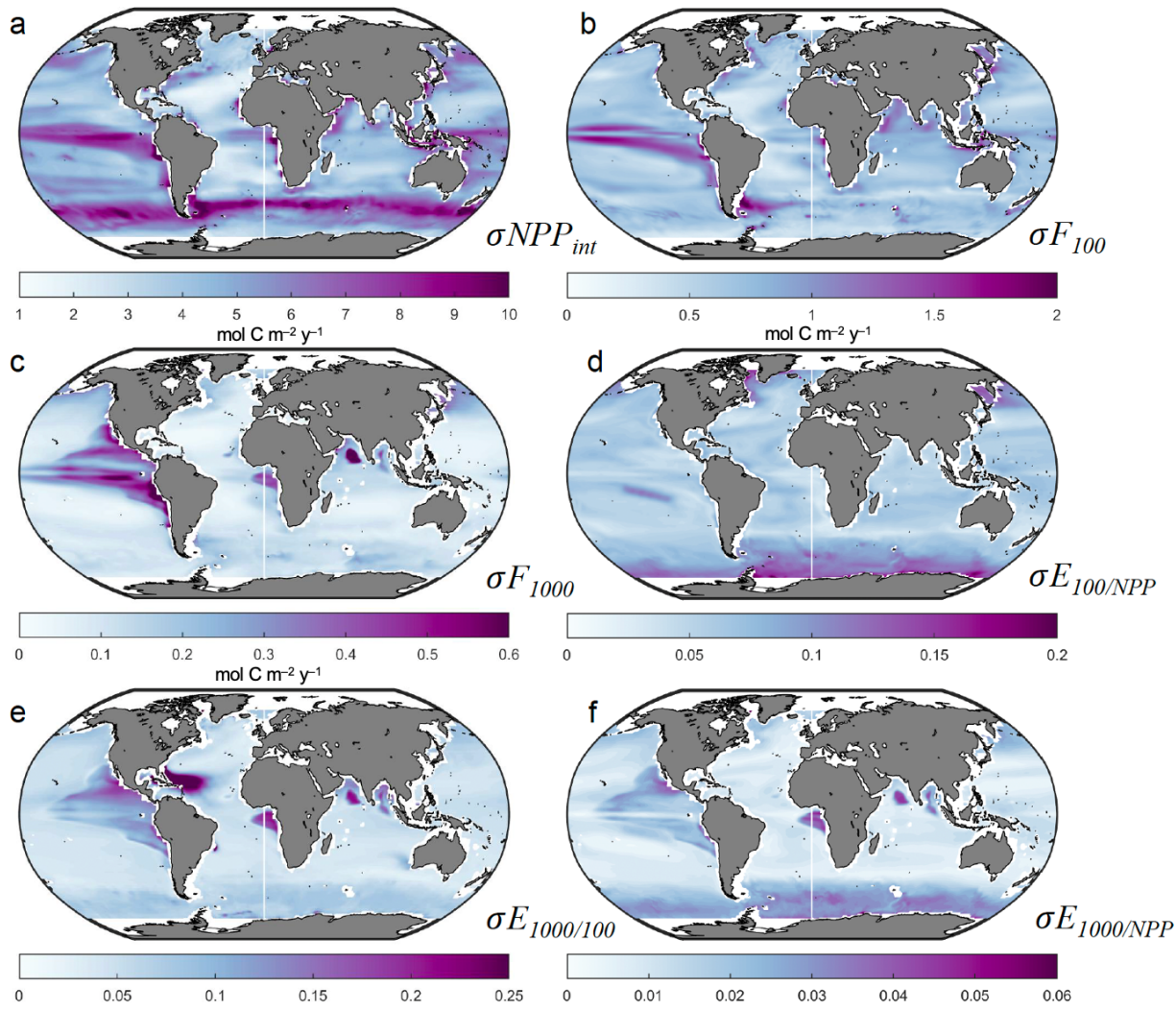
1414     The REgional Carbon Cycle Assessment and Processes (RECCAP) project is a coordinated, international  
1415     effort to constrain contemporary ocean carbon air-sea fluxes and interior storage trends using a combination  
1416     of field observations, inverse model products, and ocean biogeochemical hindcast simulations. The second  
1417     phase, RECCAP2, extends the original synthesis using additional years of ocean observational data and  
1418     updated numerical results (DeVries et al., 2023) as well as expanding the scope of the observational and model  
1419     analysis, in this case into the biological carbon pump magnitude and efficiency.

1420

1421     **Supplement Figures**

1422

1423



1424

1425

1426

1427

**Figure S1.** Maps of within-ensemble standard deviation of biological pump parameters. Standard deviations across model ensemble members are computed relative to the average model ensemble presented in Figure 1 for: (a) vertically integrated primary productivity  $\sigma_{NPP}$ , (b) particulate organic carbon export fluxes at 100 m  $\sigma F_{100}$ , and (c) 1000 m  $\sigma F_{1000}$ , all in moles C m<sup>-2</sup> y<sup>-1</sup>, and (d) surface export efficiency ratio  $E_{100/NPP} = F_{100}/NPP$ , (e) mesopelagic transfer efficiency at 1000 m  $E_{1000/100} = F_{1000}/F_{100}$ , and (f) export efficiency to the deep ocean  $E_{1000/NPP} = F_{1000}/NPP$ , all ratios unitless.

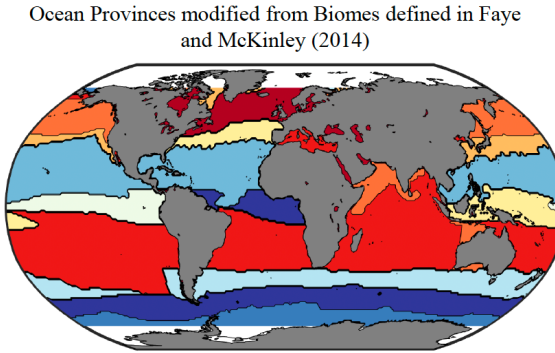
1434

1435

1436

1437

1438



Biome Number	Biome Acronym	Biome Description
18	SOSPSS	Southern Ocean Subpolar Seasonally Stratified
17	NaAEQU	N. Atlantic Equatorial
16	SOICE	Southern Ocean Ice
15	NPICE	North Pacific Ice
14	NPSTPS	N. Pacific Subtropical Permanently Stratified
13	NaSTPS	N. Atlantic Subtropical Seasonally Stratified
12	SOSTSS	Southern Ocean Subtropical Seasonally Stratified
11	BARENTS	Barents Sea
10	PEQUE	Eastern Equatorial Pacific
9	PEQUW	Western Equatorial Pacific
8	NAICE	N. Atlantic Ice
7	NaSTSS	N. Atlantic Subtropical Seasonally Stratified
6	NPSTSS	N. Pacific Subtropical Seasonally Stratified
5	NPSPSS	N. Pacific Subpolar Seasonally Stratified
4	INDSTPS	Indian Ocean Subtropical Permanently Stratified
3	MED	Mediterranean Sea
2	SASTPS	S. Atlantic Subtropical Permanently Stratified
1	NaSPSS	N. Atlantic Subpolar Seasonally Stratified

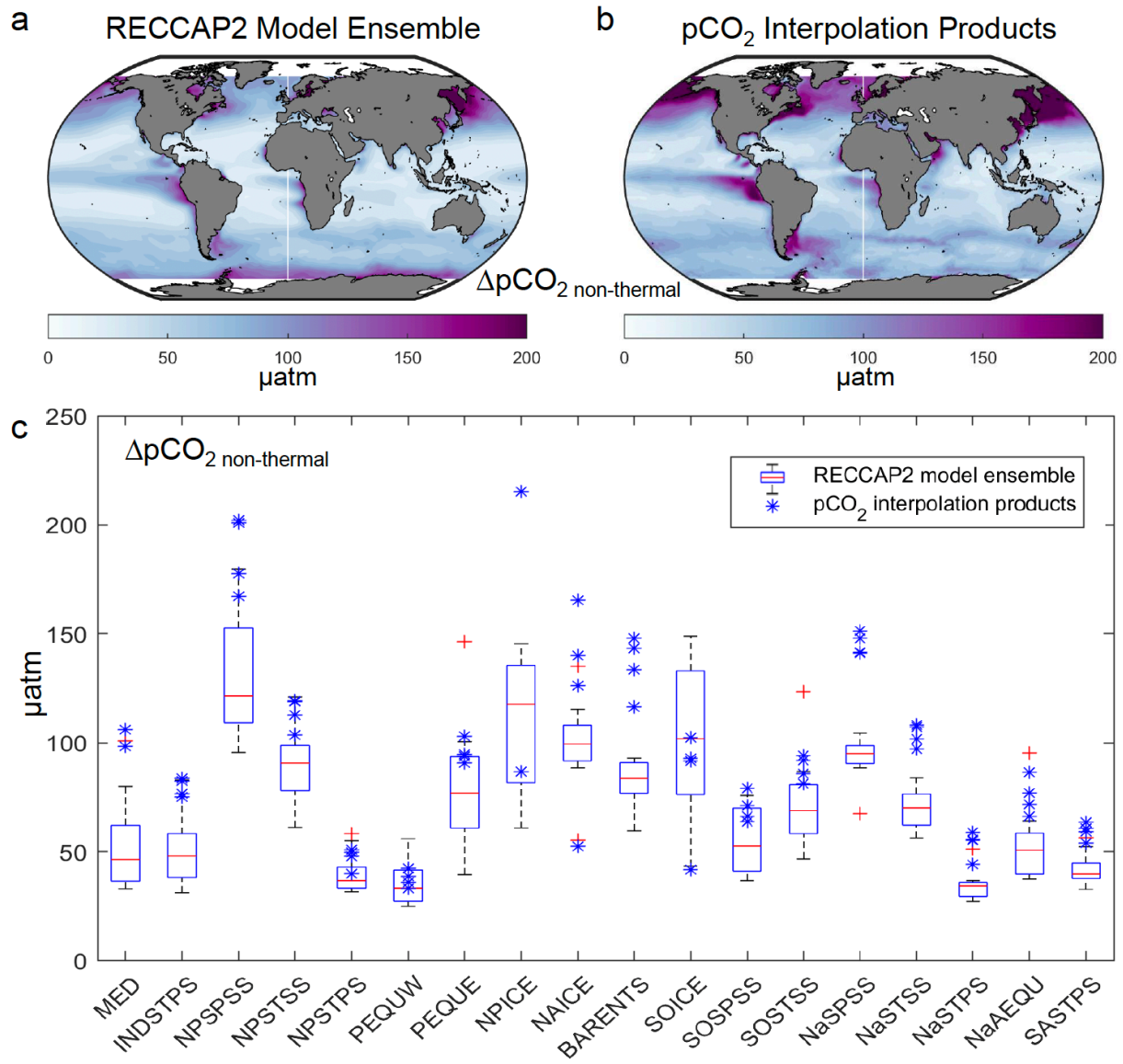
1439

1440

1441 **Figure S2.** Map of standard RECCAP2 biomes by ocean basin (Fay and McKinley, 2014). The  
 1442 biomes include polar (ICE), subpolar seasonally-stratified (SPSS), subtropical seasonally stratified  
 1443 (STSS), subtropical permanently stratified (STPS), and equatorial regions (EQU); note the  
 1444 equatorial Pacific is divided into western and eastern sub-basins. The equatorial eastern Pacific  
 1445 and Atlantic, monsoon-influenced Indian, and seasonally-stratified biomes generally exhibited  
 1446 relatively high NPP,  $F_{100}$ , and  $F_{1000}$ . Polar and sub-polar biomes exhibited relatively high  $E_{100}$ .

1447

1448

1449  
1450

1451 **Figure S3.** Analysis of the seasonal cycle of non-thermal  $\Delta pCO_2$  non-thermal (a) spatial map of  
 1452 RECCAP2 multi-model ensemble average, (b) spatial map from pCO<sub>2</sub> observational data products,  
 1453 and (c) box-whisker plot of RECCAP2 multi-model ensemble medians, interquartile ranges, and  
 1454 outliers pooled into Fay and McKinley biomes (Figure S2).  
 1455

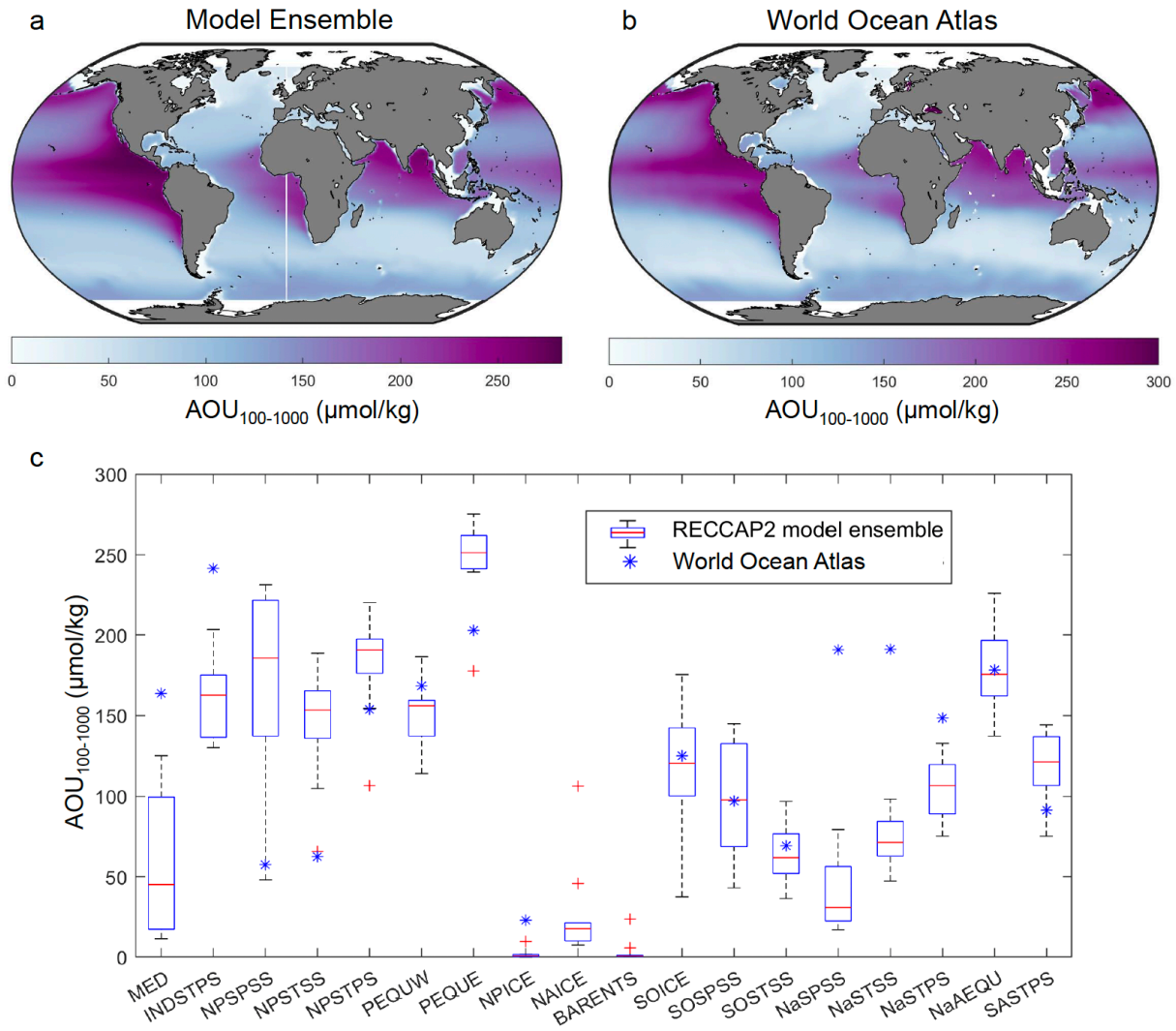


**Figure S4.** Analysis of apparent oxygen utilization (AOU) vertically averaged over the mesopelagic zone (100-1000 m) (a) spatial map of RECCAP2 multi-model ensemble average, and (b) spatial map from WOA observational data set, and (c) box-whisker plot of RECCAP2 multi-model ensemble medians, interquartile ranges, and outliers pooled into Fay and McKinley biomes (Figure S2).

#### Supporting Information Tables

1467 **Table S1.** Interannual variability (1985-2018) for the RECCAP2 simulations (simulation A) for  
 1468 global-integrated, annual-mean variables: vertically integrated net primary productivity *NPP* and  
 1469 particulate organic carbon export fluxes at 100 m  $F_{100}$  and 1000 m depth  $F_{1000}$ . Interannual  
 1470 variability (standard deviation) are in Pg C  $y^{-1}$ .

1471

	CCSM- WHOI	CESM- ETHZ	CNRM- ESM2	ECCO- Darwin	EC- Earth3	FESOM - RECoM _LR	MOM6- Princeto n	MPIOM - HAMO CC	MRI- ESM2-0	Nor_ES M- OC1.2	ORCA1 -LIM3- PISCES	PlankT OM12
NPP	0.1914	0.3743	0.2000	0.7272	0.2194	0.3878	0.3204	1.5377	0.4127	0.3518	0.2286	0.3655
F100	0.0352	0.0491	0.0304	0.1966	0.0412	0.1079	0.0383	0.2004	0.0736	0.0717	0.0484	0.1447
F1000	0.0024	0.0140	0.0000	0.1107	0.0000	0.0143	0.0000	0.0419	0.0103	0.0283	0.0000	0.0000

1472

1473 **Table S2.** Long-term temporal trends (1985-2018) for the RECCAP2 simulations (simulation A)  
 1474 for global-integrated, annual-mean variables: vertically integrated net primary productivity *NPP*  
 1475 and particulate organic carbon export fluxes at 100 m  $F_{100}$  and 1000 m depth  $F_{1000}$ . Trends are in  
 1476 Pg C  $y^{-1}/year$ ,

1477

	CCSM- WHOI	CESM- ETHZ	CNRM- ESM2	ECCO- Darwin	EC- Earth3	FESOM - RECoM _LR	MOM6- Princeto n	MPIOM - HAMO CC	MRI- ESM2-0	Nor_ES M- OC1.2	ORCA1 -LIM3- PISCES	PlankT OM12
NPP	-0.0140	-0.0172	0.0005	-0.0727	0.0017	-0.0094	0.0102	0.0028	-0.0047	0.0009	0.0190	0.0184
F100	-0.0031	-0.0020	0.0000	-0.0209	0.0000	0.0013	0.0010	0.0001	0.0002	0.0017	0.0029	0.0237
F1000	-0.0002	-0.0002	0.0000	-0.0117	0.0000	0.0004	0.0000	0.0013	0.0000	-0.0001	0.0000	0.0000

1478

1479